Mechanical behavior of composite corrugated structures for skin of morphing aircraft.

Dayyani, Iman

Prifysgol Abertawe
Swansea University

Mechanical Behavior of Composite Corrugated Structures for Skin of Morphing Aircraft

Iman Dayyani

Supervised by

Professor Michael Friswell

Submitted to Swansea University in fulfilment
of the requirements for the degree of

Doctor of Philosophy in

Mechanical Engineering

Swansea University

December 2014

Abstract

Corrugated panels have gained considerable popularity in a range of engineering applications, particularly in morphing skin applications due to their remarkable anisotropic characteristics. They are stiff to withstand the aerodynamic loads and flexible to enable the morphing deformations. In this thesis a detailed review of the literature on corrugated structures is presented. The specific characteristics of corrugated structures such as: high anisotropic behaviour, high stiffness and good durability, lightness and cost effectiveness are discussed comprehensively. However for the application in morphing aircraft, the optimal design of the corrugated panels requires simple models of these structures to be incorporated into multi-disciplinary system models. Therefore equivalent structural models are required that retain the dependence on the geometric parameters and material properties of the corrugated panels. In this regard, two analytical solutions based on homogenization and super element techniques are presented to calculate the equivalent mechanical properties of the corrugated skin. Different experimental and numerical models are investigated to verify the accuracy and efficiency of the presented equivalent models. The parametric studies of different corrugation shapes demonstrate the suitability of the proposed super element for application in further detailed design investigations. Then the design and multi-objective optimization of an elastomer coated composite corrugated skin for the camber morphing aerofoil is presented. The geometric parameters of the corrugated skin are optimized to minimize the in-plane stiffness and the weight of the skin and to maximize the flexural out-of-plane stiffness of the corrugated skin. A finite element code for thin beam elements is used with the aggregate Newton's method to optimize the geometric parameters of the coated corrugated panel. The advantages of the corrugated skin over the elastomer skin for the camber morphing structure are discussed. Moreover, a finite element simulation of the camber morphing internal structure with the corrugated skin is performed under typical aerodynamic and structural loadings to check the design approach.

Declarations and Statements

1. This work has not previously been accepted in substance for any degree and is not being concurrently submitted in candidature for any degree.

   Signed ... . (candidate)

   Date .....12/02/2015.....

2. This thesis is the result of my own investigations, except where otherwise stated. Other sources are acknowledged by footnotes giving explicit references. A bibliography is appended.

   Signed .... (candidate)

   Signed ..... (supervisor)

   Date .....12/02/2015.....

3. I hereby give consent for my thesis, if accepted, to be available for photocopying and for inter-library loan, and for the title and summary to be made available to outside organisations.

   Signed .... (candidate)

   Date .....12/02/2015.....

Acknowledgements

It would not have been possible to write this doctoral thesis without the help and support of the kind people around me, to only some of whom it is possible to give particular mention here.

I would like to thank my parents and brothers for their unbounded helps and encouragements. For sure without their supports this success would have not been possible.

I would like to thank my supervisor, Professor Michael Friswell for all his contributions of time and ideas to make my Ph.D. experience productive and stimulating. Because of his supports, I had the opportunity to be recruited as a fulltime research assistant and simultaneously to be enrolled as a full time Ph.D. student in Swansea University. I acknowledge funding from the European Research Council through Grant No. 247045 entitled ''Optimisation of Multiscale Structures with Applications to Morphing Aircraft''. I would like to thank the head of College of Engineering and all staff members in Swansea University for their support of this project.

I appreciate the intimate support and friendship of Dr. Erick Saavedra Flores and Dr. Hamed Haddad-Khodaparast during this project. I like to thank Professor Saeed Ziaei-Rad and Dr. Mohammad Silani for their sincere friendship and supports.

Table of Contents:

List of Figures:

List of Tables:

List of Notation:

a_1, a_2, a_3, h	Corrugation geometric parameters
b	Width of the corrugated panel
c, s	$\cos(\theta)$ and $\sin(\theta)$ of corrugation angle
d_s	Distance between two adjacent stringers
$\overrightarrow{e_t}, \overrightarrow{e_n}$	Tangent and normal unit vectors
f_4	Force due to elastomer tension
$f(x)$	Mathematical function of x defining the corrugation curve
g	Virtual force
l	Length
$n_{stringers}$	Number of stringers of the morphing internal structure, FishBAC
t	Thickness
t_c, t_e	Thickness of corrugated core and elastomer coating
$\overline{A}_{ij}$	In plane stiffness components
A_c and I_c	Cross section and second moment of area
$\overline{B}_{ij}$	Coupled in plane and out of plane stiffness components
CFn	Crossover fraction in genetic algorithm
$\overline{D}_{ij}$	Out of plane stiffness components
D_x	Equivalent orthotropic flexural rigidities in the x direction
D_y	Equivalent orthotropic flexural rigidities in the y direction
E	Young's modulus
G	Shear modulus
I	Compliance matrix
K	Equivalent tensile in-plane stiffness
L_{uc}	Length of a corrugation unit cell
L_{uc_a}	Minimum allowable length of a corrugation unit cell
N	Number of corrugation unitcells
$N_{unitcells}$	Number of corrugation unit cells between FishBAC stringers

$\bar{N}_{x,}$ $\bar{N}_y$ $\bar{N}_{xy}$ $\bar{M}_x$ $\bar{M}_y$ $\bar{M}_{xy}$	Equivalent force and moment components in the global coordinate system of the corrugated sheet
R, M_R	Reaction force and reaction moment
U	Strain energy
α	Force factor in elastomer members
δ	Displacement
δ_{hu}	Displacement of a half of corrugation unit cell
$\bar{\varepsilon}_x$ $\bar{\varepsilon}_y$ $\bar{\gamma}_{xy}$ $\bar{k}_x$ $\bar{k}_y$ $\bar{k}_{xy}$	Equivalent strain components in the global coordinate system of the corrugated sheet
η	Strength knock down factor
υ	Poisson's ratio
ρ	Density
σ_x	Stress in the longitudinal direction, x direction
σ_y	Stress in the transverse direction, y direction
σ_{xc}	Critical stress in the longitudinal direction, x direction
σ_{yc}	Critical stress in the transverse direction, y direction
τ	In-plane shear stress
τ_c	Critical In-plane shear stress
τ_I	The stress of interactive buckling mode
τ_G	The global failure stress
τ_L	The local buckling failure stress
τ_Y	The yield stress of the material

Chapter 1:
A Review on Corrugated Structures for the Application in Morphing Aircraft

1-1 Introduction

Improving the performance of an aircraft is important for a variety of reasons, such as: reducing the energy consumption, decreasing the toxic emissions and noise pollution or increasing the maneuverability of the aircraft. The only way of achieving these objectives is through better engines, more aerodynamically efficient wings, and lighter structures. However, the problem with the design of current aircraft wing is that they cannot be optimized for every single point of the flight envelope, for example take off, cruise and landing. In other words the wings of an aircraft are a compromise that limits the flight to a range of conditions where the performance of the aircraft at each condition is sub-optimal. Hence, a new generation of aircraft, known as morphing aircraft, are needed for further improvement of the aircraft performance without unacceptable penalties in terms of cost, complexity and weight.

Morphing aircraft have the ability to adapt their shape in flight so as to be always in the optimal configuration. However the requirements for morphing aircraft are conflicting. For instance, the skin is one of the main critical components of the morphing wing which must be stiff to withstand the aerodynamic loads, but also flexible to enable the shape changes. Among all possible structures for morphing skins such as segmented structures, reinforced elastomers or flexible matrix composite tubes embedded in a low modulus membrane, corrugated skins has attracted more attention in the literature. This is because the corrugated skins have exceedingly anisotropic behaviour; they are stiff along the corrugation direction, but flexible in the transverse direction. In addition, corrugated skins have other remarkable characteristics, such as high ratio of strength to density, good energy absorption and easy fabrication.

In this chapter a review of the mechanical behaviour of the corrugated structures is presented. Several investigations of these structures are studied in terms of different fields of structural engineering research, such as: bending, tensile, shear, compression and buckling analysis. Homogenization techniques and equivalent modelling are considered as well as optimization methods as necessary tools for the efficient design of these structures. Finally, the application of corrugated skin for morphing aircraft is discussed comprehensively.

1-2 A general description of corrugated structures

The term ''corrugated'' in general describes a series of parallel ridges and furrows (Merriam-Webster.com, 2014). In mechanical engineering any structure which has a surface with the shape of corrugation either made by folding, moulding, or any other manufacturing methods is called a corrugated structure. Three typical corrugated structures: a corrugated pipe, a corrugated sheet and a corrugated panel are shown in Fig. 1-1. The main common feature of all corrugated structures is their exceedingly anisotropic behaviour; high stiffness transverse to the corrugation direction in contrast to the compliance along the corrugation direction (Yokozeki et al., 2006). Because of this important feature, these structures have been widely used in industrial applications and academic research.

(a) Corrugated pipe
(www.allplasticpipe.com)

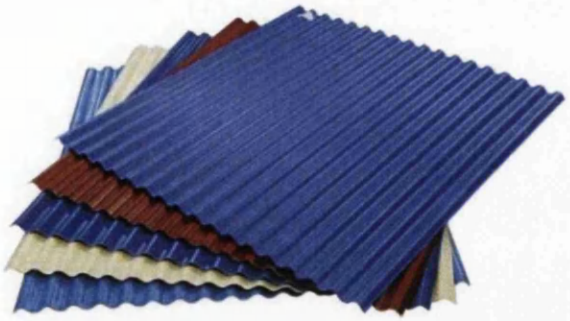

(b) Corrugated sheet
(www.yesgeneraltrading.com)

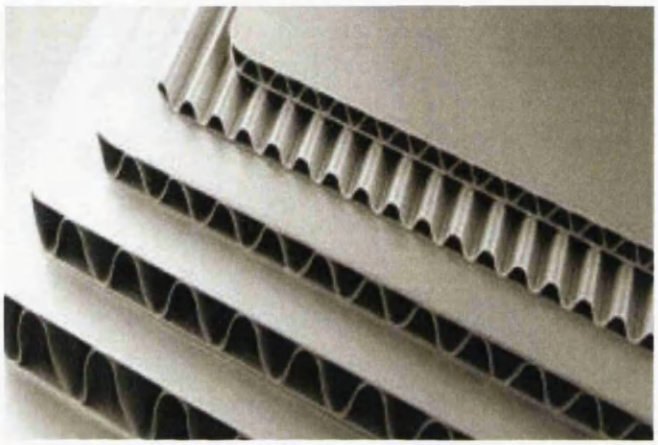

(c) Corrugated panels (http://ammonitum.com)

Figure 1-1: Three typical corrugated structure

By adding two face sheets (also known as liners) as upper and lower surfaces to the corrugated core (also known as medium or fluting) a new geometry would be obtained known, as a corrugated panel which is shown in Fig.1-1(c) (Gilchrist et al., 1998). By selecting the appropriate shape, dimensions and materials of the face sheets and corrugated core, a variety of stiffness and strength at low weight of the corrugated panel will be achieved. The structural characteristics of this corrugated structure depend mainly on the lightweight core which separates the face sheets and provides the necessary stiffness for the panel. However by considering different material stiffness for the face sheets and the core, different mechanical behaviour of the identical geometry would be expected.

If the stiffness of the material of face sheets is higher than or equal to the stiffness of the material of the core, the structure would be recognized as a corrugated sandwich panel (Carlsson et al., 2001). Such a sandwich panel demonstrates higher shear, bending and tensile stiffness to weight ratio than an equivalent panel made of

only the core material or the face-sheet material (Mallick et al., 2014). This is because the flexural stiffness of the panel is proportional to the cube of its thickness. Hence the function of a core in the sandwich panel is to increase the stiffness of the panel by effectively thickening it with a low-density core material. This results in the increase of the stiffness significantly for very little additional weight of the panel. The behaviour of such a sandwich panel under a bending load is similar to an I-beam where the facings of the sandwich panel act as the I-beam flanges where the upper and lower face sheets are subject to the in-plane compression and tension, and the core material acts as the beam's shear web where the core is subject to shear (Patel et al., 1997). It can be concluded that one of the most important characteristics of a core is to keep the face sheets apart and stabilize them by resisting the out of plane deformations which increases the shear strength and stiffness of the panel.

1-3 Applications of corrugated structures

Corrugated structures have wide application in engineering due to their special characteristics such as: anisotropic behaviour, high stiffness to weight ratio and high capacity of energy absorption. The applications of these structures can be classified into the following categories in which more value is given to the especial features of these structures. Figure 1-2 shows some applications of these structures.

1-3-1 Packaging industry

Corrugated boards, either made of plastic or cardboard are used extensively to produce rigid shipping containers of almost any shape or size. The packaging containers are exposed to various load conditions such as: static loads due to the compression of packages in a stack during transport and storage and vibration loads during transport. The reason that the corrugated sandwich panels have received huge interest in the packaging industries is because of their stiffness and durability, lightness and cost effectiveness as well as the recyclability and sustainability with the environment (Twede and Selke, 2005; Singh et al., 2006).

1-3-2 Civil structures

The wide application of corrugated structures in civil engineering may be classified mainly as: beams with corrugated web, corrugated roofs and walls and corrugated pipes.

Beams with corrugated web

The main benefit of applying corrugated web beams in supporting roofs, floors and columns in steel structural buildings are that the corrugated webs increase the beam's stability against buckling. Applying these corrugated web beams in the components of the building results in a very economical design by reducing the required web stiffeners and leads to a significant weight reduction in these beams compared with hot-rolled or welded ones (Dubina et al. 2013).

Corrugated sheets in roof and walls

Corrugated sheets are among the best candidates for application in construction elements, for roofs, claddings and walls, of modern industrial buildings owing to their high strength to weight ratio, much lighter and lower cost than flat isotropic panels of the same strength (Ng and Zheng, 1998). Corrugated metal sheets for instance are frequently used as the roof of buildings that have steep slopes to dispose of rainwater quickly. Their combination of high stiffness and lightweight nature lightens the load on the installation and the underlying building structures.

Corrugated tunnel and pipe

Large metal corrugated pipes or arches are frequently used in tunnel structures to transport the aggregate and ore across various points on their properties. The need to maximize the surface area on such sites necessitates the use of tunnels for transporting bulk materials under roadways and processing these materials. The application of corrugated pipes and arcs in these tunnels offers advantages in the design, installation and operation of these projects such as: reducing the design time and related costs; simplicity of construction which leads in to the reduction of installation and maintenance costs (Nol et al., 2009).

Corrugated pipes are often used in sewerage and drainage applications because of their light weight, high strength and compliance which lead into long life

performance. The strength of the pipes arises from the corrugated design of the outer wall rather than the wall thickness, in contrast to the normal solid wall pipes. The advantages of the corrugated pipes in general can be classified as their lightness and flexibility. The lightness of these structures reduces the manpower needed for installation and the costs of transportation whereas the flexibility reduces the damages during storage and handling and ease the natural settlements to be tolerated without suffering cracks or leakages (Corma.com, 2011).

1-3-3 Marine structures

The corrugated sandwich panel has offered a wide range of attractive design solutions to operational shipboard problems in which structural performance and weight are an important design issue. The applications of these structures include decks, bulkheads, helidecks and accommodation modules (Knox et al., 1998). Another application of the corrugated sandwich panels is in the combatant deckhouse structure of a naval ship since these structures show a good resistance to the possible blast loads (Liang et al., 2001).

1-3-4 Mechanical engineering structures

Corrugated hoses

Corrugated hoses are another case of important engineering structures which are exploiting from corrugation characteristics. Because of the special properties of the corrugation structure, these hoses can withstand very high pressure and provide maximum leak tightness. Corrugated hoses also exhibit corrosion resistance and pressure tightness under the most extreme conditions, such as aggressive seawater, extreme temperatures found in space and conveying very hot or cold substances. The other advantage of corrugated hoses is their flexibility which makes them a good candidate to connect elements where they are subjected to movement, thermal expansion and vibrations (Hachemi et al., 2011). Due to these characteristics they are frequently used in hydraulic circuits, protection for electrical cables and light conductors or exhaust gas installations.

Corrugated gasket

Surface configuration of the corrugated gaskets enables them to adapt to rough or irregular flange surfaces without requiring excessive compressive load. This provides an efficient seal under varying conditions of temperature and pressure. The substrate corrugation geometry promotes the recovery and resilience through thermal cycles and extended service life. Hence they are excellent products for both standard flange and heat exchanger gaskets where low bolt load are present or where high gasket stresses are available (Brown, 2002).

1-3-5 Aerospace and aeronautics application concepts

Corrugated sandwich panels are used in aerospace engineering because of their multifunctional characteristics. These structures offer insulation as well as load-bearing capabilities in addition to their lightness. These multifunctional integral thermal protection structures protect the spacecraft from extreme reentry temperatures, and possess load-carrying capabilities (Bapanapalli et al., 2006; Martinez et al., 2007). Moreover, because of their exceedingly anisotropic behaviour of these structures they have been proposed as a flexible skin for the wings of morphing aircraft. This is due to the fact that wing structures must be stiff so as to withstand bending due to aerodynamic forces, and flexible so they can deform efficiently in flight due to morphing actuation (Thill et al., 2010a). This application is explained exhaustively in section 1-6.

(a) Packaging
(http://www.gwp.co.uk/)

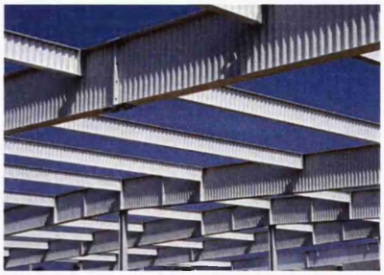

(b) Beams with corrugated web
(https://www.hera.org.nz)

(c) Corrugated roof and walls
(http://www.gulfcoastsupply.com)

(d) Corrugated tunnel
(http://www.robgalbraith.com)

(e) Corrugated pipe
(www.corrugatedsteelpipe.org)

(f) Corrugated hose
(http://processhose.com/)

(g) Corrugated bulkheads in ships
(http://www.nassco.com)

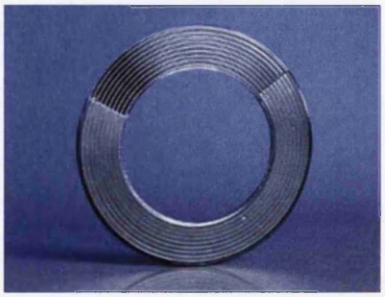

(h) Corrugated gasket
(http://www.klinger.co.za/)

Figure 1-2: Some applications of corrugated structures in engineering

1-4 Corrugated structures developments and concepts

As discussed so far, corrugated structures have noticeable impacts on the engineering applications due to their superior structural characteristics which mainly

arise from their geometric properties. However the structural performance of these structures is being developed further in the literature by introducing more geometric parameters or using different material properties. Some of the concepts regarding the development of these structures are reviewed in this section.

1-4-1 Innovation based on different material properties

Elastomeric face sheets

There are some specific applications of corrugated panels such as morphing skins (Thill et al., 2007) in which a change in material properties of the corrugated sandwich panel is considered. The corrugated core is coated with elastomeric face sheets. Although the geometry of this corrugated panel is similar to the corrugated sandwich panel the function is much different. This is because the stiffness of the elastomeric coatings is significantly smaller than the stiffness of the material of the corrugated core. The purpose of the elastomeric face sheets in this structure is not to increase the stiffness of the panel but to provide a continuous external surface to maintain the efficient aerodynamic performance during the flight (Yokozeki et al., 2006). More details of the mechanical behaviour of the corrugated core with elastomeric coating are presented later in this chapter. Figure 1-3(a) shows a corrugated core with elastomeric coating.

Core materials

Another way to increase the design space of the corrugated panel is by using composite materials in the corrugated core and consequently providing further improvement opportunities through optimizing parameters such as: fibre orientations in each layup, curvilinear fibres and textile architecture of the plain woven cloth of the fibres. The works of Kazemahvazi et al. (2009 (a, b)) in which they introduced a novel composite corrugation concept to prevent the core members from buckling, is highlighted. Another example in this perspective is the interesting idea of combining multi-stable characteristics with corrugated structural performance (Norman et al., 2007) in which the multi-stability comes from the interaction between internal prestressed laminates and non-linear geometrical changes during deformation. The multi stable characteristics enable the structure to undergo large configuration changes which can be sustained into the new position with no use of any locking

mechanism while the corrugation geometry provides the high strength to weight ratio. The wide range of parameters in such a structure enables designers to tailor the stiffness properties to the required application such as morphing wings. Figure 1-3(b) illustrates the twisted bi-stable corrugated core.

1-4-2 Innovation based on geometric parameters

Bi-directional corrugated-strip-core sandwich panel

A new concept in steel bi-directional corrugated-core sandwich structures was proposed by (Ray, 1996) to improve the stiffness in the more flexible direction of the panel and to modify the transverse shear stiffness of the panel. The geometry of the typical core can be obtained by propagating the corrugated strips in both longitudinal and transverse directions. Depending on the pattern of propagation a variety of different densities and stiffnesses may be obtained. Leekitwattana et al. (2011) proposed a derivation for the transverse shear stiffness of a steel bi-directional corrugated sandwich panel using analytical methods. Dayyani et al. (2011) simulated the mechanical behaviour of the bi-directional corrugated core with and without elastomeric coatings in tensile and five point bending tests. Figure 1-3(c) show a schematic of a bi directional corrugated core.

Furthermore, Seong et al. (2010) proposed another type of bi-directional corrugated core to reduce the anisotropic characteristics of the corrugated sandwich plates which could restrict the range of the applications of these structures. The design space in this bi-directional corrugate core was extended by introducing two additional geometric parameters, pass angle and corrugation length, in order to minimize the beam buckling of the face sheets with respect to core orientations. In this concept the continuous corrugated channels were first fabricated by using a sectional forming process and then the core was attached to face sheets by means of adhesive bonding. Figure 1-3(d) shows a schematic of this concept.

Hierarchical corrugated core sandwich panel concepts

Improving the transverse compression and shear collapse mechanisms of the corrugated panel, a novel concept based on the second order hierarchical corrugation was offered by Kooistra et al (2007) as shown in Fig. 1-3(e). The idea was born from

the fact that materials with structural hierarchy can have higher stiffness to weight ratio than their single-length scale of microstructure counterparts. Hence the local corrugated elements were introduced to postpone the elastic buckling of the webs of the main corrugated core. However, the manufacturing constraints and the relative high costs of production have limited the application of hierarchical corrugated cores to large sandwich structures. Kooistra et al. (2007) derived the analytical expressions for the compressive and shear collapse strengths of the hierarchical corrugated cores and validated their model predictions by comparing to the experimental data. They reported that the strength of a second order hierarchical corrugated sandwich panel is almost ten times greater than the first order corrugated structure of the same relative density.

Pyramidal lattice truss sandwich structure

The concept of lattice truss structures was proposed as an alternative to cellular core structures in the literature to further increase the ratio of strength to weight of sandwich panels (Wadley et al., 2003). The out-of-plane and in-plane mechanical properties of these lattice truss structures are dependant to the topology of the lattice, relative density and the stiffness properties of the core material. Queheillalt et al. (2008) proposed a new approach for manufacturing the uniform pyramidal lattice truss sandwich structure. In this method, first the solid corrugated sandwich panel was fabricated by extruding the aluminium slabs through the moulds and then the corrugated core was imposed by electro discharge machining (EDM) by use of alternating pattern of triangular-shaped EDM electrodes normal to the extrusion direction. The result of the process was a lattice truss sandwich panel in which the interface between the core and face sheet possessed the identical metallurgical and mechanical properties. Figure 1-3(f) shows the schematic of the extruded pyramidal lattice truss sandwich structure.

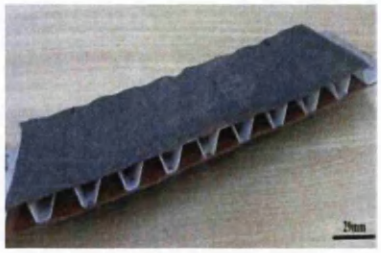

(a) Corrugated core
with elastomeric coating
(Dayyani et al. , 2013)

(b) Twisted bi-stable corrugated core
(Norman et al., 2007)

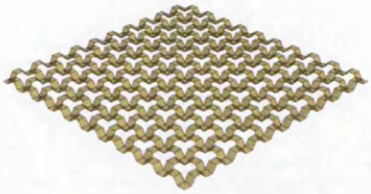

(c) Schematic of
bi-directional corrugated core
(Dayyani et al. , 2011)

(d) schematic of corrugated
bi directional core, Seong et al. (2010)

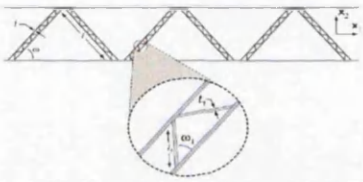

(e) Schematics of Hierarchical
corrugated core sandwich panel
(Kooistra et al., 2007)

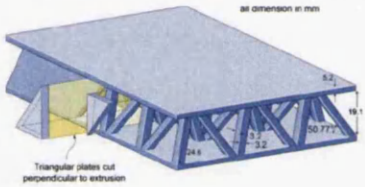

(f) Schematics of extruded pyramidal
lattice truss sandwich structure,
Queheillalt et al. (2008)

Figure 1-3: Corrugated structures developments and concepts

1-5 Mechanical properties of corrugated panels

The need to identify and manipulate the properties of a structure as a whole has led to the concept of different perspectives among designers. This is well known particularly in multidisciplinary projects where every discipline has a distinct set of concerns that require the use of knowledge in specific field of research. Despite the differences between each discipline which capture a specific design concern, they must interact consistently with each other in support of a common mission. This is important since the multidisciplinary design may greatly differ from the design of each single discipline. In order to use the corrugated panels in more complex applications such as morphing aircraft, a study which comprises interdependent resources of research such as knowledge and principles in each distinct discipline is essential. This ensures that all likely aspects of the state of problem are considered,

and integrated into a whole. In this regard investigation of mechanical behaviour of corrugated panels from different perspectives is being noticed in this section.

A comprehensive set of analyses about the flexural, tensile, shear and out of plane compressive strength of corrugated panels is developed in the literature by means of experimental and finite element analysis. These analyses have considered mainly the nonlinear effect of material properties and geometric parameters as well as analysis of various boundary conditions and loading configurations (Gilchrist et al., 1998). When possible in the literature, analytical solutions are introduced in support of these investigations (Lue et al., 1992).

1-5-1 Bending

Numerous studies have been conducted on the bending stiffness of corrugated board. These investigations have incorporated analytical solutions, finite element simulations or experiments to find the flexural rigidities of the board. Khalid et al. (2004) investigated the mechanical behaviour of structural beams with corrugated webs in three-point bending. They determined the effects of the corrugation curvature, web thickness, material properties of the corrugated web, and the corrugation direction on the beam's load-carrying capability. The experimental tests were used to validate the results obtained by nonlinear finite element analysis. The 30% difference in the flexural stiffness which was observed in the results highlighted the bending anisotropic characteristics of the composite beam with the corrugated web. It was reported also that increasing the radius of corrugation curvature led to higher bending stiffness and could reduce the beam's weight by about 14%.

Chang et al. (2005) presented a closed-form solution based on the Mindlin–Reissner plate theory to describe the linear flexural behaviour of the corrugated core sandwich plate with various boundary conditions. They reduced the three-dimensional sandwich panel to an equivalent two-dimensional structurally orthotropic thick plate continuum. They compared the numerical results of the proposed model by the experimental data available in the literature (Tan et al., 1989) and observed a good agreement. They investigated the effects of several geometric parameters of a corrugated core sandwich panel on its rigidity and state of stress and came up with some recommendations for the selection of the geometric parameters

of corrugated- core sandwich plates. These recommendations were mainly about minimizing the ratio of geometric parameters such: the ratio of the height to the thickness of the corrugated core, thickness of the corrugated core to thickness of the face sheet and the length of the corrugated unit cell to the height of corrugation. However such ratios resulted in an increase of weight of the structure and performing a multi objective optimization which considers both structural rigidities and mass of the structure is important.

Yokozeki et al. (2006) proposed a simple analytical model for the initial bending stiffness of corrugated composites in both longitudinal and transverse directions and compared the predictions with the experimental results. For the flexural modulus in the more complaint direction, they measured the deflection of one end of the corrugated core due to its own weight, while the other end of the corrugated sheet was clamped. Moreover, four-point bending load was applied to the specimens in the longitudinal direction where both ends of the corrugated core were fixed. Although the applied bending displacement was small, two modes of out of plane flexural deformation and in-plane tensile stretching were coupled. They highlighted the extremely anisotropic behaviour of the corrugated core through comparing the flexural stiffness of the corrugated sheet.

Seong et al., (2010) performed three-point bending tests on the bi-directional corrugated sandwich panels for various core orientations and demonstrated that this sandwich corrugated panel has a quasi-isotopic bending behaviour. They explained the effect of geometric parameters of the bi-directional corrugated core on the buckling strength of the face sheets during large bending deformations.

Dayyani et al. (2012) studied the flexural characteristics of a composite corrugated sheet using numerical and analytical methods and validated the results by comparing them to the experimental data. A good degree of correlation was observed in their work which evidenced the suitability of the analytical method and finite element model to predict the mechanical behaviour of the corrugated sheet in the linear and nonlinear phases of deformation. The finite element simulation exploited the node to surface and friction less contact technique, to model the interaction between the corrugated sheet and the supports. The force-displacement curves showed three distinct phases of deformation in the three-point bending test. Three phases of the

deformations were distinguished as: deformation due to pure bending of corrugated sheet, deformation due to combined bending and axial forces causing a step increase in the force-displacement curve and again deformation due to pure bending of the corrugated core. They reported that the second phase in which the step was observed arose because of simultaneous contact of the two adjacent corners of the corrugated unit cell with the support. Figure 1-4 illustrates the corrugated sheet in a three-point bending test and the corresponding force-displacement curves obtained from the experiment and simulation results.

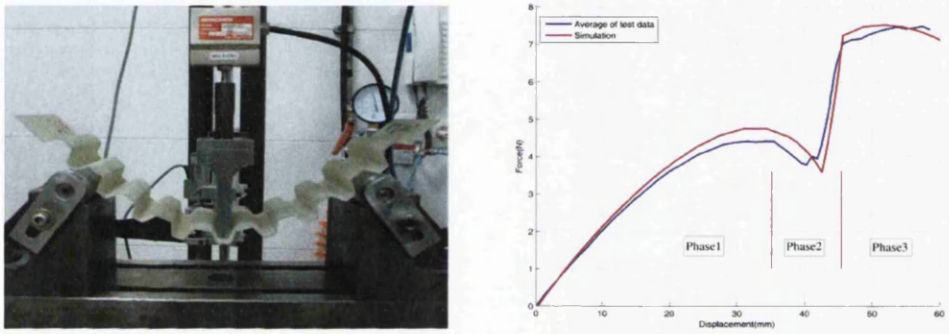

(a) Bending experimental set up (b) Force-displacement curves

Figure 1-4: Three-point Bending behaviour of a composite corrugated sheet, (Dayyani et al., 2012)

1-5-2 Tensile

Noting the extreme anisotropic stiffness properties of corrugated sheets (Yokozeki et al., 2006), Thill et al. (2007) investigated the effect of a variety of materials and parameters such as number of plies and corrugation pitch on the overall mechanical properties of the corrugated composite sheet. The output of this study was that the transverse tensile elastic modulus is dependent on the squared laminate thickness and the length of corrugated unit cell length. Three years later, they explained the obtained results via experimental, analytical and numerical analysis methods (Thill et al., 2010b). They considered trapezoidal corrugated aramid/epoxy laminates subjected to large tensile deformations transverse to the corrugation direction and highlighted the effect of local failure mechanisms of these specimens on the three stages of the tensile force-displacement graphs. They found out that the second stage, which comprised the majority of the displacement, occured because of aramid fibre compressive properties and delaminations in the corner regions of the corrugated

unit cell. This local phenomenon was compared to a pseudo-plastic hinge allowing large deformations over relatively constant stress levels.

As an extension to this work, Dayyani et al. (2012) studied the tensile behaviour of corrugated laminates made of plain woven glass/epoxy. Contrary to the literature they observed the occurrence of delamination in all of the members of the corrugated unit cell, not only to the corner regions, and evidenced that the three-stage mechanical behavior of composite corrugated core is not confined to aramid laminates and can be observed in other types of laminates. The tensile force-displacement curves in their experiment showed three distinct phases of deformation: 1-small deformations due to tension of both straight and inclined members, 2-rotation of joints at the intersection of straight and inclined members, 3-the tensile behavior of the flattened panel respectively. These three phases are shown in Fig. 1-5 where the tensile force-displacements are plotted. The plasticity was exploited in finite element simulation as a technique to model the delamination, which dissipated the strain energy of the system during the tensile testing. Assigning the plasticity to all of the regions of the corrugated unit cell resulted in a good agreement between the numerical predictions and the experimental observations. The extreme sensitivity of the composite corrugated sheet to the angle of the corrugated unit cell was also demonstrated in this work which highlighted the importance of the precision of the design and manufacturing process.

(a) Tensile experimental set up

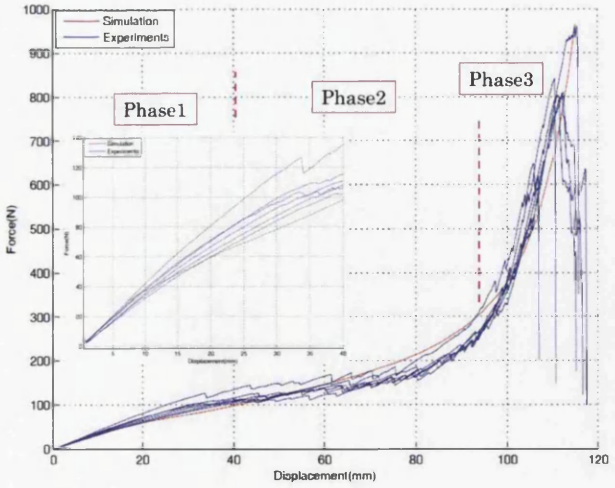

(b) Three distinct phases of the tensile force-displacement curves

Figure 1-5: The mechanical behaviour of the composite corrugated sheet in a tensile test, (Dayyani et al., 2012)

1-5-3 Shear and compression

Transverse shear stiffness of the corrugated sandwich panels is one of the important characteristics of these structures which must be accurately characterized in the performance analysis of these structures. Among the early works regarding this issue is the work of Nordstrand et al. (1994) who used curved beam theory to study the shear stiffness of a corrugated cardboard. They presented a theoretical study on how the geometry of the corrugation affects the transverse shear moduli. Firstly by assuming rigid face sheets in the corrugated cardboard they derived an upper limit of the transverse shear modulus across the corrugations and then showed how this shear stiffness reduces if deformations of the face sheets are considered in the analysis. Nordstrand and Carlsson (1997) experimentally examined the effective transverse shear moduli in the principal material directions of corrugated board using the block shear test and the three-point bend test. They observed that the shear moduli obtained by the three-point bend test were almost half of those determined by the block shear test. This discrepancy was explained by local deformation of the face sheets of the board where they were in contact with the supports in three point bending test.

Isaksson et al. (2007) considered a panel of corrugated paper board as a stack of an arbitrary number of thin virtual layers with corresponding effective elastic moduli. The elastic properties of all layers were assembled together to analyze a corrugated board as a continuous homogenous structure. They showed that exploiting the shear correction factors which were derived from the equilibrium stress field can improve the stiffness calculations. Their proposed model was validated by experiments on corrugated board panels with different geometries.

Kampner et al. (2008) investigated the possibility of using a corrugated sheet as the facings of sandwich beams to carry shear loads which are traditionally carried by the core. A compliant foam core was used as a ''cushion" between the outer skin and the internal structure in their concept. One of the main reasons for such concept was improving the performance of the panel under shock loads where stiff connections between the facings were prone to localized failure. Finite element simulations, as well as some analytical investigations were used to find out that the introduction of a

corrugated face sheet improved the capability of shear carrying and reduced the weight of the panel, predominantly for heavily loaded sandwich beams.

Leekitwattana et al. (2010) took into account the concept of a force–distortion relationship to derive a formulation for the transverse shear stiffness of a bidirectional corrugated sandwich panel by use of the modified stiffness matrix method. They showed the consistency of the proposed formulation with a three-dimensional finite element solution. The computation time for the proposed method was claimed to be 40 times lower than the FE method. They assessed the effect of geometrical parameters and compared the performance of a bi-directional corrugated sandwich panel with other one directional corrugated sandwich panels. They realized that for a specific range of parameters the bidirectional corrugated topology shows superior performance in transverse shear stiffness.

Lu et al. (2001) investigated the compressive response and failure mechanisms of a corrugated sandwich panel by use of a combined theoretical and experimental approach. In this work, the corrugated specimens were modelled by use of curved beam elements and surface contact elements. The elastoplastic material was tuned with a bi-linear constitutive model which satisfied the J_2-flow theory and assigned to the finite element model. The effects of boundary conditions, geometrical parameters, and material properties, and geometrical imperfections on the compressive strength of corrugated boards were studied. As a result, they found out that the panel has the highest compression strength when the initially sinusoidal corrugated core deforms into a square wave pattern. Moreover, it was shown that the stress-strain curves of the corrugated panel had an undulating behaviour in compression, which reflects the initiation, spreading and arrest of the localised plastic collapse mechanisms.

Rejab and Cantwell (2013) investigated a series of experimental and numerical analyses on the compression response and subsequent failure modes of the corrugated core sandwich panels which were made of three different materials: aluminium alloy, glass fibre reinforced plastic and carbon fibre reinforced plastic. Particular attention in this work was paid to the effect of the number of unit cells and the thickness of the cell walls in determining the overall deformation and local collapse behaviour of the panel. They realized that the buckling of the cell walls was

the first failure mode in these corrugated structures and increasing the compression loading will result in localised delamination as well as debonding between the skins and the core. The experimental results were compared to finite element and analytical solutions. The predictions offered by the numerical models were in good agreement. However the analytical model over-estimated the load-bearing capability of the corrugations due to the fact that the model assumed perfect bonding between the apex of the corrugated core and the skin and neglected the effect of initial imperfections along the cell walls.

As mentioned earlier, Kooistra et al. (2007) analysed the transverse compression and collapse mechanisms of a second order hierarchical corrugated sandwich panel. In contrast to a first order corrugated sandwich panel which exhibit two competing collapse modes of elastic buckling and plastic yielding, they showed that the second order corrugated panel has six competing modes of failure: elastic buckling and yielding of the larger and smaller struts, shear buckling of the larger struts, and wrinkling of the face sheets of the larger struts. Figure 1-6 shows the global and local failure modes of first order and second order corrugated sandwich panels in compression. Analytical expressions for the compressive and shear collapse strengths in each of these modes were derived and used to construct collapse mechanism maps for the second order corrugation models. They used these maps as a base for selecting the geometric parameters of second order corrugated panel to optimize the ratio of collapse strength to mass and validated the proposed model experimentally. They discovered that increasing the level of structural hierarchy does not lead to further enhancements in the stiffness of the corrugated core. In other words, for a given mass the first order corrugation exhibited slightly more stiffness than its second order counterpart suggesting that the hierarchical corrugated construction has applications in strength limited applications.

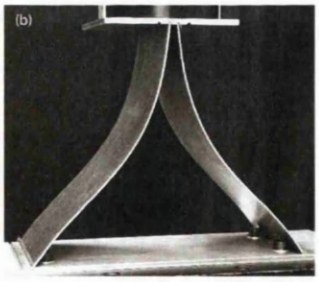

(a) First order corrugation unit cell, global elastic buckling mode

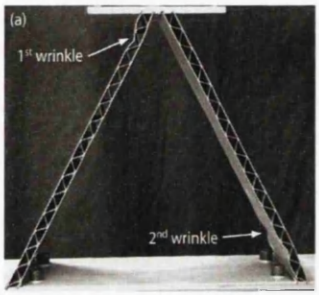

(b) Second order corrugation unit cell, local failure modes

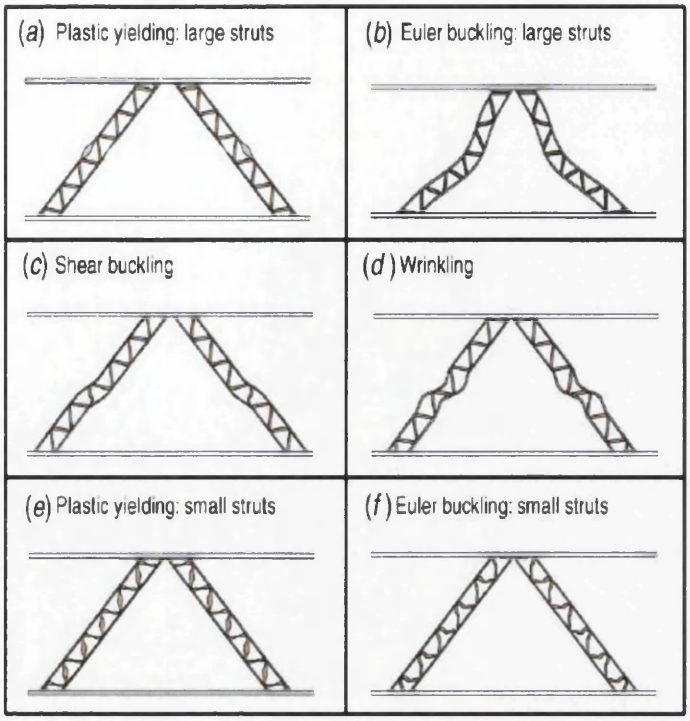

(c) Schematics of the failure modes in the second order corrugated unit cell

Figure 1-6: Global and local failure modes of first order and second order corrugated sandwich panels in compression, (Kooistra et al. 2007)

Likewise, the effect of hierarchy on the stiffness of corrugated structures in compression has been followed by other researchers such as Kazemahvazi et al. (2009). They applied sandwich panel with PMI foam to the local inclined members of the global corrugated core and experimentally studied a range of different failure modes of these structures depending on their geometrical and the material properties. In this regard, first the collapse mechanism maps of different corrugation configurations were analytically obtained (Kazemahvazi and Zankert, 2009). The stiffness model exploited the contribution in stiffness from the bending and the shear deformations of the local core members in addition to the stretching deformation. They claimed that the proposed hierarchical corrugated core can have more than 7 times higher weight specific strength compared to its monolithic counterpart, if designed correctly. The difference in strength arose mainly due to the increase in buckling resistance of the sandwich core members compared to the monolithic corrugated core. It was observed that when the density of the core increases, the

monolithic core members get thicker and more resistant to buckling and thus the benefits of the hierarchical structure reduces.

1-5-4 Buckling

Buckling occurs when a structure makes a rapid change of configuration due to applied load - this applied load may be compression, shear or multi-axial. A structure is often said to have failed when buckling occurs (for example when a column collapses under axial compression), and in these cases all that must be understood is when the onset of buckling will occur, which is usually a linear problem that can generally be achieved through classical analytical methods or using finite element analysis. However, in certain cases (such as in-plane shear buckling of a panel) some stability remains after buckling, and this so called post-buckle strength may be exploited. The study of post-buckling is often more complex than that of buckling, and the complex deformations formed during buckling often require the use of nonlinear analysis.

One of the most common methods to analyse buckling of corrugated plate or shell structures is to use a model to homogenize the corrugation as an orthotropic panel, and then to find global buckling modes using analysis similar to conventional panels. Many examples of this approach are presented subsequently. Although a variety of homogenization methods exist, an FEA unit cell may be used to derive the equivalent properties if an analytical process is not available.

Moreover it is usually possible to make further checks on corrugated structures especially for the configurations which have flat sections, such as trapezoidal corrugations. However, this approach cannot be applied in a straight forward manner to continuous profiles e.g. sinusoidal corrugations. If it is not feasible to simply check local and global modes separately, or greater accuracy is required, higher fidelity analyses must be used. Clearly, Finite Element methods have a broad role to play, however other higher fidelity methods exist. Liew et al. (2006) used the mesh free Galerkin method to analyse the buckling modes of a plate in. This method was an alternative to FEA analysis, with the advantage that it could avoid certain problems with element distortion. Pignataro et al. (2000) used a finite strip method, with nonlinear kinematics, to study in detail the situations where the global mode interacts with local modes to create a localised region of buckling in the post buckled

shape, and reduce the critical load. The work also considered how these interactions led to sensitivity to initial imperfections. It is discussed in following how deep-shell approaches were applied to locate both local and global modes (and interactions between them) that can be found with a single analysis.

Buckling of corrugated structures is widely discussed in the literature mainly in terms of the following applications: webs of beam sections, shell structures, naval structures, and the packaging industry.

Buckling of corrugated webs for beam sections

Corrugations have been widely used in I-beams as webs as shown in Fig. 1-2(b). The purpose of the web in an I-beam serves to resist shear force, so shear is the primary cause of buckling in these cases. It seems that much of the current literature on shear buckling of corrugations has been driven by this application. An early work in this field is given by Libove (1973), where it is briefly demonstrated that shear effects may be important in the analysis, and that therefore homogenized equivalent orthotropic approaches may have poor accuracy. The work then goes on to develop a shell model approach, giving expressions for the total potential energy that can therefore be used in variational analysis to find the buckling modes. The model uses nonlinear Von-Karman strains in the local material, with shear effectively accounted for in the global deformation.

However, assumedly due to the complexity of the model given, later works have adopted an approach using the equivalent orthotropic properties. Elgaaly et al. (1996) discussed the global shear buckling of corrugated panels in terms of equivalent homogeneous properties. Their formula for the global buckling mode's critical shear stress has been cited by many authors since:

$$\tau_c = 36\beta \frac{D_y^{1/4} D_x^{3/4}}{tl^2} \tag{1-1}$$

where D_x and D_y were the equivalent orthotropic flexural rigidities in the x and y directions respectively, t was the thickness and l was the length of the panel along the corrugation channels. β was a constant, between 0 and 1.9 depending on boundary conditions.

At a similar time, Luo and Edlund (1996) presented numerical analysis of both buckling and post buckling under shear force applied to a beam with a trapezoidally corrugated web. It was noted that three types of buckling may occur; local buckling (of a single flat section within the corrugation), global buckling (where the entire panel fails) and 'zonal' buckling, which was similar to a local mode but could extend over more than one panel. The nonlinear results were compared to some earlier analytical models for shear buckling, which were shown to have only approximate accuracy.

Yi et al. (2008) presented a work that focussed on the 'zonal' mode, although they refered to it as the 'interactive' mode. They compared it to a range of previous analytical formulas in previous literature, which were all of a form similar to

$$\frac{1}{(\tau_I)^n} = \frac{1}{(\tau_L)^n} + \frac{1}{(\tau_G)^n} + \frac{1}{(\tau_Y)^n} \tag{1-2}$$

Where τ_I is the resulted stress due to interactive buckling mode, τ_L is the local buckling failure stress, τ_G is the global failure stress and τ_Y is the yield stress of the material and n is an integer between 1 and 4 depending on the model used. Inspecting the form of this equation shows that if the critical mode of failure (as appearing in the terms on the right) is much lower than the others, it will dominate the overall interactive mode; however if the individual modes are similar, the resulting interactive failure will be lower than all of them. It is shown by comparison to numerical and previously published experimental data that these methods are approximately accurate, but require empirical corrections when operating near the yield limit of the material. Sause and Braxtan (2011) extended the work of Yi et al. (2008) with further comparisons to experiment, and further suggested corrections to allow for empirically found areas where the derived models were non-conservative.

Buckling of corrugated shells

Corrugations have been considered as a way of improving the stability of shells (Semenyuk and Neskhodovskaya, 2002(a;b)) provided a comprehensive analysis of these problems using deep shell theory. It was shown that under certain conditions, the use of corrugation on a cylindrical shell can substantially raise the critical buckling load. These papers presented some every intriguing possibilities for refined

analytical approaches to corrugations, because they did not depend on homogenised approaches, so that local buckling modes were calculated simultaneously with global effects. Furthermore, the shell approach used suggested that an adaptation to the curved surfaces of a true wing may be feasible, and maybe a further extension to include the effects of surface pressure along the lines of Semenyuk et al. (2007). The constraints of this approach would be a restriction to single layer geometries with smooth corrugation profiles.

Buckling of corrugated structures in naval applications

The American Bureau of Shipping regulations ABS (2004) include guidelines for the use of metal corrugated panels, and these are summarised and explained by Sun and Spencer (2005). The overall approach is to separately consider buckling cases of in plane shear (as discussed in the above section) and compressive loading in both directions and also lateral pressure, and combine them so that a safe design is defined by

$$\left(\frac{\sigma_x}{\eta\sigma_{xc}}\right)^2 + \left(\frac{\sigma_y}{\eta\sigma_{yc}}\right)^2 + \left(\frac{\tau}{\eta\tau_c}\right)^2 < 1 \qquad (1\text{-}3)$$

where η is a strength knock down factor. These results are shown to be reasonably conservative in comparison to FEA. This work also includes a formula to consider buckling in the corrugation caused by lateral pressure; at present it has not been possible to view the original source of how this was derived, but the final form appears to be that of a local buckling mode. However, accuracy is again reliant on empirical factors so this may not be directly applicable to morphing applications.

Buckling of corrugated panels in packaging application

Many treatments of corrugation come from the packaging industry due to the widespread use of corrugated cardboard, and this provides some valuable data. Indeed, one of few publications to discuss buckling of corrugations where the material is not isotropic is given by Biancolini and Brutti (2003), in a study of the ability to stack boxes on one another. This work extends equivalent stiffness formulae for sinusoidal corrugations found by Briassoulis (1986) to allow an

orthotropic source material, and uses these to calculate the global buckling load. However, further buckling modes are neglected.

In a study on corrugated board, where the effects of the face sheets are included, Nordstrand (2004) looks at global buckling and post buckling in the presence of imperfections. The analysis is very clear, and could easily be adapted for the purpose of morphing. Johnson and Urbanik (1989) provide analysis of a similar structure in, with an approach that can be potentially be adapted to any prismatic structure; however their focus is on local buckling modes with the assumption that these initiate failure.

1-5-5 Homogenization and equivalent modelling

Over the last two decades, homogenisation-based modelling techniques have attracted considerable attention within the computational mechanics community (Michel et al., 1999, 2002; Pellegrino et al., 1999; Suquet, 1993; Saavedra Flores and de Souza Neto, 2010). The importance and increasing interest in this area stems mainly from the ability of these techniques to capture the effective response of complex microstructures under a wide range of conditions. In such cases, the structural response has to be approximated to avoid the computational modelling of the corrugations and thus, circumvent the major drawback of excessive computing times. Often the loads are well distributed and only the overall deflections are required. If the dimensions of the whole corrugated panel are much larger than the period of the corrugations, then a suitable approach is the use of homogenisation techniques, in which the corrugated panel is replaced by an orthotropic plate with equivalent stiffness properties (Yokozeki et al., 2006; Thill et al., 2010b; Xia et al., 2012).

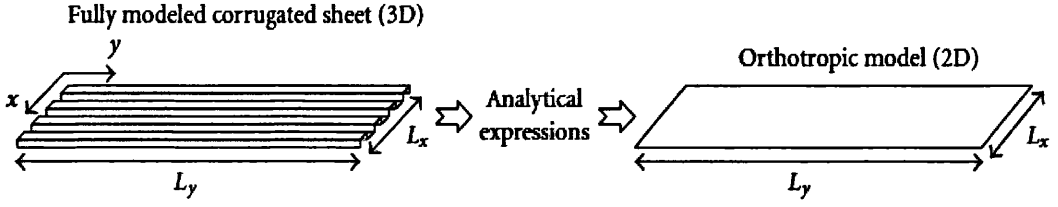

Figure 1-7: Schematic representation of a fully modelled corrugated sheet and its equivalent orthotropic model (Wennberg et al., 2011)

In homogenisation-based equivalent models, the effective response is calculated by means of a representative volume element (RVE) of material or structure. The RVE is such that its domain Ω has a characteristic length much smaller than that of the macroscopic continuum and, at the same time, is sufficiently large to represent the macroscopic mechanical behaviour in an averaged sense. Figure 1-8 shows the choice of a typical RVE of a corrugated structure.

Periodic boundary conditions are often adopted to model corrugated sheets. Periodic boundary conditions are typically associated with the modelling of periodic media. In this particular case, the RVE is a so-called unit cell whose periodic repetition generates the entire heterogeneous macrostructure (Saavedra Flores and de Souza Neto, 2010). Here, the fundamental assumption consists of prescribing identical displacement vectors u for each pair of opposite points, y_+ and y_-, of the RVE boundary domain $\partial\Omega$, such that, $u(y_+) = u(y_-)$.

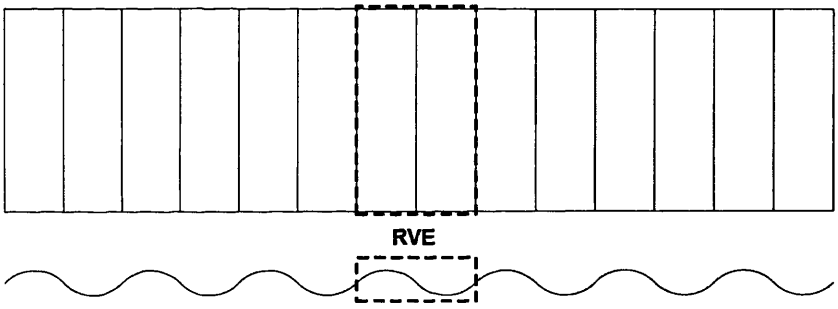

Figure 1-8: Typical RVE chosen for the modelling of a corrugated structure (Winkler, 1981)

In the context of modelling of corrugated panels, Briassoulis (1986) and McFarland (1967) investigated the equivalent flexural stiffness of sinusoidal and rectangular corrugations. Briassoulis (1986) studied corrugated shells on the assumption of thin and uniform thickness, and proposed new expressions for their equivalent orthotropic properties. McFarland (1967) investigated the static stability of corrugated rectangular plates loaded in pure shear. Dayyani et al. (2012) proposed numerical and analytical solutions for the modelling of composite corrugated cores under tensile and three-point bending tests. Their results revealed that the mechanical behavior of the core in tension is sensitive to the variation of core height.

Kress and Winkler (2010) and Winkler and Kress (2010) derived analytical expressions for an equivalent orthotropic plate with circular corrugations. Later, Kress and Winkler (2011) studied corrugated laminates by solving a set of six load cases under the assumption of generalised plane-strain. The first three cases correspond to in-plane loading states which are associated with extension along the x-direction ($\bar{N}_x$) and y-direction ($\bar{N}_y$), and shear in the xy-plane ($\bar{N}_{xy}$). Here, the x and y-axes are assumed to define the plane of the corrugated sheet. The other three cases correspond to out-of-plane loading states represented by bending along the x-direction ($\bar{M}_x$) and y-direction ($\bar{M}_y$), and twist out of the xy-plane ($\bar{M}_{xy}$). These six cases are independent and can be combined linearly to form any generic loading state as long as the superposition principle holds. This is generally true for linear analyses. Figure 1-9 shows the schematic representation of these six basic cases.

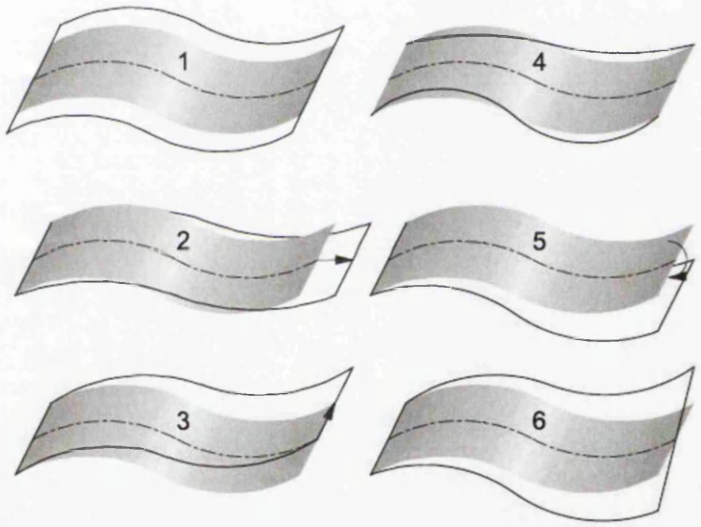

Figure 1-9: Six basic deformation mechanisms (Kress and Winkler, 2011)

By assuming that the mechanical response of the corrugated sheet can be established in terms of these six independent cases, the constitutive equation of the equivalent orthotropic plate is determined as (Xia et al., 2012)

$$\begin{Bmatrix} \bar{N}_x \\ \bar{N}_y \\ \bar{N}_{xy} \\ \bar{M}_x \\ \bar{M}_y \\ \bar{M}_{xy} \end{Bmatrix} = \begin{bmatrix} \bar{A}_{11} & \bar{A}_{12} & 0 & 0 & 0 & 0 \\ \bar{A}_{12} & \bar{A}_{22} & 0 & 0 & 0 & 0 \\ 0 & 0 & \bar{A}_{66} & 0 & 0 & 0 \\ 0 & 0 & 0 & \bar{D}_{11} & \bar{D}_{12} & 0 \\ 0 & 0 & 0 & \bar{D}_{12} & \bar{D}_{22} & 0 \\ 0 & 0 & 0 & 0 & 0 & \bar{D}_{66} \end{bmatrix} \begin{Bmatrix} \bar{\varepsilon}_x \\ \bar{\varepsilon}_y \\ \bar{\gamma}_{xy} \\ \bar{k}_x \\ \bar{k}_y \\ \bar{k}_{xy} \end{Bmatrix} \quad (1\text{-}4)$$

where $\bar{\varepsilon}_x$, $\bar{\varepsilon}_y$, $\bar{\gamma}_{xy}$, $\bar{k}_x$, $\bar{k}_y$ and $\bar{k}_{xy}$ are the strain components in the global coordinate system of the corrugated sheet associated with their corresponding force and moment components $\bar{N}_x$, $\bar{N}_y$, $\bar{N}_{xy}$, $\bar{M}_x$, $\bar{M}_y$ and $\bar{M}_{xy}$, respectively. In the above equation, the coupling terms between in-plane strains and out-of-plane loads have been ignored.

For the definition of each of the components $\bar{A}_{ij}$ and $\bar{D}_{ij}$ (with $i,j = 1,2,6$) in Eq. (1-4), several authors have proposed analytical expressions for different geometries of corrugation. Refer, for instance, to those expressions proposed by Samanta and Mukhopadhyay (1999), Xia et al. (2012), Ahmed and Badaruzzaman (2003), Briassoulis (1986), Yokozeki et al. (2006), Ye et al. (2014) and Seydel (1931), among many others.

One approach to implement the above constitutive laws Eq. (1-4), within a standard commercial finite element software is to uncouple the in-plane and out-of-plane mechanical responses. That is, for in-plane loading conditions we have the following constitutive equation

$$\begin{Bmatrix} \bar{N}_x \\ \bar{N}_y \\ \bar{N}_{xy} \end{Bmatrix} = \begin{bmatrix} \bar{A}_{11} & \bar{A}_{12} & 0 \\ \bar{A}_{12} & \bar{A}_{22} & 0 \\ 0 & 0 & \bar{A}_{66} \end{bmatrix} \begin{Bmatrix} \bar{\varepsilon}_x \\ \bar{\varepsilon}_y \\ \bar{\gamma}_{xy} \end{Bmatrix} \tag{1-5}$$

and for out-of-plane conditions we have

$$\begin{Bmatrix} \bar{M}_x \\ \bar{M}_y \\ M_{xy} \end{Bmatrix} = \begin{bmatrix} \bar{D}_{11} & \bar{D}_{12} & 0 \\ \bar{D}_{12} & \bar{D}_{22} & 0 \\ 0 & 0 & \bar{D}_{66} \end{bmatrix} \begin{Bmatrix} \bar{k}_x \\ \bar{k}_y \\ \bar{k}_{xy} \end{Bmatrix} \tag{1-6}$$

For an orthotropic sheet subject to in-plane loads, the following constitutive equation applies:

$$\begin{Bmatrix} \bar{\varepsilon}_x \\ \bar{\varepsilon}_y \\ \bar{\gamma}_{xy} \end{Bmatrix} = \begin{bmatrix} \frac{1}{E_x} & -\frac{\nu_{xy}}{E_x} & 0 \\ -\frac{\nu_{xy}}{E_x} & \frac{1}{E_y} & 0 \\ 0 & 0 & \frac{1}{G_{xy}} \end{bmatrix} \begin{Bmatrix} \bar{\sigma}_x \\ \bar{\sigma}_y \\ \bar{\tau}_{xy} \end{Bmatrix} \tag{1-7}$$

By comparing Eq. (1-5) with the inverse relation of Eq. (1-7), it is straightforward to obtain the following expressions for the in-plane equivalent mechanical properties. The Young's modulus along the x-direction (according to Fig. 1-7), that is, along the corrugation direction, is given by

$$E_x = \frac{\bar{A}_{11}\bar{A}_{22} - \bar{A}_{12}^{\,2}}{t\bar{A}_{22}} \tag{1-8}$$

and the Young's modulus along the y-direction is

$$E_y = \frac{\bar{A}_{11}\bar{A}_{22} - \bar{A}_{12}^{\,2}}{t\bar{A}_{11}} \tag{1-9}$$

where the parameter t is the thickness of the equivalent plate. Furthermore, the in-plane Poisson's coefficient is

$$\upsilon_{xy} = \frac{\bar{A}_{12}}{\bar{A}_{22}} \tag{1-10}$$

and the corresponding in-plane shear modulus is

$$G_{xy} = \frac{\bar{A}_{66}}{t} \tag{1-11}$$

On the other hand, for an orthotropic sheet subject to out-of-plane loading conditions, the following stress-strain expression applies:

$$\begin{Bmatrix} \bar{\sigma}_x \\ \bar{\sigma}_y \\ \bar{\tau}_{xy} \end{Bmatrix} = \frac{12}{t^3}\begin{bmatrix} \bar{D}_{11} & \bar{D}_{12} & 0 \\ \bar{D}_{12} & \bar{D}_{22} & 0 \\ 0 & 0 & \bar{D}_{66} \end{bmatrix}\begin{Bmatrix} \bar{\varepsilon}_x \\ \bar{\varepsilon}_y \\ \bar{\gamma}_{xy} \end{Bmatrix} \tag{1-12}$$

By comparing Equation (1-7) with the inverse relation of Equation (1-12) we obtain the following equivalent mechanical properties. The Young's modulus along the x-direction is

$$E_x = \frac{12\left(\bar{D}_{11}\bar{D}_{22} - \bar{D}_{12}^{\,2}\right)}{t^3\bar{D}_{22}} \tag{1-13}$$

and the Young's modulus along the y-direction is

$$E_y = \frac{12\left(\bar{D}_{11}\bar{D}_{22} - \bar{D}_{12}{}^2\right)}{t^3\bar{D}_{11}} \tag{1-14}$$

In addition, the in-plane Poisson's coefficient is

$$\nu_{xy} = \frac{\bar{D}_{12}}{\bar{D}_{22}} \tag{1-15}$$

and the corresponding in-plane shear modulus is

$$G_{xy} = \frac{12\bar{D}_{66}}{t^3} \tag{1-16}$$

With the above equivalent mechanical properties at hand, it is straightforward to introduce them in a commercial finite element program and model the corrugated geometry via a standard shell-type finite element without resorting to more computationally expensive modelling techniques.

As commented earlier, the previous modelling strategy relies on the linear combination of six independent cases, which is generally valid for linear problems. However, non-linear effects have also been investigated. Samanta and Mukhopadhyay (1999) performed non-linear geometric analyses on trapezoidal corrugated panels. They proposed an equivalent orthotropic model by taking into account both extensional and bending rigidities. Peng et al. (2007) investigated the equivalent elastic properties of sinusoidal and trapezoidal corrugated plates by means of a mesh-free Galerkin method. Liew et al. (2007) used this method for the geometrically nonlinear analysis of stiffened and unstiffened corrugated plates. Large deflection von Karman theory was adopted in the nonlinear analysis of the orthotropic plate. Both the equivalent flexural and extensional properties were employed in the analyses.

In the particular context of morphing wings, corrugated laminates represent an ideal solution for the design of morphing skins in adaptive aircraft structures. Yokozeki et al. (2006) developed a simple model for the in-plane stiffness of corrugated composites. They manufactured carbon fibre plain woven fabrics as candidates for flexible structural components. They tested them under tensile and bending loads in both in-plane longitudinal and transverse directions and their results

were compared with the analytical predictions. Thill et al. (2008b, 2010b) compared the homogenised plate properties for candidate morphing aircraft skins to experimental results by adopting the same procedure proposed by Samanta and Mukhopadhyay (1999).

1-5-6 Optimization

The design of corrugated structures can be improved significantly by implementing the optimization techniques in which the geometrical parameters and material properties of the structure play a dominant role. Some of the goals for the optimization may be represented as: minimizing the weight of the structure, maximizing the structural stiffness of the structure, postponing the buckling load of the structure as much as possible, and maximizing the distance between the natural frequencies of the structure and the excitation frequencies and maximizing the impact energy absorption. However the key question in the optimal design of these structures is the measure of what is desirable about a design. In practical applications, the design process is often measured with respect to multiple objectives which are often conflicting. In other words achieving the optimal value for one objective requires compromise on other objectives. In this case the goal may be to find a representative set of Pareto optimal solutions, and/or quantify the trade-offs in satisfying the different objectives, and/or finding a single solution that satisfies the subjective preferences of a human decision maker. In this section a review of the literature for the optimization of the mechanical behaviour of the corrugated structures is presented.

Liang et al. (2001) investigated the optimum design of metallic trapezoidal corrugated core sandwich panels subjected to blast loads by using a combined algorithm in which the Feasible Direction Method (Rao, 1996) was coupled with the Backtrack Program technique (Bitner and Reingold, 1984). A simple-beam theory and small-deflection plate theory were adopted to model the behaviour of the corrugated core sandwich panels. They considered a simply supported boundary condition for the panel and estimated the blast load by an equivalent static pressure. Geometric parameters such as: the corrugation leg, corrugation angle, face sheet thickness, core thickness and corrugation pitch were selected as design variables. The optimization problem was performed with the objective of minimizing the

weight of the corrugated sandwich panel with regards to explicit constraints arising from structure buckling and failure behaviour. Manufacturing limitations on the sizes or shape of corrugations were considered as implicit constraints. They realized that the corrugation leg, corrugation angle, core thickness and corrugation pitch were important design parameters for the core component with respect to buckling strength. For the face sheet with respect to axial stress, the corrugation leg and face sheet thickness were key design parameters.

Rathbun et al. (2005) implemented a general methodology for the design of the geometry of light weight sandwich panels. They considered several core topologies, such as: square-section truss members in pyramidal and tetrahedral configurations, square honeycombs and triangular corrugated sheets. Closed-form analytical solutions were proposed for the optimal design when the number of design parameters was up to three; however for a further parameter which was needed to fully characterize the corrugation geometry, they used numerical techniques. The geometric parameters they considered were: face sheet thickness, core thickness, height of corrugation and corrugation length. The four possible failure modes of the structure including face yielding, face buckling, core yielding and core buckling were represented as constraints in the optimization problem. Minimizing the weight of the structure for a prescribed load, a numerical procedure described by Wicks and Hutchinson (2001) was used. The results revealed that the four parameter optimization was kind of marginal benefit; i.e. leading to a design weight slightly lighter than that of the three parameters optimization. It was shown that the variations in the weights of the optimized panels were quite small in almost all cases, specifically in contrast to the weight of a solid panel. However for the case of a transverse corrugated core panel, the optimized weight was reported almost twice as heavy as the others. They concluded that other objectives or constraints, representing the manufacturing costs and prospect of multifunctionality must be considered in the optimization problem. The structural analysis, however should have been developed further to take to account the coupled effects arising from the anisotropy of the structure; i.e. different characteristics of longitudinal and transverse orientations.

Daxner et al. (2007) optimized the corrugated paper board with the purpose of attaining the maximum reduction in the area-specific weight of the structure in the

presence of bending stiffness constraints as well as local and global stability constraints. They considered only the geometrical parameters of the sinusoidal corrugated profile in the optimization (as shown in Fig. 1-10(a)) and studied the effective mechanical behaviour of the structure within the limits of linear shell theory by application of appropriate periodicity boundary conditions. Both isotropic and orthotropic material models were considered in their analysis; the corrugated board with isotropic material was analysed by a semi-analytical approach and for orthotropic material, the optimization algorithm was wrapped around a finite element model. Calculation of the critical loads with respect to local instabilities involved a minimization scheme within the optimization loop in order to find the critical buckling wavelength and the unit cell size was adjusted accordingly (Fig. 1-10(b)). In their analysis, the function 'NMinimize' in Mathematica was used with different optimziation techniques: Downhill-Simplex method and a genetic algorithm to solve the problem. The optimized results (as shown schematically in Fig. 1-10(c)) introduced a set of parameters describing a new design of corrugated board with the same buckling strength, but an area-specific weight which was reduced by more than 18% with respect to the original design.

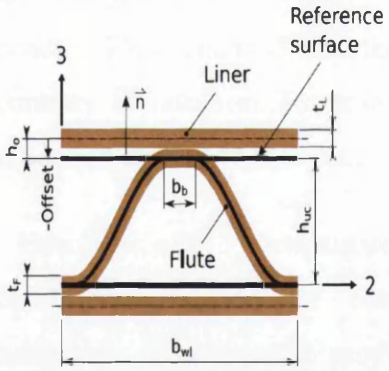

(a) Geometric parameters of optimization

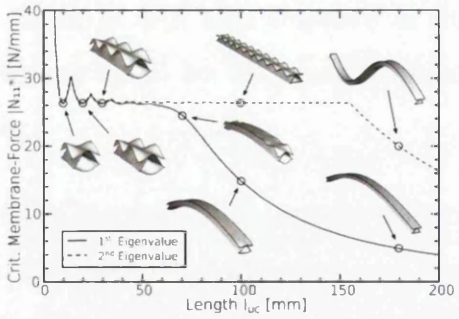

(b) Effect of variation of the unit cell length on the critical compressive membrane force

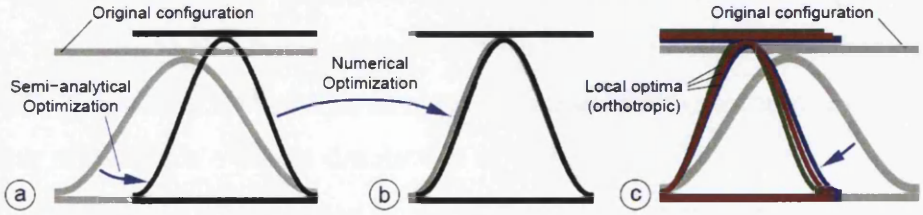

(c) The original and optimized geometry by the semianalytical optimization for isotropic material, best three designs for orthotropic material model

Figure 1-10: Optimum design of corrugated board under buckling constraints, Daxner et al. (2007)

Bapanapalli et al. (2006), proposed the corrugated sandwich panel as a candidate of the integral thermal protection system of the space vehicle from extreme aerodynamic heating, due to their heat transfer and load bearing capabilities. They developed an optimization problem as a part of the design process with the objective of minimizing the mass per unit area of the trapezoidal corrugated sandwich panel. The constraints were represented in terms of heat transfer and structural mechanics, such as: sustaining the face sheets temperature below certain limit and maintaining the structure far from the global and local buckling due to mechanical and thermal forces. The response surface approximations (Roux et al., 1998) of transient heat transfer and buckling analyses were constructed by use of finite element software, ABAQUS. The FE toolbox was a function called in the optimization process which was performed by use of fmincon command in Matlab. The optimized results showed that the corrugation webs should be as thin as possible in order to reduce the mass of the structure as well as the amount of heat entering the corrugated sandwich panel. In other words, they realized that the material for the corrugation webs should have a very low conductivity and high Young's modulus. They suggested that the conductivity of the webs can be decreased further by removing some material from the corrugation webs which will also reduce the weight of the corrugated sandwich panel. They claimed that the buckling capacity will also improve in this case, contrary to intuition. However, a disadvantage could be the shear stiffness of the sandwich panel which reduces considerably.

Hou et al. (2013) investigated the effects of the shape (trapezoidal and triangular configurations) and the corresponding geometrical parameters on the crash behaviour of corrugated sandwich panels. Two different types of impact loading were considered in their analysis: the low-velocity local impact and the global planar impact which were simulated using ANSYS Parametric Design Language (APDL) and LS-DYNA finite element software. The surrogate modelling method (Forrester et al., 2008) was used as an approximate modelling technique to mimic the behaviour of the finite element simulations as closely as possible, while reducing the cost of computations. For the case of low velocity local impact, the corrugated core with both trapezoidal and triangular corrugation profiles was optimized with the purpose of maximizing the energy absorption (internal energy) of the structure. However for the case of global planar impact, a multi-objective particle swarm

optimization (Mostaghim et al., 2003) was performed with the objectives of maximising the internal energy and minimizing the peak crushing force. The comparison of two optimal configurations with the identical face sheet thickness and core density showed that the triangular configuration has better crashworthiness performance.

1-6 Corrugated skin for morphing wing

Improving the performance of an aircraft is important for a variety of reasons such as: reducing the energy consumption, decreasing the toxic emissions and noise pollution or increasing the maneuverability of the aircraft (Argüelles et al., 2001; European Commission., 2011; Barbarino et al., 2011). The problem with current traditional aircraft is that they cannot be optimized for every single point of the flight envelope (Chekkal et al., 2014). Hence, a new generation of the aircraft, known as Morphing aircraft, is needed to overcome this problem. Morphing aircraft have the ability to adapt their shape in flight so as to always match the optimal configuration. Three major types of the morphing deformations which can be envisaged for an aircraft wing maybe classified as: planform alteration involving span, chord, and sweep changes; out-of plane transformation including twist, dihedral/gull and spanwise bending; as well as aerofoil adjustment such as camber and thickness alteration. However, the requirements of morphing aircraft are conflicting. For instance the design of a proper skin is a huge challenge and a key issue. The skin must be stiff to withstand the aerodynamic loads, but flexible to enable the expected large shape changes.

1-6-1 General requirements of the corrugated skin for morphing wing

A variety of possible materials and structures such as: elastomer matrix composites and auxetic materials are suggested as morphing skins in the literature (Thill et al., 2008a). Among the potential candidates mentioned in the literature, corrugated cores have exceedingly anisotropic behaviour; they are stiff along the corrugation direction, but flexible in the transverse direction. Yokozeki et al. (2006) demonstrated the use of corrugated composite sheets as a candidate material for flexible wing skins. As mentioned earlier, the mechanical properties of the corrugated sheets obtained by experiments were presented and followed by a simple

analytical model. They proposed the use of stiff rods within the corrugated skin in the longitudinal direction to increase further the anisotropy of the skin and suggested the use of elastomeric coating to maintain the smooth aerodynamic surface of the skin.

However the optimal design of these structures requires high-fidelity models of the coated corrugated skin to be incorporated into multi-disciplinary system models. Hence numerical and experimental investigations were required which maintain the dependence on the nonlinear static and dynamic behaviour of these structures. Dayyani et al. (2013) noticed this necessity and studied the nonlinear effects of the elastomeric coating and the mechanism of deformation of the composite corrugated core. They performed a series of experiments such as: static and cyclic tensile tests on the standard samples of composite laminates and elastomeric strips; static and cyclic tensile tests on the composite corrugated skin with and without elastomeric coating and three–point bending test on the coated corrugated skin. More details on the experimental setups of this work are presented later in chapter 2. The linear stress–strain curves of the glass fibre laminates demonstrated the high stiffness of corrugated core. The large elastic deformation capacity of the elastomers was also demonstrated; the elastomeric specimens stretched 1.5 and 3.3 times over their original length in longitudinal and transverse directions respectively. Figure 1-11 shows the tensile and flexural behaviour of the coated corrugated skin obtained by experiment and FE simulations. The tensile behaviour of the coated corrugated skin, i.e. the three stages of the deformation mechanism with respect to the function of the elastomer coating was discussed before and after the failure of the corrugated core. In terms of the flexural behaviour of the coated corrugated skin, they realized that the elastomer coating functioned as springs that undergo only tension. In other words the elastomer coating resisted the gap opening between two adjacent corners of each unit cell of the corrugated core. Because of the membrane function the elastomer coating showed, the other elastomer coating, which was subjected to the compressive forces, wrinkled and caused a non-smooth surface for the skin during bending. This was maybe the main drawback of the corrugated skin for maintaining the aerodynamic performance as high as possible. However they suggested two concepts to deal with this drawback: pre-stretching the elastomer coating and a reentrant corrugated configuration.

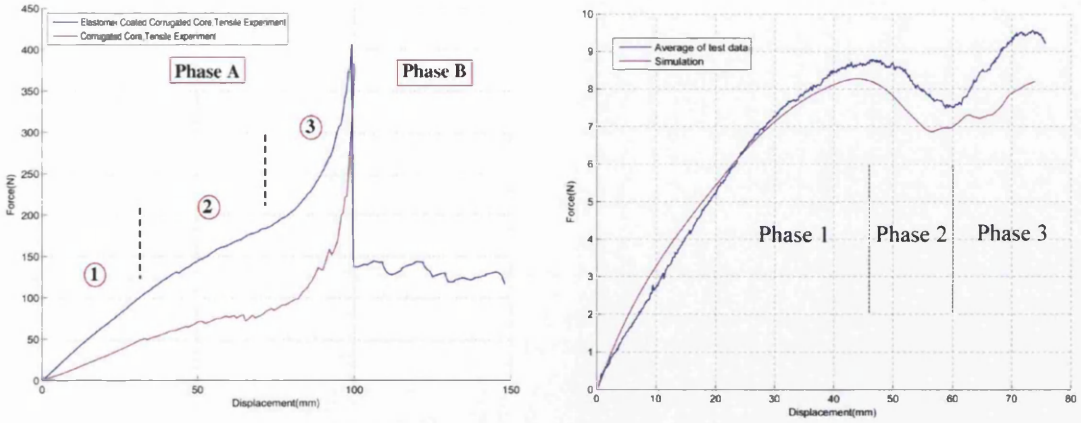

(a) Tensile properties of the corrugated core with and without elastomeric coatings

(b) Bending force-displacement behaviour; experiment and simulation

Figure 1-11: Experiments and FE simulations of the coated corrugated skin in tensile and bending tests, (Dayyani et al., 2013)

Structural components which are subjected to cyclic loading may yield due to fatigue, causing them to fail at stress levels lower than static mechanical loading. The cyclic loading behaviour of composite corrugated skin for morphing applications, where the source of cyclic stresses may be the aerodynamic flow over the skin or the actuator, is important. In this regard, Dayyani et al. (2013) investigated the cyclic loading behaviour of the corrugated skin with and without elastomeric coating before and after the elastic limit and compared the energy dissipation in each case. It must be mentioned that the authors of this paper interpreted the load at which the delamination cracks initiated and started dissipating the strain energy of the structure as the elastic limit. They observed the Mullins effect (Diani et al., 2009) in the elastomer coatings even before the elastic limit of the corrugated skin, because of the microscopic damage which resulted in considerable energy dissipation in the elastomeric coatings.

However the optimal design of these corrugated skins requires simple models of the structure to be incorporated into multi-disciplinary morphing system models. Therefore equivalent structural modelling and homogenization techniques are required to retain the dependence on the geometric parameters and material properties of the coated corrugated skin, while reducing the cost of computations.

1-6-2 Corrugated skin for different morphing applications

To the knowledge of the author the investigations for the application of the corrugated skin is so far limited to the camber morphing, winglet morphing and span wise morphing extension. Although each of these applications have their own specific boundary conditions, structural and aerodynamic loading configuration as well as the geometric and manufacturing constraints; the corrugated skin shows these two main characteristics in common: highly anisotropic behaviour and lightness. In addition the aerodynamic performance in all these applications is highly dependent on the corrugation geometry and Reynolds number. The aerodynamic performance however can be improved further if the corrugated skin is coated by pre stretched elastomeric face sheet, a segmented skin or used with foam slices filling the empty surface between the corrugated unit cells. On the other hand these solutions lead to increases in the mass of the structure. Hence any concept for modifying the performance of the corrugated skin should pass through the multi-objective optimization and multidisciplinary system level design. Low fidelity analysis in the first steps are necessary for these system level analyses and optimization, since they provide a feasible estimate of each design objective while keeping the computations efficient in terms of time and cost. This section reviews the literature of the corrugated skin with the given focus to camber morphing, winglet morphing and span extension morphing.

1-6-2-1 Corrugated skin in camber morphing

One of the effective ways to change the aerodynamic forces generated by a wing is through actively varying the aerofoil's camber, which allows for control of the aircraft flight path and optimization of the aerodynamic performance over different flight regimes. In addition to the fixed-wing applications, rotary aircraft have also followed the concept of the change in camber to postpone effectively the occurrence of stall and vibration control of the rotary blades. However, the concept of camber variation is not a recent novel achievement and has been traditionally been implemented through the use of discrete trailing edge flaps. Nevertheless, a smooth and continuous change in camber is still valuable in the aerospace industries to reduce significantly the drag and noise penalty associated with rigid flap deflections. A smooth and continuous change in the camber through a highly anisotropic skin can

also lead to a further reduction in the system complexity which decreases the mass of the structure and also the production and maintenance cost. In this section, the applications of the corrugated skin for camber morphing structures which are proposed in the literature are discussed.

Thill et al. (2010a) used composite corrugated sheets for the skin of the trailing edge of a NACA 0024 aerofoil section. Both cord wise extension and camber morphing deformations were considered for the trailing edge section which was about 35% of the 1 meter length cord. They used a simple scissor mechanism to extend the length of the cord and adjusted the manual camber deflections by use of locating pins. The skin was manufactured by attaching and filling foam into two corrugated laminates. Considering the manufacturing limits, the dimension of a corrugated unit cell was between 5-10 mm, which represented about 1% of the chord length for acceptable aerodynamic performance. Low speed wind tunnel testing and the open source code XFOIL as well as a two-dimensional computational fluid dynamics (CFD) panel method with viscous effects (Derla, 1989) were used to explore the limitations of these concepts. The Reynolds number and Mach number which were used in the analysis were about $2*10^6$ and 0.1 respectively, over a range of angles of attack for the NACA 0024 with morphing trailing edge. Figure 1-12 shows the trailing edge section of the morphing NACA 0024 aerofoil with a corrugated skin, as it is stretched up to 4% and deflected up to 12◦. The main problem of this concept was the lack of internal structure to support the skin against the aerodynamic and structural loadings. This problem caused the global buckling of the lower skin during the actuation, as it is subjected to compressive strains. The wind tunnel results highlighted a major increase in drag generation, when the morphing arifoil was compared to the conventional NACA 0024. To improve the aerodynamic surface of the skin, they suggested the use of discontinuous segmented composite laminates on top of the corrugated sheets.

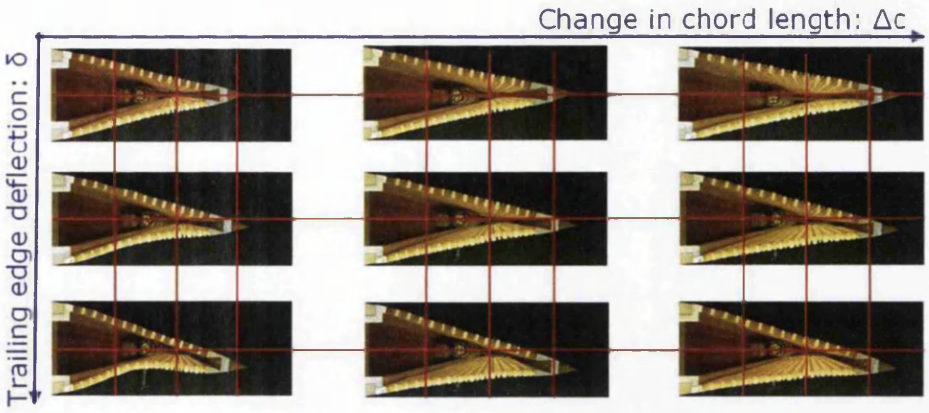

Figure 1-12: The trailing edge section of the morphing NACA 0024 aerofoil with corrugated skin, (Thill et al., 2010a)

Yokozeki et al. (2014) proposed a camber morphing aerofoil in which the corrugated sheet was used as the internal structure in the trailing edge section. The morphing section consisted of a circular corrugated structure and upper thin skin, both of which were made of carbon fibre reinforced plastic. The lower surface of the corrugated region was coated by a thin plastic sheet. The morphing section consisted almost 30% of the chord length, as shown in Fig. 1-13. Nonlinear finite element analysis was used to confirm the feasibility of the proposed morphing system in terms of actuation force and displacement. They developed a low speed (30 m/s) wind tunnel test for the camber morphing aerofoil (Wortmann FX63-137 baseline), inside which two servomotors were used as the actuation system to control the aerofoil shape by the chord-wise tension of the connected wires. The aerodynamic performances of the morphing and hinged mechanism wing were compared together and it revealed that the morphing model exhibited superior properties in lift coefficients. However the proposed concept had some restrictions as it limited the morphing deformation to downwards trailing edge displacement. Although this might be useful for "flaps" and low speed maneuvers such as take-off and landing, it is not suitable for higher speed maneuvers. In addition the unsmooth lower surface of the morphing trailing edge has considerable impact on increasing the generated drag.

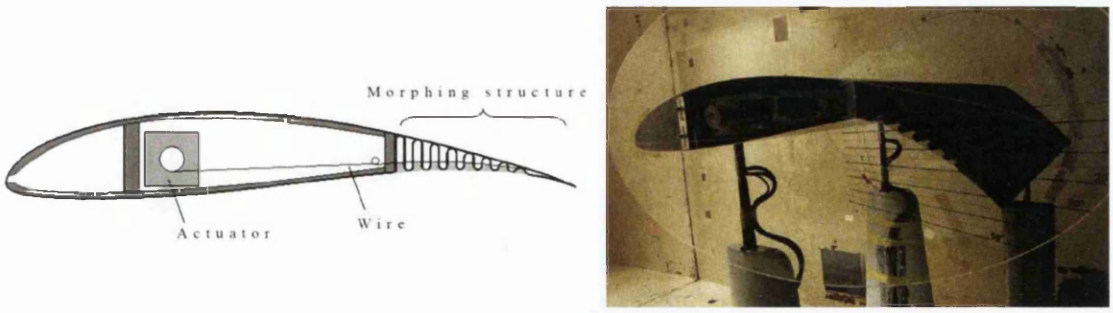

(a) Schematic representation (b) Wind tunnel testing

Figure 1-13: Camber morphing aerofoil with corrugated structure in the trailing edge, (Yokozeki et al., 2014)

As mentioned before the role of internal structure for the support of corrugated skin in the camber morphing deformation is very important. This is because the internal structure supports the skin against the aerodynamic loadings, structural shear and buckling loads and vibration. In addition the internal structure has a main role in enforcing the morphing trailing edge to move on the right path from the start point of the actuation to the desired destination. A further point of discussion of the role of the internal structure is the influence of the structure on the actuation energy required to morph, as the correct design of the internal structure can lead to minimizing the power required for actuation.

Furthermore the study of buckling in morphing concepts is important since the compression due to bending in the upper surface of a wing may lead to issue of buckling. Nevertheless the literature on the buckling of the corrugated skins in morphing applications is fairly light, specifically when the effect of the internal structure should be considered. Many of the key publications on morphing analysis or experimental work have briefly discussed buckling but give little detail on the methods used, for an unusual corrugation incorporating rigid stiffener sections. However it is possible that much of the work in literature with regard to buckling in general applications could be reapplied to the context of morphing corrugations, however the following modifications would be required:

- Allowance for the use of orthotropic materials instead of just isotropic materials.
- End conditions that are more applicable to a morphing structure, instead of a structure where the corrugation could be restrained by welded joints.

- Considering the orthotropic behaviour of the composite corrugated sheets as nearly all of the literature appears to lie in regions where failure is influenced by the yield strength of the isotropic material.

Shaw et al. (2015) investigated the optimization problem for the buckling loads along the spanwise direction of the wing. Weight, buckling performance, and actuation compliance of the corrugated skin were the three objectives. Classical buckling models with homogenised plate properties were used to derive the equivalent plate properties of the skin to obtain approximate estimates of the buckling loads. Figure 1-14(a) shows the trend of maximum loads with out-of-plane stiffness for optimal solutions for a variety of corrugation geometries. In addition to the global and local out-of-plane buckling modes of the skin, they observed the existence of a further buckling mode which occurs entirely in-plane. This unique in-plane mode was due to extreme anisotropic behaviour of the skin. As shown in Fig. 1-14(b), this mode affected deep, finely pitched corrugations where the transverse in-plane stiffness became less than the out of plane stiffness. Finite element analysis was used to evaluate the accuracy of the results obtained by the optimization method which exploited the equivalent methods.

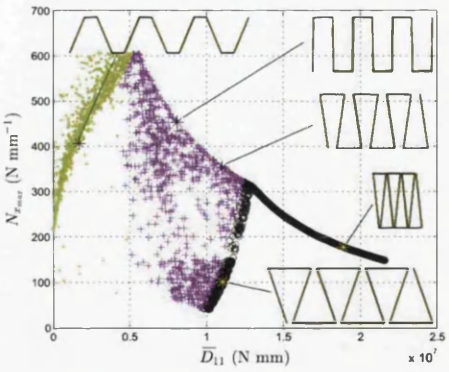

(a) Trend of max loads with out-of-plane stiffness for optimal solutions of a corrugation

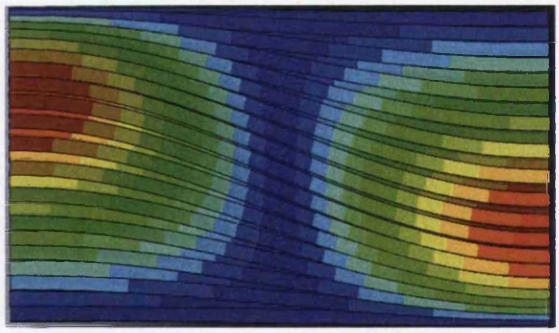

(b) In plane buckling mode of a corrugated skin subjected to compressive load in the vertical direction

Figure 1-14: Multi objective optimization of the corrugated skin with regards to buckling constraints, (Shaw et al., 2015)

The aerodynamic performance of the skin is perhaps the main challenge of the morphing wing. In this regard, Xia et al. (2014) investigated the 2D aerodynamic performance, particularly lift and drag characteristics of the NACA0012 aerofoil with unsmooth rigid corrugated surface. The effects of corrugation size and

Reynolds number were analysed and quantified experimentally and numerically in comparison to the standard NACA0012 aerofoil. They evidenced that the increase in the roughness of the surface i.e. increasing the corrugation size, had a negative impact on both lift and drag. In addition, the aerodynamic performance of corrugated aerofoils reduced at low angles of attack i.e. the lift-to-drag ratio decreased slightly as the Reynolds number was increased. They showed through CFD simulations how the local flow maintained an attached flow as eddies filled the corrugation troughs and smoothed the shape of the corrugated aerofoil, similar to flow around streamlined aerofoils. In particular, for a deformable trailing edge, the increased drag from the camber morphing skin is a trade off with the reduced drag obtained from avoiding the sharp changes in camber at the hinge mechanism which leads to flow separation.

1-6-2-2 Corrugated skin for winglet and span extension morphing application

In addition to camber morphing, there are some other effectiv ways to change the aerodynamic forces generated by a wing, such as through an actively varying winglet and wing span. Both these methods can control the aircraft performance over different flight regimes and can increase the range and endurance of the aircraft (Shelton et al., 2006). For example, the increase in the wingspan leads to a higher aspect ratio and wing surface; hence it results in a higher lift and higher lift to drag ratio in some aerodynamic configurations (Beaverstock et al., 2013). As a result, the range or endurance of the aircraft increases although the wing-root bending moment can increase considerably due to the larger span. Therefore both aerodynamic and structural characteristics of the aircraft should be investigated in the design of winglet and span extension morphing wings. Corrugated skins may be a good candidate for both concepts, when the corrugation profile is swept along the aerofoil, as shown in Fig. 1-15. The extreme anisotropic behaviour of the corrugated skin provides sufficient compliance for the actuation and increases the out of plane stiffness of the wing to withstand more aerodynamic and inertial loads. This is because of the combination of the global aerofoil curvature along the wing span and the local curvature of the corrugations. Furthermore, since the corrugation lines are along the flow direction the aerodynamic performance is less influenced than the camber morphing application. However from a structural perspective, the

combination of the global aerofoil curvature along the wing span and the local curvature of the corrugation makes the mechanical behaviour of the structure much more complex in contrast to the camber morphing application. Although the concept of the application of a corrugated skin in winglet and span extension morphing is attractive, little effort has been devoted to these concepts in the literature, maybe because of the complexity of the manufacturing method and the required 3D structural and aerodynamic analysis.

Ursache et al. (2008) presented a preliminary demonstration of a morphing wingtip with a corrugated skin in span wise direction, as shown in Fig. 1-15(a). One of the key challenges in the demonstration of the corrugated skin in the span wise direction is the special manufacturing process required to hand lay the composite laminates around the corrugated mould with air foil cross section. They preferred the plain woven Kevlar over other materials because of its ease of manufacture into corrugations and its special characteristics such as: lightness, good durability and impact resistance, as well as high stiffness and strength. Finite element simulation was performed to assess the mechanical behaviour of the corrugated skin while undergoing winglet morphing deformation. The FE results and the trends of the deformation showed some local instabilities of the skin and highlighted the need to update the model to enhance shape adaptability.

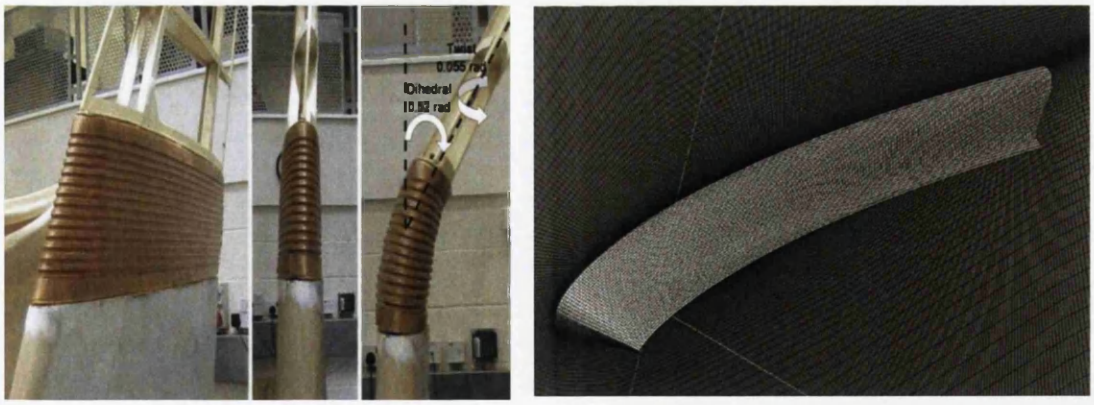

(a) Demonstration of morphing wingtip with corrugated skin in span wise direction, (Ursache et al., 2008)

(b) Structural and aerodynamic mesh of a half of a corrugated unit cell in span wise direction, (Fincham et al., 2014)

Figure 1-15: The application of corrugated skin in the span wise direction, winglet and span extension morphing

Xia et al. (2014) studied the feasibility of the concept of using a corrugated skin for a span extension morphing wing. The geometric parameters of the corrugated skin

were optimized to minimize the axial stiffness of the skin with respect to out-of-plane de`formation constraints. The equivalent structural properties of the skin were calculated by ANSYS APDL finite element simulation based on the global and local geometric parameters. They estimated the aerodynamic performance of the skin using the low fidelity aerodynamic solvers: Tornado Vortex Lattice Method (Melin, 2000) and XFOIL, in which the effect of camber thickness and airflow in corrugated channels were neglected. The results showed that the constraint on maximum out of plane displacement forced the optimizer to choose fewer corrugations in the span direction.

Fincham et al. (2014) noted the sharp leading edges generated in the span wise application of the corrugated skin and examined the low pass filtering and arc fitting for rounding of the leading edge to improve the aerodynamic performance. They examined the effect of corrugation wavelength and corrugation depth on the aerodynamic performance, in both 2D and 3D CFD simulations. They concluded that that corrugation wavelength has a minor effect in the aerodynamic efficiency of the wing in contrast to the corrugation depth which incurred a significant performance penalty. They emphasised that the aerodynamic penalty of the corrugated surface would be too large to be practical without some kind of compliant skin covering the corrugated surfaces.

1-7 A brief introduction of the thesis

Considering the detailed information about corrugated structures, as reviewed above, the purpose of this thesis is to provide further knowledge about the mechanical behaviour and design of the corrugated skins for application to morphing aircraft.

In the second chapter of this thesis, a simple equivalent analytical model for the mechanical properties of the corrugated skin with elastomer coating is proposed. Several experimental and numerical models are investigated to verify the accuracy and efficiency of the presented homogenized model. The importance of this chapter is that it provides simple models of the coated corrugated skin to incorporate into multi-disciplinary system models and further multi objective optimization studies.

In the third chapter, a generic super element of a corrugated core unit cell is investigated. The super element captures the small deformation of a 2D thin curved beam with variable curvature and is based
on an exact analytical equivalent model which avoids any homogenization assumption. The super element uses the geometric and mechanical properties of the corrugated skin as variables that may be applied for further topology optimization studies.

In the fourth chapter, the design of an elastomer coated composite corrugated skin for a camber morphing aerofoil is presented. The geometric parameters of the coated composite corrugated panels are optimized to minimize the in-plane stiffness and the weight of the skin and to maximize the flexural out-of-plane stiffness of the corrugated skin. The details of the multi-objective optimization of a trapezoidal corrugated core with elastomer coating are presented. It describes how Newton's aggregate method is selected to solve the optimization problem and the approach validated by comparing to the GA multi-objective optimization technique. The trend of the optimized objectives and parameters are discussed in detail. The obtained results provide important insights into the design of morphing corrugated skins. The advantages of the corrugated skin over the elastomer skin for a camber morphing structure are discussed and a finite element simulation of the internal structure with the corrugated skin is performed under typical aerodynamic and structural loadings to check the design approach.

In the fifth chapter, a conclusion to the results obtained in the previous chapters is presented and some suggestions for the future design of the corrugated skins in morphing applications are proposed.

Chapter 2:
Equivalent Models of Composite Corrugated Cores with Elastomeric Coatings

2-1 Introduction

The optimal design of the corrugated structures requires simple models of the panels that may be incorporated into multi-disciplinary system models. Therefore equivalent structural models are required that retain the dependence on the geometric parameters of the coated corrugated panels. Taking into account the geometric and mechanical properties of the coated corrugated panel, an analytical homogenization model is investigated in this chapter. The importance of this work is that it provides a simple equivalent analytical model which uses the geometric and mechanical properties of panel as variables that can be applied for further optimization studies. This is because the numerical modeling of composite corrugated sheets can be very expensive and time consuming if many corrugation periods are spanned or an actuation system and internal structure are involved. In this regard, two analytical

solutions to calculate the equivalent tensile and bending flexural properties of a coated composite corrugated core in the longitudinal and transverse directions are presented. Then different experimental and numerical models are investigated to verify the accuracy and efficiency of the presented equivalent model. The comparison studies demonstrate the suitability of the proposed method for application in further complex design investigations.

2-2 Analytical Homogenization Methods

In this section, two analytical solutions to calculate the equivalent tensile and bending flexural properties of a coated composite corrugated core in the longitudinal and transverse directions are presented. Fig. 2-1(a) shows a schematic of the corrugated core coated with elastomeric skins in tension. The panel is assumed to have periodic corrugations in the longitudinal direction only. The corrugation pattern consists of trapezoidal segments. The objective is to approximate the response of the coated corrugated panel using two longitudinal and transverse beam models whose properties are selected to be equivalent to those of the original panel. Since the ratio of the elastomer Young's modulus to the glass fibre Young's modulus is very small, a good assumption is to neglect the elastomer coating in the areas overlapped with the composite corrugated core. This assumption is reasonable because these two materials are well adhered together and have the same displacement. Thus the strain energy terms of the elastomer in contact with the glass fibre maybe neglected. Furthermore, since the out of plane and compression stiffnesses of the elastomer coatings are very low, they may be modelled as springs that undergo only tension. In other words their action resists the gap opening between two adjacent corners of each unit cell of the corrugated core. On the other hand since the structure is indeterminate in terms of loading in the longitudinal direction, the equilibrium and compatibility equations are used to find the force distribution in the elastomeric members. Then the whole structural stiffness of the panel is obtained using Castiglione's second theorem. Finally, the analytical solutions are compared to experimental and numerical results.

2-2-1 Longitudinal in plane stiffness

2-2-1-1 Problem definition

Fig. 2-1(a) shows a schematic of the constructed corrugated core coated with elastomeric skins in tension. The required parameters to define the geometry of the coated corrugated core are shown in Fig. 2-1(b)

(a) Periodic unit cells in tension (b) Sketch of unit cell

Figure 2-1: Schematic of the coated corrugated core in the longitudinal direction

2-2-1-2 Solution

To calculate the tensile displacement of the corrugated core, a unit cell of the corrugated core is considered as shown in Fig. 2-1(b). Since the unit cell is symmetric along the axis passing through the center of the unit cell, only one half of the cell is studied in the calculation. Considering the concept of periodicity and Saint-Venant's principle (Toupin, 1965) in the theory of elasticity, the global applied force F would pass through the neutral axis located at the center of the panel. In other words the eccentric local effect of the load becomes very small at sufficiently large distances from the load segment, where the external load is applied.

As illustrated in Fig. 2-2, in order to avoid dealing with the indeterminate loading configuration of the structure, half of the corrugated core unit cell is subdivided into two corrugated parts such that each has half of the original thickness of the structure. The idea is to calculate the stiffness of each subdivision and then add them together. Considering the nonlinearity in the formulation of the second moment of area with respect to the thickness, it is important to state that this parameter is calculated about the separating centre line of the original configuration, so that the total stiffness of the structure would be the same as the original configuration after the summation of these two substructures. Thus, from the parallel axis theory, $I_c$for the subdivided

corrugated core unit cell is calculated as: $\frac{4bt^3}{96}$. Where b and t denote the width and thickness of the corrugated core unit cell respectively. Moreover, because of the periodicity and symmetry, it is assumed in Fig. 2-2 that the nodes at the end of spring S_1 and the corrugated unit cell have equal displacement.

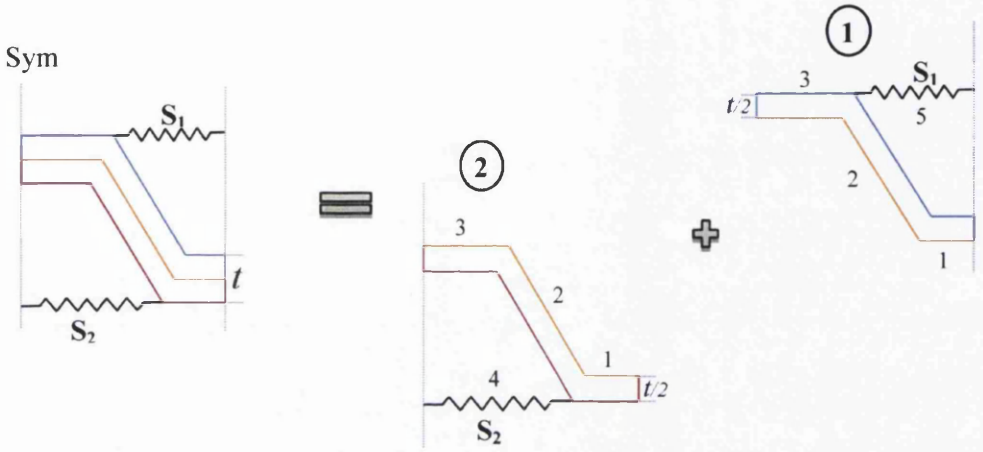

Figure 2-2: Subdivision of half of the corrugated core unit cell into two corrugated partitions in tensile solution

Figure 2-3 illustrates a schematic of the second substructure of corrugated core in tension. In this figure f_4, and M_R are the force from spring S_2, reaction force and reaction moment, respectively. According to Castigliano's second theorem in order to calculate the displacement at node P, the virtual force g must be applied to the structure at this node.

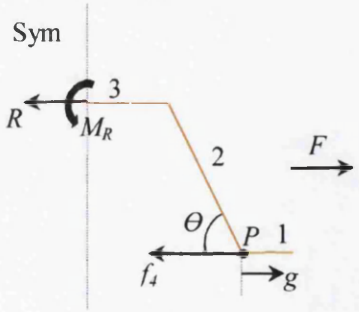

Figure 2-3: Schematic of the second substructure of corrugated core in tension

Therefore the strain energy of each member due to the bending moment and axial forces may be calculated as:

$$U_i = U_{i,A} + U_{i,B} \quad , \quad i = 1,2,3 \tag{2-1}$$

where:

$$U_{1A} = \frac{F^2 l_1}{2E_c A_c} \quad , \quad U_{1B} = \frac{F^2 h^2 l_1}{8E_c I_c} \tag{2-2}$$

$$U_{2A} = \frac{(F + g - f_4)^2 c^2 l_2}{2E_c A_c} \tag{2-3}$$

$$U_{2B} = \frac{1}{2E_c I_c}\left[(Fh/2)^2 l_2 - (Fh/2)(F + g - f_4) s {l_2}^2 + \frac{(F + g - f_4)^2 s^2 {l_2}^3}{3}\right]$$

$$U_{3A} = \frac{(F+g-f_4)^2 l_3}{2E_c A_c} \quad , \; U_{3B} = \frac{h^2((F/2)+g-f_4))^2 l_3}{2E_c I_c} \tag{2-4}$$

Here h, E_c, A_c and I_c represent the height, Young's modulus, cross section and second moment of area of the subdivided corrugated core respectively. Moreover c and s denote $\cos(\theta)$ and $\sin(\theta)$ respectively. Differentiating the strain energy of each member respect to this virtual force g, the displacement of each member would be obtained from following relations.

$$\delta_{iA} = \left.\frac{\partial U_{iA}}{\partial g}\right|_{g=0}, \quad \delta_{iB} = \left.\frac{\partial U_{iB}}{\partial g}\right|_{g=0} \quad , \quad i = 1,2,3 \tag{2-5}$$

By following a straight forward formulation and adding these terms, the total displacement would be expressed as:

$$\delta = \frac{(F - f_4)(c^2 l_2 + l_3)}{E_c A_c} + \frac{1}{2E_c I_c}\left[-\frac{Fh s {l_2}^2}{2} + \frac{2(F - f_4) s^2 {l_2}^3}{3}\right] + \frac{h^2 l_3((F/2) - f_4)}{E_c I_c} \tag{2-6}$$

Considering that the force in the elastomeric members are proportional to the applied structural load, i.e. $f_4 = \alpha_4 F$, the force displacement relation may be rewritten in the following form:

$$\delta = F\left[\frac{(1 - \alpha_4)(c^2 l_2 + l_3)}{E_c A_c} + \frac{-3hs {l_2}^2 + 4(1 - \alpha_4) s^2 {l_2}^3 + 6h^2 l_3 (1 - 2\alpha_4)}{12E_c I_c}\right] \tag{2-7}$$

Compatibility implies that $\delta = \frac{f_4 l_4}{E_e A_e} = \frac{\alpha_4 l_4}{E_e A_e} F$ for the elastomeric member, where $E_e$and A_e represent the Young's modulus and cross section of the elastomeric coating respectively. Therefore α_4 is obtained as:

$$\alpha_4 = \frac{\left(\frac{c^2 l_2 + l_3}{E_c A_c} + \frac{-3hsl_2{}^2 + 4s^2 l_2{}^3 + 6h^2 l_3}{12E_c I_c}\right)}{\left(\frac{c^2 l_2 + l_3}{E_c A_c} + \frac{s^2 l_2{}^3 + 3h^2 l_3}{3E_c I_c} + \frac{l_4}{A_e E_e}\right)} \tag{2-8}$$

Considering Fig. 2-2, and by repeating the same procedure for the first substructure of the half of periodic unit cell, α_5 is obtained as:

$$\alpha_5 = \frac{\left(\frac{c^2 l_2 + l_1}{E_c A_c} + \frac{-3hsl_2{}^2 + 4s^2 l_2{}^3 + 6h^2 l_1}{12E_c I_c}\right)}{\left(\frac{c^2 l_2 + l_1}{E_c A_c} + \frac{s^2 l_2{}^3 + 3h^2 l_1}{3E_c I_c} + \frac{l_5}{A_e E_e}\right)} \tag{2-9}$$

After finding the distribution of forces in the elastomeric members i.e. α_4 and α_5, the total mechanical behaviour of the second substructure of half of the unit cell would be calculated by adding the displacement of the first member as: $\delta_{1A} = F(\frac{l_1}{E_c A_c})$ and $\delta_{1B} = F\left(\frac{h^2 l_1}{4E_c I_c}\right)$. Therefore the force-displacement relation for the second subdivision of half of the unit cell would be obtained as:

$$\delta_{hu=} F\left[\frac{l_1 + (1-\alpha_4)(c^2 l_2 + l_3)}{E_c A_c} + \frac{3h^2 l_1 - 3hsl_2{}^2 + 4(1-\alpha_4)s^2 l_2{}^3 + 6h^2 l_3(1-2\alpha_4)}{12E_c I_c}\right] \tag{2-10}$$

Consequently the stiffness of the second substructure of half of the unit cell illustrated in Fig. 2-2 would be obtained as:

$$K_2 = \frac{1}{\frac{l_1 + (1-\alpha_4)(c^2 l_2 + l_3)}{E_c A_c} + \frac{3h^2 l_1 - 3hsl_2{}^2 + 4(1-\alpha_4)s^2 l_2{}^3 + 6h^2 l_3(1-2\alpha_4)}{12E_c I_c}} \tag{2-11}$$

In the similar way, the stiffness of the first subdivision of half of the unit cell would be obtained by replacing l_1 with l_3 and α_4 with α_5 in the Eq. (2-11) to give

$$K_1 = \frac{1}{\frac{l_3 + (1-\alpha_5)(c^2 l_2 + l_1)}{E_c A_c} + \frac{3h^2 l_3 - 3hs{l_2}^2 + 4(1-\alpha_5)s^2{l_2}^3 + 6h^2 l_1(1-2\alpha_5)}{12E_c I_c}} \tag{2-12}$$

Finally, the total stiffness of half of the corrugated unit cell is the summation of these two terms. Consequently the tensile stiffness of a panel consisting of N periodic unit cells would be: $\frac{(K_1+K_2)}{2N}$. On the other hand, the tensile force displacement behaviour for an equivalent beam with the same length of the panel is: $F = \frac{(AE)_{Eq_L}}{(2N)(l_1+l_2c+l_3)}\delta$. Therefore the equivalent longitudinal tensile modulus can be presented as:

$$(AE)_{Eq_L} = (l_1 + l_2 c + l_3)\,(K_1 + K_2) \tag{2-13}$$

2-2-2 Longitudinal out of plane stiffness

As mentioned before, since the out of plane and compression stiffness of the elastomer coatings are very low, it is assumed that they act like springs that undergo only tension. In other words, the role of the upper elastomeric coating which is subjected to tensile loading is modelled as springs resisting the gap opening between two adjacent corners of each unit cell of the corrugated core. The minor effect of the coating subjected to compression forces during the bending is neglected.

2-2-2-1 Problem definition

As illustrated in Fig. 2-4(a), the coated corrugated core is symmetric along the axis passing through the center of the panel. Hence only one half is considered in the analytical solution. Fig. 2-4(a) depicts the schematic of generic coated corrugated core which includes $N + 1$ unit cells in half of the span of the simulated three-point bending experiment. It is expected that the maximum gap opening in the structure, and consequently the maximum stretching of the elastomeric coating, happens at node $N + 1$ which is in the center of the panel. The more distance the marked nodes in Fig. 2-4(a) have from the symmetry line of the panel, the less gap opening and

consequently the less resisting force they would have. The idea here is to find a relation for the distribution of forces in the elastomeric members.

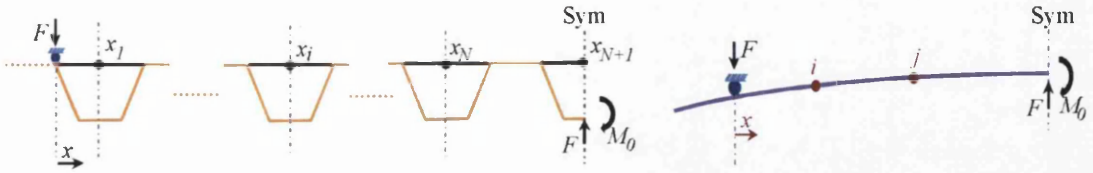

(a) coated corrugated core in longitudinal direction

(b) typical beam

Figure 2-4: Schematic representation of a coated corrugated core and a typical beam in three-point bending

2-2-2-2 Solution

In order to find the distribution of the forces in the elastomeric members and to avoid solving complex coupled multi equations of compatibility for these members, the Euler-Bernoulli beam in a three point bending test is considered as illustrated in Fig. 2-4(b). In this figure, for any two arbitrary points resting on a line parallel to the neutral axis, the ratio of their off axis strains in the x direction, are equal to the ratio of their coordinates, i.e.:

$$\varepsilon_i x_j = \varepsilon_j x_i \tag{2-14}$$

By assuming a displacement model for the corrugated structure based on an Euler-Bernoulli beam, and by analogy to Eq. (2-14), the force of the elastomer coating in each unit cell due to the gap opening is proportional to forces in the other cells. Thus it is assumed that the upper coating of the sandwich panel acts like a beam in three-point bending. That is, Eq. (2-14) is used here as an assumption to make a proportional relation between the forces of the elastomeric members and the one located in the center of panel. This relation can be stated as: $\frac{x_i}{x_{N+1}} = \frac{f_i}{f_{N+1}}$.

To see how valid this assumption is, the ratio of strains and in plane axial forces for the nodes marked in Fig. 2-4 (a) for 9 periodic unit cells, i.e. N=9, are calculated, tabulated and compared with FE results in Table 2-1. (More details of the FE simulation are presented in section 2-3-2.)

Table 2-1: Ratio of strains and stresses corresponding to nodes for the elastomeric members marked in Fig. 2-4(a)

(x_i/x_{N+1})	Coordinate ratios	FE Strain ratios	Error %
(x_1/x_{10})	0.0341	0.0346	1.47
(x_2/x_{10})	0.1414	0.1430	1.13
(x_3/x_{10})	0.2488	0.2520	1.29
(x_4/x_{10})	0.3561	0.3610	1.38
(x_5/x_{10})	0.4634	0.4700	1.42
(x_6/x_{10})	0.5707	0.5790	1.45
(x_7/x_{10})	0.6780	0.6880	1.47
(x_8/x_{10})	0.7854	0.7960	1.35
(x_9/x_{10})	0.8927	0.9050	1.38

The matrix form of the forces in the elastomeric members can be written as following symmetric matrix relation, in which $\mathrm{f_{el}}(ij)$ for $i,j = 1{:}(\mathrm{N}+1)$is the elastomeric force that the corners of the unit cells exert on each other, as shown in Fig. 2-5(b). Thus

$$\mathbf{f_{el}} = \mathrm{f_{el}}(ij) = \begin{cases} f\left[\dfrac{L_{np} + (i-1)L_{uc}}{L_{np} + NL_{uc}}\right] & , \quad i+1 = j \\ 0 & , \ i+1 \neq j \end{cases} \tag{2-15}$$

where L_{np} and L_{uc} are the length of non-periodic part and periodic unit cell respectively. Next, in order to determine the distribution of force in the elastomeric member located at the center of panel, i.e. f in Eq. (2-15) and Fig. 2-5(a), the displacement at node q is calculated first. In this regard, again according to Castigliano's second theorem, the virtual force g is applied to the structure at this node. Differentiating the strain energy of each member respect to this force, the displacement in each member can be obtained. As mentioned before the strain energy of each member is due to the axial force and bending moment:

$$U_{ij} = U_{ij,A} + U_{ij,B}\,, \qquad i = 1{:}\mathrm{N}+1 \ ; \ j = 1,2,3,4,5 \tag{2-16}$$

where the indices i and j denote the cells and members of each cell respectively, as shown in Fig. 2-5(b).

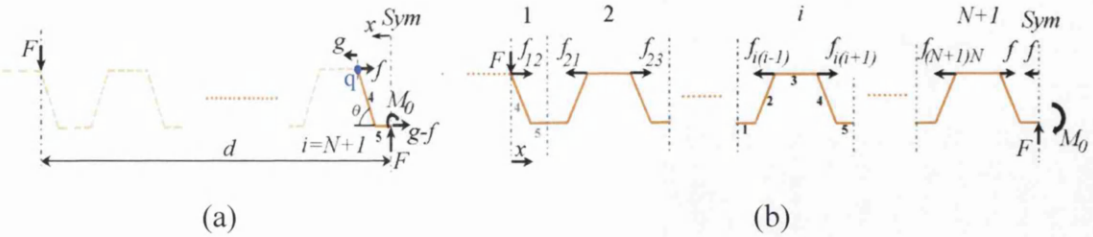

(a) (b)

Figure 2-5: Schematic of half of the coated corrugated core in bending

Considering equilibrium equations, the axial forces and bending moments of the illustrated members in Fig. 2-5(a), i.e. $i = N + 1$ and $j = 4,5$, are

$$T_{(N+1)5} = (g - f)$$
$$M_{(N+1)5} = F(d - x) + (g - f)h \tag{2-17}$$

where $d = L_{np} + NL_{uc}$ and represents half of the bending span, as shown in Fig. 2-5(a). By differentiating the obtained strain energy due to the axial forces and bending moments with respect to the virtual force, the relative displacement in each member is obtained. In Eqs.(2-18) to (2-22) the factor w has been introduced so as to keep the format of equations simple and clear. Thus

$$\delta_{(N+1)5_A} = f\left(-\frac{l_5}{\mathrm{E}_c\mathrm{A}_c}\right) = fw_1$$
$$\delta_{(N+1)5_B} = F\left(\frac{hl_5(d - l_5)}{2\mathrm{E}_c\mathrm{I}_c}\right) + f\left(-\frac{l_5h^2}{\mathrm{E}_c\mathrm{I}_c}\right) = Fw_2 + fw_3 \tag{2-18}$$

Likewise for the next member, i.e. $i = N + 1$ and $j = 5$,

$$T_{(N+1)4} = (g - f)c - Fs$$
$$M_{(N+1)4} = \big(F(d - l_5) + h(g - f)\big) - x\big((g - f)s + Fc\big) \tag{2-19}$$

and for the tensile axial and flexural displacement:

$$\delta_{(N+1)4_A} = F\left(-\frac{l_4 cs}{\mathrm{E}_c\mathrm{A}_c}\right) + f\left(-\frac{l_4 c^2}{\mathrm{E}_c\mathrm{A}_c}\right) = Fw_4 + fw_5$$

$$\delta_{(N+1)4_B} = F\left(\frac{(d-l_5)(2l_4 h - {l_4}^2 s) + c\left(-h{l_4}^2 + \frac{s{l_4}^3}{3}\right)}{2\mathrm{E}_c\mathrm{I}_c}\right) + f\left(\frac{-\mathrm{h}(2l_4 h - {l_4}^2 s) - s\left(-h{l_4}^2 + \frac{s{l_4}^3}{3}\right)}{2\mathrm{E}_c\mathrm{I}_c}\right) = Fw_6 + fw_7 \quad (2\text{-}20)$$

Considering the compatibility of the elastomeric member, the displacement of node q which is the summation of these relative displacements is

$$\delta = \sum_{j=4}^{j=5}\left(\delta_{(N+1)4j_A} + \delta_{(N+1)4j_B}\right) = F(w_2 + w_4 + w_6) + f(w_1 + w_3 + w_5 + w_7) = \left(\frac{f(l_e/2)}{\mathrm{A}_e\mathrm{E}_e}\right) \quad (2\text{-}21)$$

where l_e is the length of the elastomeric member which is located between two adjacent corners of two consecutive unit cells of corrugation. Then the relation between the applied global force and the resisting force due to the gap opening in the elastomeric member is

$$f = F\left[\frac{(w_2 + w_4 + w_6)}{\left(\frac{l_e}{2\mathrm{A}_e\mathrm{E}_e}\right) - (w_1 + w_3 + w_5 + w_7)}\right] = \alpha F \quad (2\text{-}22)$$

Obtaining Eq. (2-22) and considering Eqs. (2-15) and (2-16) the force distribution in the elastomeric members are identified and hence the structure is determinate. In other words the force in each elastomeric member is proportional to the global applied force F, i.e. $f_{i(i+1)} = \alpha_{i(i+1)}F$. Similar to Eq. (2-15) $\alpha_{i(i+1)}$ is the symmetric matrix given by $\alpha_{\mathrm{i(i+1)}} = \alpha\left[\frac{\mathrm{L_{np}+(i-1)L_{uc}}}{\mathrm{L_{np}+NL_{uc}}}\right]$. By differentiating the whole strain energy of the structure with respect to the global applied load F in Fig. 2-5(b), the vertical displacement for the center of the panel would be obtained. Considering Fig. 2-5(b), Eq. (2-16) can be divided into periodic and non-periodic parts as:

$U = U_{np} + \sum_{i=2}^{i=N+1} \sum_{j=1}^{j=5} U_{ij}$.

Considering Eq. (2-15) and Eq. (2-22) and following the same procedure, the axial forces and bending moment of the members of the non-periodic part, i.e. $i = 1$, can be calculated. The axial and bending deformation of these members are calculated as

$$\delta_{14_A} = F\left(\frac{-(s + \alpha_{12}c)^2 l_4}{\mathrm{E}_c\mathrm{A}_c}\right) = FC_{14_A}$$

$$\delta_{14_B} = F\left(\frac{(\alpha_{12}s - c)^2 {l_4}^3}{3\mathrm{E}_c\mathrm{I}_c}\right) = FC_{14_B}$$

$$\delta_{15_A} = F\left(\frac{-(\alpha_{12})^2 l_5}{\mathrm{E}_c\mathrm{A}_c}\right) = FC_{15_A} \qquad (2\text{-}23)$$

$$\delta_{15_B} = F\left(\frac{(l_5 + l_4 c - \alpha_{12}h)^3 - (l_4 c - \alpha_{12}h)^3}{3\mathrm{E}_c\mathrm{I}_c}\right) = FC_{15_B}$$

In Eq. (2-23) to Eq. (2-35) C_{ij} is the flexibility factor has been introduced so as to keep the format of equations simple and clear. According to Fig. 2-5(b), for the periodic unit cells of the structure, the length parameter L_i is introduced as

$$L_i = \left[L_{np} + (i-2)L_{uc}\right] + \sum_1^{j-1} L_j \qquad (2\text{-}24)$$
$$i = 2{:}\,N+1 \quad \text{and} \quad j = 1,2,3,4,5$$

where L_i is the distance from the support to the member of each periodic unit cell. Considering Fig. 2-5(b), for the first member of each periodic unit cell, i.e. $i = 2{:}\,N+1$ and $= 1$, the axial and bending moment is stated as:

$$T_{i1} = f_{(i-1)i} = F\left(\alpha_{(i-1)i}\right)$$
$$M_{i1} = f_{(i-1)i}h - F(x + L_i) = F\left(\alpha_{(i-1)i}h - L_i - x\right) \qquad (2\text{-}25)$$

The relative displacements due to the axial and bending forces for this member is then

$$\delta_{i1_A} = F\left(\frac{-(\alpha_{(i-1)i})^2 l_1}{E_c A_c}\right) = FC_{i1_A}$$
$$\delta_{i1_B} = F\left(\frac{\left(l_1 - (\alpha_{(i-1)i}h - L_i)\right)^3 + (\alpha_{(i-1)i}h - L_i)^3}{3E_c I_c}\right) = FC_{i1_B} \quad (2\text{-}26)$$

In a similar way, for the second member of each periodic unit cell, i.e. $j = 2$, the axial and bending moment is

$$T_{i2} = Fs - f_{(i-1)i}c = F(s - \alpha_{(i-1)i}c)$$
$$M_{i2} = (Fc + f_{(i-1)i}s)x + (FL_i - f_{(i-1)i}h) = F[(c + \alpha_{(i-1)i}s)x + (L_i - \alpha_{(i-1)i}h)] \quad (2\text{-}27)$$

and the deformations corresponding to these forces are

$$\delta_{i2_A} = F\left(\frac{(s - \alpha_{(i-1)i}c)^2 l_2}{E_c A_c}\right) = FC_{i2_A}$$
$$\delta_{i2_B} = F\left(\frac{\left((c + \alpha_{(i-1)i}s)l_2 + (L_i - \alpha_{(i-1)i}h)\right)^3 - (L_i - \alpha_{(i-1)i}h)^3}{3E_c I_c(c + \alpha_{(i-1)i}s)}\right) = FC_{i2_B} \quad (2\text{-}28)$$

Similarly, for the third member of each periodic unit cell, i.e. $j = 3$, the axial and bending moment is

$$T_{i3} = 0$$
$$M_{i3} = F(L_i + x) \quad (2\text{-}29)$$

Therefore the deformations corresponding to these forces are:

$$\delta_{i3_A} = 0$$
$$\delta_{i3_B} = F\left(\frac{(L_i + l_3)^3 - {L_i}^3}{3E_c I_c}\right) = FP_{i3_B} \quad (2\text{-}30)$$

Likewise, for the fourth member of each periodic unit cell, i.e. $j = 4$, the axial force and bending moment are:

$$T_{i4} = Fs + f_{i(i+1)}c = F(s + \alpha_{i(i+1)}c)$$
$$M_{i4} = FL_i + (Fc - f_{i(i+1)}s)x = F[L_i + (c - \alpha_{i(i+1)}s)x] \quad (2\text{-}31)$$

Similarly, the deformations corresponding to these forces are:

$$\delta_{i4_A} = F\left(\frac{-\left(s + \alpha_{i(i+1)}c\right)^2 l_4}{\mathrm{E}_c\mathrm{A}_c}\right) = FC_{i4_A}$$
$$\delta_{i4_B} = F\left(\frac{\left(\left(L_i + \left(c - \alpha_{i(i+1)}s\right)l_4\right)\right)^3 - {L_i}^3}{3\mathrm{E}_c\mathrm{I}_c\left(c - \alpha_{i(i+1)}s\right)}\right) = FC_{i4_B} \quad (2\text{-}32)$$

Finally, for the fifth member of each periodic unit cell, i.e. $j = 5$, the axial and bending moment is

$$T_{i5} = f_{i(i+1)} = F\left(\alpha_{i(i+1)}\right)$$
$$M_{i5} = f_{i(i+1)}h - F(L_i + x) = F\left(\alpha_{i(i+1)}h - L_i - x\right) \quad (2\text{-}33)$$

and the deformations are

$$\delta_{i5_A} = F\left(\frac{-\left(\alpha_{i(i+1)}\right)^2 l_5}{\mathrm{E}_c\mathrm{A}_c}\right) = FC_{i5_A}$$
$$\delta_{i5_B} = F\left(\frac{\left(l_5 - \left(\alpha_{i(i+1)}h - L_i\right)\right)^3 + \left(\alpha_{i(i+1)}h - L_i\right)^3}{3\mathrm{E}_c\mathrm{I}_c}\right) = FC_{i5_B} \quad (2\text{-}34)$$

The vertical displacement for the half of the panel then is obtained as:

$$\delta = \left(\sum_{j=4}^{j=5}(\delta_{1j_A} + \delta_{1j_B}) + \sum_{i=2}^{i=N+1}\sum_{j=1}^{j=5}(\delta_{ij_A} + \delta_{ij_B})\right) = F\sum_{i=1}^{i=N+1}\sum_{j=1}^{j=5}\left(C_{ij_A} + C_{ij_B}\right) = FC_{total} \quad (2\text{-}35)$$

Comparing this relation, with the cantilever beam with length equal to half of the original three point bending span, i.e. d, the equivalent flexural stiffness would be obtained as:

$$(EI)_{Eq_L} = \frac{(L_{np} + NL_{uc})^3}{3C_{total}} \quad (2\text{-}36)$$

It is worthwhile to notice that C_{total} is a function of the number of periodic unit cells and hence the equivalent flexural stiffness is dependent to the number of periodic unit cells.

2-2-3 Transverse stiffness

In order to predict the transverse stiffness modulus of the coated corrugated core, a straight Euler –Bernoulli beam is considered. As illustrated in Fig. 2-6(a) and Fig. 2-6(b), calculation of the in plane and out of plane stiffness of the beam in the transverse direction leads to formulation of the equivalent transverse modulus of stiffness.

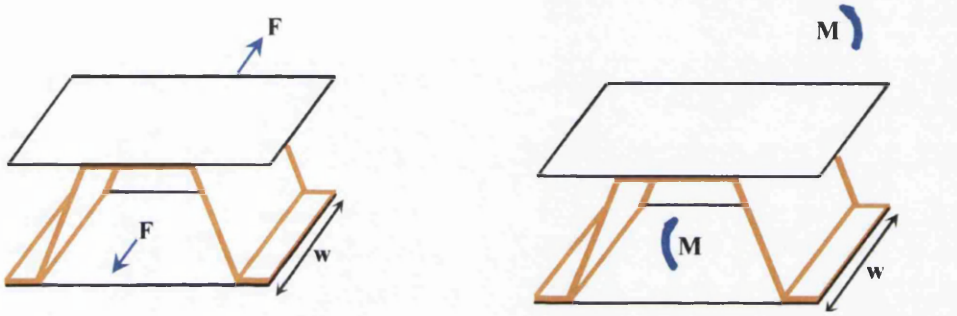

(a) Transverse in plane stiffness (b) Transverse out of plane stiffness

Figure 2-6: Schematic of a unit cell of coated corrugated core in the transverse direction

2-2-3-1 Transverse in plane stiffness

Composite corrugated core and elastomeric members act like parallel springs in the transverse direction. Therefore the total stiffness of a unit cell of coated corrugated core in the transverse direction is given by:

$$K_T = K_{c_T} + K_{e_T} = \frac{A_{e_T}E_e + A_{c_T}E_c}{W_T} \tag{2-37}$$

where A_{c_T}, A_{e_T} and W_T denote the cross section area of the corrugated core and elastomeric coating and the width of the panel in the transverse direction, respectively. The axial stiffness for the equivalent bar is:

$$K_{Eq_T} = \frac{(AE)_{Eq_T}}{W_T} \tag{2-38}$$

Hence by comparing Eq. (2-37) and Eq. (2-38) the equivalent stiffness in the transverse direction is:

$$(AE)_{Eq_T} = A_{e_T}E_e + A_{c_T}E_c \approx A_{c_T}E_c \tag{2-39}$$

2-2-3-2 Transverse out of plane stiffness

As mentioned in the previous section, since the composite corrugated core and elastomeric members act like parallel springs in the transverse direction, the total out of plane stiffness of a unit cell of coated corrugated core is given by:

$$(EI)_{EqT} = E_c I_{c_T} + E_e I_{e_T} \approx E_c I_{c_T} \tag{2-40}$$

It is evident that in Eq. (2-39) and Eq. (2-40) that the role of the elastomeric members in the transverse direction may be neglected since the elastomer Young's modulus is small compared to the composite material.

2-3 Validation

Different experimental and numerical models are considered in this section to verify the accuracy and efficiency of the presented equivalent model. In the experimental part, both coated and uncoated corrugated cores are studied in tensile and three point bending tests and their mechanical behavior are compared to those predicted by the analytical solution. In the numerical section, the mechanical behavior of coated corrugated cores predicted by the analytical model is compared to the finite element results obtained by ABAQUS simulation (SIMULIA, 2011). The effect of combined loading and the number of unit cells on the mechanical behavior of the structure are investigated and verified with numerical simulations.

2-3-1 Experimental validation

In order to validate the analytical model for different levels of complexity of the geometry of the structure, the mechanical behavior of both coated and uncoated corrugated cores in tensile and three point bending tests (Dayyani et al., 2013) are compared to those predicted by the analytical solution. More details of the experiments for the uncoated corrugated cores are presented in (Dayyani et al., 2012).

2-3-1-1 Problem definition

In this section a brief description of the literature (Dayyani et al., 2013) on the manufacturing method and material characterization of the coated corrugated panel is presented.

Coated corrugated core fabrication

To manufacture the composite corrugated cores, prepreg laminates of glass fibre plain woven cloth were hand-laid on a trapezoidal machined aluminium mould. More details of the manufacturing process as well as the schematic of the trapezoidal mould and the prepreg laminates of glass fibre are presented in the author's previous work (Dayyani et al., 2012). Afterwards, both the upper and lower faces of the corrugated core were covered by elastomer which is widely used in applications where low stiffness and a high elastic strain are required.

Coated corrugated core geometry

The length of the coated composite corrugated core investigated in this section was 300 mm. The widths of tensile and bending test specimens were 25 mm and 100 mm, respectively. Figure 2-7 illustrates the constructed coated composite corrugated core which included 10 unit cells. The thickness of the corrugated core and elastomer skin was 1.00 mm and 0.80 mm, respectively. The values of the dimensions given in Fig. 2-1(b) are tabulated in Table 2-2.

Figure 2-7: The coated composite corrugated core, (Dayyani et al., 2013)

Table 2-2: Dimensions of the corrugated core unit cell, (Dayyani et al., 2013)

Dimensions	Values(mm)
a_1	3.75
a_2	5.50
a_3	5.30
h	9.50

Coated corrugated core material characterization

The corrugated core was made of three-plies of woven glass fibres with epoxy resin. Moreover, to evaluate the mechanical properties of this material, uniaxial tensile tests were carried out on five flat samples with unidirectional embedded fibres. The average Young's modulus of fibres, E_{fibre}, was 9 GPa, while the effect of the matrix was neglected. The elastomer coatings were made of synthetic rubber Polyurethane (PU) which was knitted by a circular interlock weft method. To evaluate the mechanical properties of the elastomer, a total of six strips of elastomer sheet were cut and subjected to simple tensile tests. Table 2-3 describes the average Young's modulus of the elastomer coating in three phases of stretching.

Table 2-3: Tangent modulus of the elastomer in different phases of stretching, (Dayyani et al., 2013)

Elasticity	Initial stretch	Medium stretch	Final stretch
Tangent modulus	13.5 MPa	10.25 MPa	108.00 MPa

2-3-1-2 Experiments on coated composite corrugated core

Tensile test of coated composite corrugated core

Using the ASTM D3039 standard (ASTM-D, 2000) as a basis for the tensile standard testing, six specimens of the coated composite corrugated core were tested experimentally in tension, transverse to their corrugations. Figure 2-8(a) illustrates the investigated composite corrugated core with elastomeric coatings for the tensile test. A comparison of the average data from the experiment for the corrugated core with and without elastomeric coatings in the tensile tests is shown in Fig. 2-9(a).

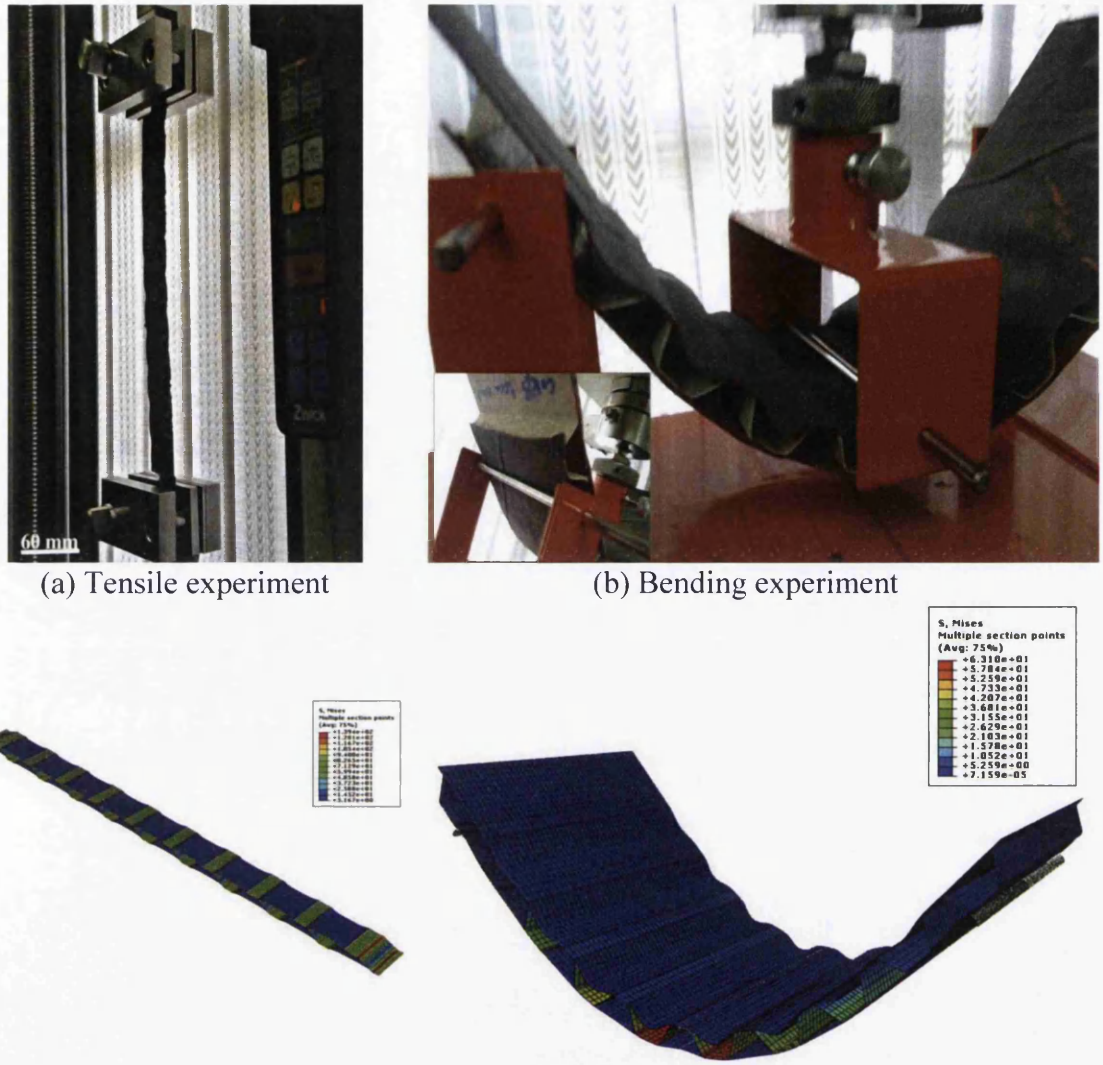

(a) Tensile experiment (b) Bending experiment

(c) Tensile simulation (d) Bending simulation

Figure 2-8: Composite corrugated core with elastomeric coatings in structural tests and corresponding simulations, (Dayyani et al., 2013)

Three-point bending test of a coated composite corrugated core

Likewise, according to ASTM C393 (ASTM-C, 2000), six specimens of the coated composite corrugated core were tested experimentally by a three point bending test. The span and diameter of the support rollers were 193 mm and 5 mm, respectively. Figure 2-8(b) illustrates testing machine and the coated composite corrugated core during the three point bending test. A comparison of the average data from the experiment for the corrugated core with and without elastomeric coatings in the three-point bending test is shown in Fig. 2-9(b).

2-3-1-3 Analytical modeling of experiments

The analytical modelling consists of two steps: first, the equivalent isotropic material properties for the plain woven fabrics are estimated and second, the equivalent tensile and bending flexural property of the coated composite corrugated core for 10 unit cells are evaluated. In the first step, since the plain woven fabrics are a type of heterogeneous orthotropic material, the equivalent Young's modulus is calculated based on the finite element model described in detail in (Dayyani et al., 2012; Li et al., 2008). However the equivalent Young's modulus can also be calculated from the rule of mixtures. Since the analytical solution is proposed for linear small deformations of the structure, the initial stretching behaviour of the elastomer is considered. Therefore, the equivalent Young's modulus of the composite, E_c and the elastomer E_e are estimated as 4.5 GPa and 13.5 MPa respectively.

Longitudinal in plane stiffness

Considering Eqs. (2-11) and (2-12) and the fact that the tensile stiffness of the panel consisting of 10 periodic unit cells would be equal to $\frac{(K_1+K_2)}{20}$, the force displacement curves for both coated and uncoated structures are plotted in Fig. 2-9(a). It must be mentioned that by setting the Young's modulus of the elastomer to zero the proposed analytical solution would be identical to the analytical method proposed in (Dayyani et al., 2012) and matches with the first phase of mechanical behaviour for the uncoated corrugated core in the experiment. Then by increasing the Young's modulus of the elastomer up to 13.5 MPa, the proposed analytical solution would correlate with the first phase of the mechanical behaviour of elastomeric coated corrugated core in the experiment. By considering the low stiffness of the corrugated core in the initial stages (Dayyani et al., 2012), the effect of the elastomer is evident. The elastomer functions as a spring which is parallel with the corrugated core and thus resists the deformation of the whole structure.

Longitudinal out of plane stiffness

The span in the three-point bending test was 193 mm. Hence, considering the values listed in Table 2-2 and Fig. 2-5(b), one half of the bending span included one

non periodic part and three periodic unit cells. In this regard Eq. (2-15) is rewritten as:

$$\mathbf{f_{el}} = \begin{bmatrix} 0 & f_{12} & & & & \\ f_{21} & 0 & f_{23} & & & \\ & f_{32} & 0 & f_{34} & & \\ & & f_{43} & 0 & f_{45} & \\ & & & f_{54} & 0 & \end{bmatrix} = f \begin{bmatrix} 0 & 0.1 & & & & \\ 0.1 & 0 & 0.4 & & & \\ & 0.4 & 0 & 0.7 & & \\ & & 0.7 & 0 & 1 & \\ & & & 1 & 0 & \end{bmatrix} \qquad (2\text{-}41)$$

The force displacement curves for both coated and uncoated structures are plotted in Fig. 2-9(b). By setting the Young's modulus of the elastomer to zero the proposed analytical solution would be the same as the analytical method proposed in (Dayyani et al., 2012) and matches with the first phase of mechanical behaviour of uncoated corrugated core in the three-point bending experiment. However by increasing the Young's modulus of elastomer to 13.5 MPa, the proposed analytical solution correlates with the first phase of the mechanical behaviour of the elastomeric coated corrugated core in the bending experiment.

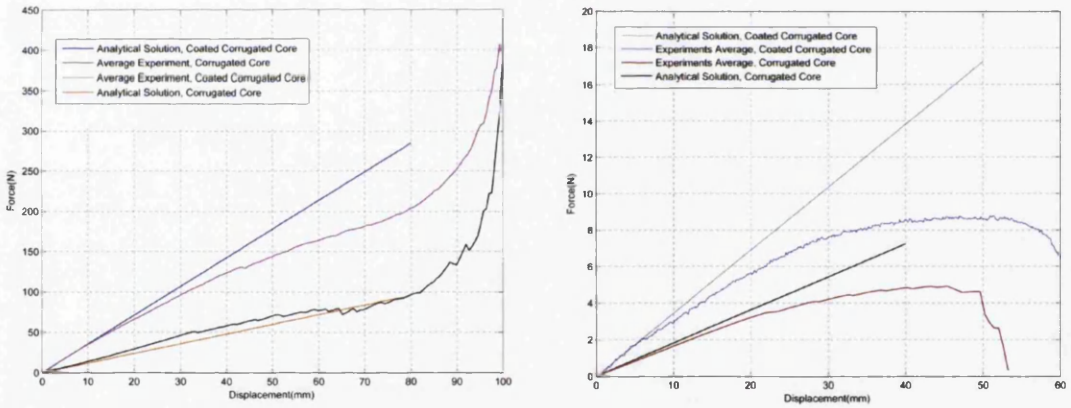

(a) Tensile (b) Bending

Figure 2-9: Mechanical behaviour of coated and uncoated corrugated core, experiments and analytical solution

2-3-2 Finite element validation

In this section the mechanical behavior of coated corrugated cores predicted by the analytical model is compared to the finite element results obtained by ABAQUS simulation. Two different effects on the mechanical behavior of the structure are investigated and verified by numerical simulations. In both cases the geometric dimensions and material properties are selected as those presented in section 2-3-1-1.

In both cases a fine mesh of 2D beam elements which interpolates the deformations by use of cubic shape functions was considered. The size of each element was 1 mm and 3 degrees of freedom for each node was considered. A mesh convergence study was performed to confirm the mesh independency of the solution.

2-3-2-1 The effect of the number of unit cells

As mentioned before the coated corrugated core acts as a series of springs in tension. However, for the bending case the situation is slightly different. It is evident in Eqs. (2-23) to (2-36) that the flexibility factor, i.e. C_{ij}, itself is a quadratic function of the number of unit cells. On the other hand, considering Eq. (2-36) the bending stiffness is a cubic function of the length of the bending span which is dependent to the number of unit cells. As a result, in both tensile and bending cases the stiffness has an inverse relation with the number of unit cells. Figure 2-10(a) compares the tensile stiffness of the panel versus N, the number of periodic unit cells, obtained by the equivalent model and the finite element simulation. Figure 2-10(b) shows a comparison of the bending stiffness of the panel versus the number of periodic unit cells in half of the bending span, obtained by the equivalent model and the finite element simulation.

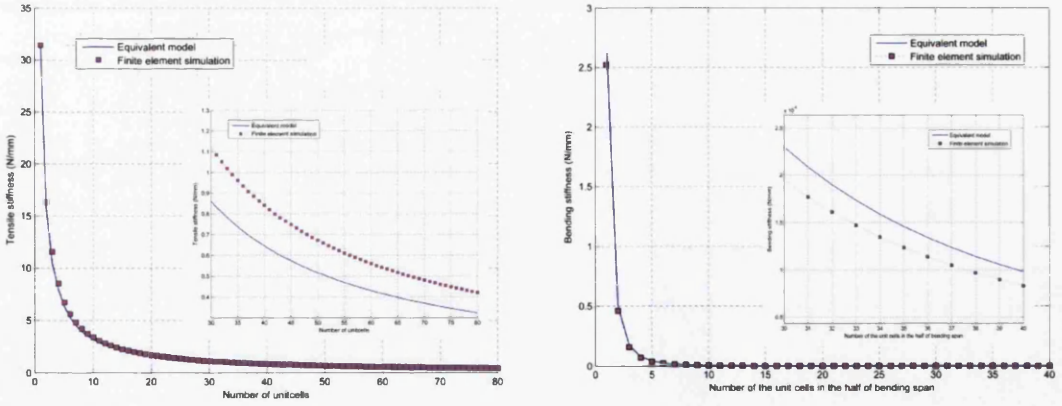

(a) Tensile (b) Bending

Figure 2-10: The stiffness of the panel versus the number of unit cells

2-3-2-2 The effect of combined loading

This section shows the suitability of the proposed method to replace the coated corrugated core with an equivalent structure under a complex combination of load

and boundary conditions, by analyzing two finite element models corresponding to these structures.

Firstly a coated corrugated core with equivalent material properties and the same dimensions of the tensile specimens given in section 2-3-1-1, were modelled as beam elements. The boundary conditions were selected such that one end of the panel was fixed and the other was subjected to a horizontal displacement of 10mm in the longitudinal direction. Furthermore, in terms of loading, one side of the coated corrugated core was subjected to a vertical uniform pressure of 1000 kPa. Secondly an equivalent beam model was simulated with an in plane stiffness, i.e. $(EA)_{Eq_L}$, of 1035.8 N and an out of plane stiffness, $(EI)_{Eq_L}$, of 12931N/mm^2; the same boundary conditions and loading were modeled independently in ABAQUS.

In both cases fine meshes and linear small displacement theory were considered. The results obtained corresponded to the reaction forces at the fixed end and the nodal displacements of the moving end are tabulated and compared in Table 2-4. The error in both the horizontal and vertical cases is less than 6.7%, which demonstrates the efficiency of the proposed method under complex combined load and boundary conditions.

Table 2-4: Stiffness comparison of the corrugated panel in combined loading, finite element model and the analytical equivalent method

Method \ Stiffness	Force to displacement ratio (N/mm)	
	Horizontal direction	Vertical direction
Finite Element Method	3.3820	0.0388
Analytical Equivalent Model	3.5500	0.0362
Error (%)	4.7300	6.7000

2-4 Discussion

Considering the geometric dimensions and material properties of the panel presented in section 2-3-1-1, and regarding Eqs. (2-8),(2-9) and (2-22), the relation between the coefficient of the force distribution in the elastomeric members, i.e. α, and the Young's modulus of the elastomer is shown in Fig. 2-11 for the tension and bending cases in the longitudinal direction respectively. The curve shows a plateau when the Young's modulus of the elastomer tends to infinity, which is expected

because of the geometric constraints. The physical description of the behaviour is that by increasing the Young's modulus of the elastomer sufficiently there would be a rigid geometric constraint between two adjacent corners of the unit cells. In other words the rigid link would prohibit any change in the distance between two adjacent corners of subsequent unit cells. Therefore the rigid link would have a constant axial force. However it must be mentioned that this behaviour is true only in terms of theory. In reality, by increasing the Young's modulus of the elastomer up to a certain level the mechanical behaviour of the elastomer would change from membrane into shell behaviour. Moreover the deformation mechanism would also change since the skins of the sandwich panel would have a greater Young's modulus than the composite corrugated core. Fig. 2-11(a) and Fig. 2-11(b) illustrate the relation between α and the Young's modulus of the elastomer in the longitudinal tensile and bending tests respectively. In addition, the effect of the length of the elastomeric members on the distribution of force in each elastomeric member (i.e. different α_4 and α_5), which is due to the different geometric parameters, are shown in Fig. 2-11(a).

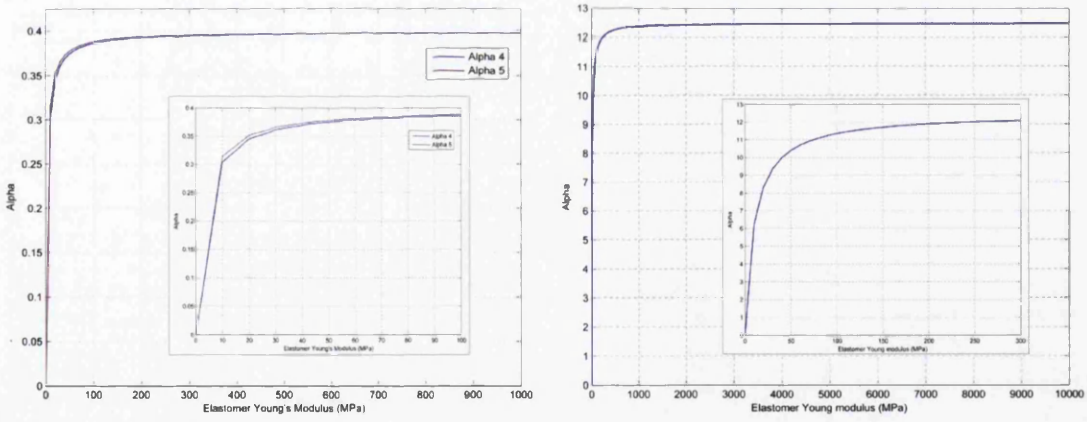

(a) Tensile (b) Bending

Figure 2-11: The relation between α and the Young's modulus of the elastomer

2-5 Conclusion

Two analytical solutions to calculate the equivalent tensile and bending flexural property of the coated corrugated core in the longitudinal and transverse directions are presented based on Castigliano's second theorem. The results obtained by the analytical model were compared to those given by numerical simulations and experiments. In the experimental part, both coated and uncoated corrugated cores

were studied in tensile and three point bending tests. The ratio of the in plane and out of plane stiffness of coated corrugated structure to uncoated corrugated structure was 2.28 and 2.14, respectively. This provides a better insight into the mechanical behavior of coated composite corrugated panels as candidates for morphing wing applications. Furthermore, the effect of combined loading and the number of unit cells on the mechanical behavior of the coated corrugated core are investigated and verified with numerical simulations. The physical description of the behavior that the relation between the coefficient of the distribution of forces in the elastomeric members and the Young's modulus of the elastomer converges when the Young's modulus of elastomer tends to infinity was also discussed. The comparison studies demonstrate the suitability of the proposed method for further design investigations.

Chapter 3:
A General Super Element for a Curved Beam

3-1 Introduction

Considering the geometric and mechanical properties of the corrugated panel, a generic super element of corrugated core unit cell with elastomeric coating for morphing structures is investigated in this chapter. The super element captures the small deformation of a 2D thin curved beam with variable curvature. The importance of this work, in contrast to the previous chapter, is that it provides a precise analytical equivalent model which avoids any homogenization assumptions. In this regard, the stiffness matrix of a general curved beam element for a corrugated unit cell with elastomeric coating is derived. Different geometries are investigated to verify the accuracy and efficiency of the presented super element. The super element uses the geometric and mechanical properties of the panel as variables that may be applied for further topology optimization studies. The parametric studies of different corrugation shapes demonstrate the suitability of the proposed super element for application in further detailed design investigations.

3-2 Problem statement; Motivation and Approach

Although some research is available in the field of analytical homogenization of both uncoated and coated corrugated cores, the applicability of these studies to further optimization and design of morphing skins is still a matter of question as discussed in chapters 1 and 2. For instance, the equivalent flexural property of both uncoated and coated corrugated cores is dependent on the length of panel. Figure 3-1(a) shows a comparison of the predicted equivalent flexural property of both coated and uncoated corrugated panels from finite element analysis, ABAQUS (SIMULIA, 2011). The details of the geometry of the coated corrugated unit cell are presented in the literature (Dayyani et al., 2012). A fine mesh of 2D beam elements which interpolates the deformations by use of cubic shape functions was considered for the analysis. The size of each element was 1 mm and 3 degrees of freedom for each node was considered. A mesh convergence study was performed to confirm the mesh independency of the solution. The ascending trend of the curve for the coated corrugated panel is due to the elastomeric coatings, which act as springs parallel to corrugation unit cell, as discussed in the previous chapter. Figure 3-1(a) shows that, for the detailed FE analysis of a corrugated panel, the equivalent flexural property of a sufficiently large number of unit cells is about 9% more than one unit cell. This difference is higher than that predicted from the assumptions and limitations of the theories used. The curvature of an aerofoil, especially at the leading edge of the morphing wing, is another issue that must be considered when using the homogenized tensile and flexural properties of the corrugated panel in the literature. The literature describing the equivalent tensile and flexural properties of coated and uncoated corrugated cores is limited to straight flat panels and does not capture the effect of curvature. Figure 3-1(b) illustrates the application of the coated corrugated core as a skin of a Fish-BAC internal structure (Woods and Friswell, 2012) of an aerofoil in a leading and trailing edge morph. Thus the limitations identified above, motivate the development of a generic super element for a coated corrugated unit cell.

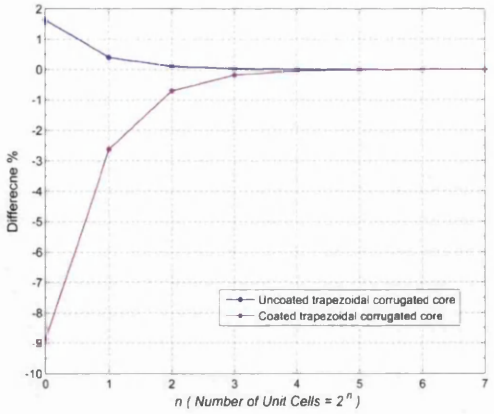

(a) The convergence of the equivalent bending stiffness of a corrugated panel

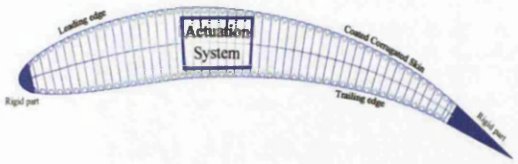

(b) The application of the coated corrugated core as a skin of camber morphing aerofoil

Figure 3-1: The motivations for the general super element

Figure 3-2(a) shows a schematic of the corrugated core unit cell coated with an elastomeric skin. The panel is assumed to have periodic corrugations in the longitudinal direction. In comparison to the literature (Bartolozzi et al., 2013) only one side of the corrugated core is coated with the elastomer skin. This approach reduces the weight of the morphing skin and also results in a smaller actuation force required to stretch the skin to morph to the desired position. Figure 3-2(a) shows that any coated corrugation unit cell has three components. Considering the shear deformation between the elastomeric coating and the corrugated core, the regions labelled 1 provide significant area to bond the elastomer and corrugated core. The curved component, labelled 2, causes the main deformations of the skin. The shape and curvature of this member has a major impact on the ratio of the out of plane stiffness to the in-plane stiffness of the skin, which must be optimized for the specific application of morphing. The elastomeric skin is labelled 3. Since the ratio of the elastomer Young's modulus to Young's modulus of corrugated core material is very small, a good assumption is to neglect the elastomer coating in the areas overlapped with the composite corrugated core. This assumption is reasonable because these two materials are well bonded together and have the same displacement. Thus the strain energy terms of the elastomer in contact with the glass fibre maybe neglected (Dayyani et al., 2013). Considering the points mentioned above, the objective of this chapter is first to represent an equivalent element for the

curved component 2, and then to assemble its stiffness matrix with the stiffness matrix of the elastomeric member 3.

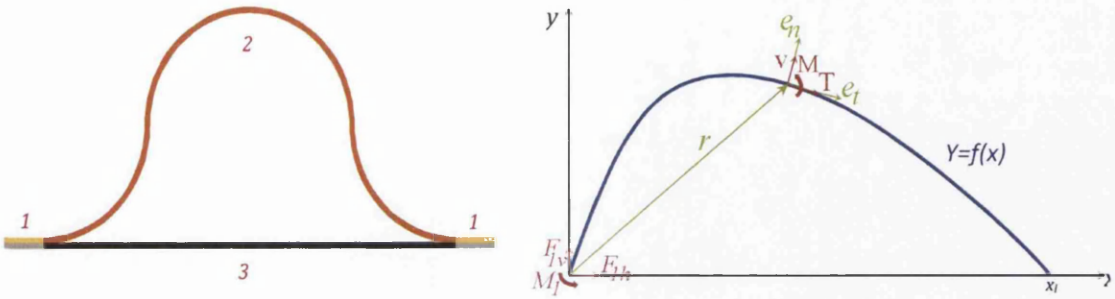

(a) (b)

Figure 3-2: Schematic of the corrugation unit cell and its curve function

3-3 Theory

In this section the direct stiffness method and Castigliano's second theorem are used to derive the stiffness matrix of an arbitrary corrugation curve. Figure 3-2(b) shows a schematic of an arbitrary corrugation curve that can be a mathematical function of x , i.e. $f(x)$.The Cartesian and normal and tangent $(n-t)$ coordinate systems are selected for the global and local coordinate systems. For any arbitrary point on the curve the position vector is:

$$\vec{r} = \begin{pmatrix} x \\ f(x) \end{pmatrix} \tag{3-1}$$

The unit vectors of the tangent and normal directions are defined as:

$$\overrightarrow{e_t} = \frac{1}{\sqrt{1+\left(\acute{f}(x)\right)^2}} \begin{pmatrix} 1 \\ \acute{f}(x) \end{pmatrix}$$
$$\overrightarrow{e_n} = \frac{1}{\sqrt{1+\left(\acute{f}(x)\right)^2}} \begin{pmatrix} -\acute{f}(x) \\ 1 \end{pmatrix} \tag{3-2}$$

In vector notation, the applied forces on node 1, which is located at the origin of coordinate systems, is:

$$\overrightarrow{F_{1h}} = F_{1h} \begin{pmatrix} 1 \\ 0 \end{pmatrix} \tag{3-3}$$

$$\overrightarrow{F_{1v}} = F_{1v}\begin{pmatrix}0\\1\end{pmatrix}$$

where indices h and v represent the horizontal and vertical directions. The projection of these vectors in the tangent and normal directions are:

$$Proj_{\overrightarrow{e_t}}^{\overrightarrow{F_{1h}}} = \overrightarrow{F_{1h}}.\overrightarrow{e_t} = \frac{F_{1h}}{\sqrt{1+\left(\acute{f}(x)\right)^2}}$$

$$Proj_{\overrightarrow{e_n}}^{\overrightarrow{F_{1h}}} = \overrightarrow{F_{1h}}.\overrightarrow{e_n} = \frac{-F_{1h} * \acute{f}(x)}{\sqrt{1+\left(\acute{f}(x)\right)^2}} \quad (3\text{-}4)$$

and

$$Proj_{\overrightarrow{e_t}}^{\overrightarrow{F_{1v}}} = \overrightarrow{F_{1v}}.\overrightarrow{e_t} = \frac{F_{1v} * \acute{f}(x)}{\sqrt{1+\left(\acute{f}(x)\right)^2}}$$

$$Proj_{\overrightarrow{e_n}}^{\overrightarrow{F_{1v}}} = \overrightarrow{F_{1v}}.\overrightarrow{e_n} = \frac{F_{1v}}{\sqrt{1+\left(\acute{f}(x)\right)^2}} \quad (3\text{-}5)$$

Thus the equilibrium the tangent and normal forces and the bending moment are:

$$T_1(x) = \frac{-\left(F_{1h} + F_{1v} * \acute{f}(x)\right)}{\sqrt{1+\left(\acute{f}(x)\right)^2}}$$

$$v_1(x) = \frac{\left(F_{1h} * \acute{f}(x)\right) - F_{1v}}{\sqrt{1+\left(\acute{f}(x)\right)^2}} \quad (3\text{-}6)$$

$$M_1(x) = (F_{1v} * x) - \left(F_{1h} * f(x)\right) - M_1$$

The incremental length along the curve is $ds = \sqrt{1+\left(\acute{f}(x)\right)^2}\,dx$. Hence the strain energy of the curved beam due to the axial (tangent) forces and bending moment may be represented as:

$$U_A = \int_0^{x_l} \frac{T^2}{2EA}\sqrt{1+\left(\acute{f}(x)\right)^2}\,dx$$

$$U_B = \int_0^{x_l} \frac{M^2}{2EI}\sqrt{1+\left(\acute{f}(x)\right)^2}\,dx \tag{3-7}$$

Where the indices A and B indicate axial and bending. The total strain energy is $U = U_A + U_B$. Since the theory of thin beam elements is used, the strain energy due to shear strains is neglected. From Castigliano's second theorem, the displacements and rotation at node 1, along the direction of the applied forces and moments from the axial strain energy, are obtained as:

$$\begin{aligned}\frac{\partial U_{A,1}}{\partial F_{1h}} &= F_{1h}\int_0^{x_l} \frac{dx}{EA\sqrt{1+\left(\acute{f}(x)\right)^2}} + F_{1v}\int_0^{x_l} \frac{\acute{f}(x)}{EA\sqrt{1+\left(\acute{f}(x)\right)^2}}dx \\ &= F_{1h} * I_{A,F_{1h}F_{1h}} + F_{1v} * I_{A,F_{1h}F_{1v}}\end{aligned} \tag{3-8}$$

$$\begin{aligned}\frac{\partial U_{A,1}}{\partial F_{1v}} &= F_{1h}\int_0^{x_l} \frac{\acute{f}(x)}{EA\sqrt{1+\left(\acute{f}(x)\right)^2}}dx + F_{1v}\int_0^{x_l} \frac{\left(\acute{f}(x)\right)^2}{EA\sqrt{1+\left(\acute{f}(x)\right)^2}}dx \\ &= F_{1h} * I_{A,F_{1v}F_{1h}} + F_{1v} * I_{A,F_{1v}F_{1v}}\end{aligned} \tag{3-9}$$

$$\frac{\partial U_{A,1}}{\partial M_1} = 0 \tag{3-10}$$

A series of factors are introduced from Eq. (3-8) to keep the format of equations simple and clear. The second index of these factors represents the force which the axial strain energy is differentiated to while the third index indicates which force this factor is coefficient of. For instance the second index of $I_{A,F_{1h}F_{1v}}$ in Eq. (3-8) represents the force F_{1h}which the axial strain energy $U_{A,1}$ is differentiated by, while the third index indicates that the term $I_{A,F_{1h}F_{1v}}$ is a coefficient of F_{1v}. Similarly for the bending strain energy:

$$\frac{\partial U_{B,1}}{\partial F_{1h}} = F_{1h}\int_0^{x_l}\frac{(f(x))^2\sqrt{1+\left(\acute{f}(x)\right)^2}}{EI}dx + F_{1v}\int_0^{x_l}-\frac{x*f(x)\sqrt{1+\left(\acute{f}(x)\right)^2}}{EI}dx$$
$$+ M_1\int_0^{x_l}\frac{f(x)\sqrt{1+\left(\acute{f}(x)\right)^2}}{EI}dx \qquad (3\text{-}11)$$
$$= F_{1h} * I_{B,F_{1h}F_{1h}} + F_{1v} * I_{B,F_{1h}F_{1v}} + M_1 * I_{B,F_{1h}M_1}$$

$$\frac{\partial U_{B,1}}{\partial F_{1v}} = F_{1h}\int_0^{x_l}-\frac{x*f(x)\sqrt{1+\left(\acute{f}(x)\right)^2}}{EI}dx + F_{1v}\int_0^{x_l}\frac{x^2\sqrt{1+\left(\acute{f}(x)\right)^2}}{EI}dx$$
$$+ M_1\int_0^{x_l}-\frac{x\sqrt{1+\left(\acute{f}(x)\right)^2}}{EI}dx \qquad (3\text{-}12)$$
$$= F_{1h} * I_{B,F_{1v}F_{1h}} + F_{1v} * I_{B,F_{1v}F_{1v}} + M_1 * I_{B,F_{1v}M_1}$$

$$\frac{\partial U_{B,1}}{\partial M_1} = F_{1h}\int_0^{x_l}\frac{f(x)\sqrt{1+\left(\acute{f}(x)\right)^2}}{EI}dx + F_{1v}\int_0^{x_l}-\frac{x\sqrt{1+\left(\acute{f}(x)\right)^2}}{EI}dx$$
$$+ M_1\int_0^{x_l}\frac{\sqrt{1+\left(\acute{f}(x)\right)^2}}{EI}dx \qquad (3\text{-}13)$$
$$= F_{1h} * I_{B,M_1F_{1h}} + F_{1v} * I_{B,M_1F_{1v}} + M_1 * I_{B,M_1M_1}$$

Equations. (3-8 to 3-13) may be written a symmetric matrix form as:

$$\begin{bmatrix} I_{F_{1h},F_{1h}} & I_{F_{1h},F_{1v}} & I_{F_{1h},M_1} \\ I_{F_{1v},F_{1h}} & I_{F_{1v},F_{1v}} & I_{F_{1v},M_1} \\ I_{M_1,F_{1h}} & I_{M_1,F_{1v}} & I_{M_1,M_1} \end{bmatrix}\begin{bmatrix} F_{1h} \\ F_{1v} \\ M_1 \end{bmatrix} = \begin{bmatrix} \delta_{1h} \\ \delta_{1v} \\ \theta_1 \end{bmatrix} \qquad (3\text{-}14)$$

where each element of the flexibility matrix $\boldsymbol{I}_1$ is a sum of the factors due to axial and bending strain energy. In other words, $I_{F_{1h},F_{1h}} = I_{A,F_{1h}F_{1h}} + I_{B,F_{1h}F_{1h}}$ and likewise for the rest of the components. The flexibility matrix $\boldsymbol{I}_1$ is invertible for any curve $f(x)$; a mathematical proof for this argument is behind the scope of this chapter, but a physical explanation is based on the fact that any curved beam is not rigid in any direction. Rearranging Eq. (3-14) in terms of nodal forces gives:

$$\begin{bmatrix} F_{1h} \\ F_{1v} \\ M_1 \end{bmatrix} = \begin{bmatrix} I_{F_{1h},F_{1h}} & I_{F_{1h},F_{1v}} & I_{F_{1h},M_1} \\ I_{F_{1v},F_{1h}} & I_{F_{1v},F_{1v}} & I_{F_{1v},M_1} \\ I_{M_1,F_{1h}} & I_{M_1,F_{1v}} & I_{M_1,M_1} \end{bmatrix}^{-1} \begin{bmatrix} \delta_{1h} \\ \delta_{1v} \\ \theta_1 \end{bmatrix} \quad (3\text{-}15)$$

Applying the proper boundary conditions at node 1, the corresponding forces, representing the elements of the stiffness matrix, are obtained. For $\begin{bmatrix} \delta_{1h} \\ \delta_{1v} \\ \theta_1 \end{bmatrix} = \begin{bmatrix} 1 \\ 0 \\ 0 \end{bmatrix}$

$$K_{11} = F_{1h} = \frac{\left(I_{F_{1v},F_{1v}} * I_{M_1,M_1}\right) - {I_{F_{1v},M_1}}^2}{\det(I_1)} \quad (3\text{-}16)$$

$$K_{12} = F_{1v} = \frac{\left(I_{F_{1v},M_1} * I_{M_1,F_{1h}}\right) - \left(I_{F_{1v},F_{1h}} * I_{M_1,M_1}\right)}{\det(I_1)} \quad (3\text{-}17)$$

$$K_{13} = M_1 = \frac{\left(I_{F_{1v},F_{1h}} * I_{M_1,F_{1v}}\right) - \left(I_{F_{1v},F_{1v}} * I_{M_1,F_{1h}}\right)}{\det(I_1)} \quad (3\text{-}18)$$

where $\det(I_1)$ is the determinant of the flexibility matrix $\boldsymbol{I}_1$. For $\begin{bmatrix} \delta_{1h} \\ \delta_{1v} \\ \theta_1 \end{bmatrix} = \begin{bmatrix} 0 \\ 1 \\ 0 \end{bmatrix}$

$$K_{21} = F_{1h} = \frac{\left(I_{F_{1h},M_1} * I_{M_1,F_{1v}}\right) - \left(I_{F_{1h},F_{1v}} * I_{M_1,M_1}\right)}{\det(I_1)} \quad (3\text{-}19)$$

$$K_{22} = F_{1v} = \frac{\left(I_{F_{1h},F_{1h}} * I_{M_1,M_1}\right) - {I_{F_{1h},M_1}}^2}{\det(I_1)} \quad (3\text{-}20)$$

$$K_{23} = M_1 = \frac{\left(I_{F_{1h},F_{1v}} * I_{M_1,F_{1h}}\right) - \left(I_{F_{1h},F_{1h}} * I_{M_1,F_{1v}}\right)}{\det(I_1)} \quad (3\text{-}21)$$

And for the last case if $\begin{bmatrix} \delta_{1h} \\ \delta_{1v} \\ \theta_1 \end{bmatrix} = \begin{bmatrix} 0 \\ 0 \\ 1 \end{bmatrix}$ then

$$K_{31} = F_{1h} = \frac{\left(I_{F_{1h},F_{1v}} * I_{F_{1v},M_1}\right) - \left(I_{F_{1h},M_1} * I_{F_{1v},F_{1v}}\right)}{\det(I_1)} \tag{3-22}$$

$$K_{32} = F_{1v} = \frac{\left(I_{F_{1h},M_1} * I_{F_{1v},F_{1h}}\right) - \left(I_{F_{1h},F_{1h}} * I_{F_{1v},M_1}\right)}{\det(I_1)} \tag{3-23}$$

$$K_{33} = M_1 = \frac{\left(I_{F_{1h},F_{1h}} * I_{F_{1v},F_{1v}}\right) - I_{F_{1h},F_{1v}}{}^2}{\det(I_1)} \tag{3-24}$$

Figure 3-3 shows a schematic of general curved beam in which node 1 and node 2 do not have the same y coordinate. Considering the equilibrium equations of the general curved beam the reaction forces at node 2 are:

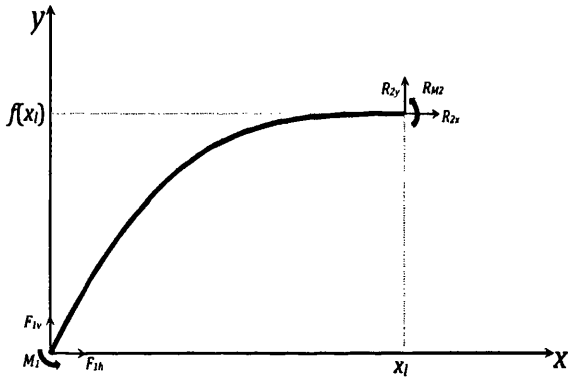

Figure 3-3: Schematic of any general curved beam

$$\begin{aligned} R_{2x} &= -F_{1h} \\ R_{2y} &= -F_{1v} \\ R_{M2} &= -\left(F_{1h} * f(x_l)\right) + \left(F_{1v} * x_l\right) - M_1 \end{aligned} \tag{3-25}$$

Considering Eq. (3-25), the rest of elements of first three rows of the stiffness matrix are as follows. For $i = 1{:}3$

$$\begin{aligned} K_{i4} &= -K_{i1} \\ K_{i5} &= -K_{i2} \end{aligned} \tag{3-26}$$

$$K_{i6} = -\left(K_{i1} * f(x_l)\right) + (K_{i2} * x_l) - K_{i3}$$

Following the same strategy as for node 1, and applying the forces and moment to node 2, the rest of the elements of the stiffness matrix are obtained. Representing the reaction forces at node 1 based on the forces at node 2, and substituting into Eq. (3-6), gives

$$T_2(x) = \frac{F_{2h} + \left(F_{2v} * \acute{f}(x)\right)}{\sqrt{1 + \left(\acute{f}(x)\right)^2}} \tag{3-27}$$

$$M_2(x) = F_{2v} * (l - x) + F_{2h} * \left(f(x) - f(x_l)\right) + M_2$$

It is clear from Eq.(3-6) and Eq.(3-27) that the axial forces have identical formats and hence

$$\begin{aligned} \frac{\partial U_{A,2}}{\partial F_{2h}} &= \frac{\partial U_{A,1}}{\partial F_{1h}} \\ \frac{\partial U_{A,2}}{\partial F_{2v}} &= \frac{\partial U_{A,1}}{\partial F_{1v}} \\ \frac{\partial U_{A,2}}{\partial M_2} &= \frac{\partial U_{A,1}}{\partial M_1} = 0 \end{aligned} \tag{3-28}$$

In other words the axial stiffness matrices are identical as expected ($[\boldsymbol{I}_{A,2}] = [\boldsymbol{I}_{A,1}]$), and whether the curve $f(x)$ has a symmetry axis at the mid-point of the curve is not important. By applying Castigliano's second theorem to derive the displacements and rotation at node 2, along the direction of the applied forces and moments, the following flexibility terms are obtained.

$$\frac{\partial U_{B,2}}{\partial F_{2h}} = F_{2h}\int_0^{x_l}\frac{\left(f(x)-f(x_l)\right)^2\sqrt{1+\left(\acute{f}(x)\right)^2}}{EI}dx$$

$$+ F_{2v}\int_0^{x_l} -\frac{(x-x_l)*\left(f(x)-f(x_l)\right)\sqrt{1+\left(\acute{f}(x)\right)^2}}{EI}dx \qquad (3\text{-}29)$$

$$+ M_2\int_0^{x_l}\frac{\left(f(x)-f(x_l)\right)\sqrt{1+\left(\acute{f}(x)\right)^2}}{EI}dx$$

$$= F_{2h} * I_{B,F_{2h}F_{2h}} + F_{2v} * I_{B,F_{2h}F_{2v}} + M_2 * I_{B,F_{2h}M_2}$$

$$\frac{\partial U_{B,2}}{\partial F_{2v}} = F_{2h}\int_0^{x_l} -\frac{(x-x_l)*\left(f(x)-f(x_l)\right)\sqrt{1+\left(\acute{f}(x)\right)^2}}{EI}dx$$

$$+ F_{2v}\int_0^{x_l}\frac{(x-x_l)^2\sqrt{1+\left(\acute{f}(x)\right)^2}}{EI}dx \qquad (3\text{-}30)$$

$$+ M_2\int_0^{x_l} -\frac{(x-x_l)\sqrt{1+\left(\acute{f}(x)\right)^2}}{EI}dx$$

$$= F_{2h} * I_{B,F_{2v}F_{2h}} + F_{2v} * I_{B,F_{2v}F_{2v}} + M_2 * I_{B,F_{2v}M_2}$$

$$\frac{\partial U_{B,2}}{\partial M_2} = F_{2h}\int_0^{x_l}\frac{\left(f(x)-f(x_l)\right)\sqrt{1+\left(\acute{f}(x)\right)^2}}{EI}dx$$

$$+ F_{2v}\int_0^{x_l} -\frac{(x-x_l)\sqrt{1+\left(\acute{f}(x)\right)^2}}{EI}dx \qquad (3\text{-}31)$$

$$+ M_2\int_0^{x_l}\frac{\sqrt{1+\left(\acute{f}(x)\right)^2}}{EI}dx$$

$$= F_{2h} * I_{B,M_2F_{2h}} + F_{2v} * I_{B,M_2F_{2v}} + M_2 * I_{B,M_2M_2}$$

The comparison of Eqs. (3-29 to 3-31) and Eqs. (3-11 to 3-13) reveals that the flexural compliance matrices are not identical ($[\boldsymbol{I}_{B,2}] \neq [\boldsymbol{I}_{B,1}]$) for a general function

$f(x)$ and depends on if the curve $f(x)$ has a symmetry point (rotational symmetry of order 2) in the middle of the curve. Similarly, by rearranging Eqs. (3-29 to 3-31) in a matrix form, the relation between the nodal forces and corresponding displacements are:

$$\begin{bmatrix} F_{2h} \\ F_{2v} \\ M_2 \end{bmatrix} = \begin{bmatrix} I_{F_{2h},F_{2h}} & I_{F_{2h},F_{2v}} & I_{F_{2h},M_2} \\ I_{F_{2v},F_{2h}} & I_{F_{2v},F_{2v}} & I_{F_{2v},M_2} \\ I_{M_2,F_{2h}} & I_{M_2,F_{2v}} & I_{M_2,M_2} \end{bmatrix}^{-1} \begin{bmatrix} \delta_{2h} \\ \delta_{2v} \\ \theta_2 \end{bmatrix} \tag{3-32}$$

where each element of the flexibility matrix $\boldsymbol{I}_2$ is a sum of the factors due to axial and bending strain energy. Again by applying the proper boundary condition on node 2 the corresponding forces, representing the elements of the stiffness matrix are obtained. For $\begin{bmatrix} \delta_{2h} \\ \delta_{2v} \\ \theta_2 \end{bmatrix} = \begin{bmatrix} 1 \\ 0 \\ 0 \end{bmatrix}$

$$K_{44} = F_{2h} = \frac{\left(I_{F_{2v},F_{2v}} * I_{M_2,M_2}\right) - {I_{F_{2v},M_2}}^2}{\det(I_2)} \tag{3-33}$$

$$K_{45} = F_{2v} = \frac{\left(I_{F_{2v},M_2} * I_{M_2,F_{2h}}\right) - \left(I_{F_{2v},F_{2h}} * I_{M_2,M_2}\right)}{\det(I_2)} \tag{3-34}$$

$$K_{46} = M_2 = \frac{\left(I_{F_{2v},F_{2h}} * I_{M_2,F_{2v}}\right) - \left(I_{F_{2v},F_{2v}} * I_{M_2,F_{2h}}\right)}{\det(I_2)} \tag{3-35}$$

where $\det(I_2)$ is the determinant of the flexibility matrix $\boldsymbol{I}_2$. For $\begin{bmatrix} \delta_{2h} \\ \delta_{2v} \\ \theta_2 \end{bmatrix} = \begin{bmatrix} 0 \\ 1 \\ 0 \end{bmatrix}$

$$K_{54} = F_{2h} = \frac{\left(I_{F_{2h},M_2} * I_{M_2,F_{2v}}\right) - \left(I_{F_{2h},F_{2v}} * I_{M_2,M_2}\right)}{\det(I_2)} \tag{3-36}$$

$$K_{55} = F_{2v} = \frac{\left(I_{F_{2h},F_{2h}} * I_{M_2,M_2}\right) - {I_{F_{2h},M_2}}^2}{\det(I_2)} \tag{3-37}$$

$$K_{56} = M_2 = \frac{\left(I_{F_{2h},F_{2v}} * I_{M_2,F_{2h}}\right) - \left(I_{F_{2h},F_{2h}} * I_{M_2,F_{2v}}\right)}{\det(I_2)} \tag{3-38}$$

For the last case if $\begin{bmatrix}\delta_{2h}\\ \delta_{2v}\\ \theta_2\end{bmatrix} = \begin{bmatrix}0\\0\\1\end{bmatrix}$

$$K_{64} = F_{2h} = \frac{\left(I_{F_{2h},F_{2v}} * I_{F_{2v},M_2}\right) - \left(I_{F_{2h},M_2} * I_{F_{2v},F_{2v}}\right)}{\det(I_2)} \tag{3-39}$$

$$K_{65} = F_{2v} = \frac{\left(I_{F_{2h},M_2} * I_{F_{2v},F_{2h}}\right) - \left(I_{F_{2h},F_{2h}} * I_{F_{2v},M_2}\right)}{\det(I_2)} \tag{3-40}$$

$$K_{66} = M_2 = \frac{\left(I_{F_{2h},F_{2h}} * I_{F_{2v},F_{2v}}\right) - I_{F_{2h},F_{2v}}{}^2}{\det(I_2)} \tag{3-41}$$

Again by considering the equilibrium equations of the general curved beam the reaction forces of node1 are:

$$\begin{aligned} R_{1x} &= -F_{2h} \\ R_{1y} &= -F_{2v} \\ R_{M1} &= \left(F_{2h} * f(x_l)\right) - (F_{2v} * x_l) - M_2 \end{aligned} \tag{3-42}$$

Considering Eq. (3-42), the rest of elements of first three columns of the stiffness matrix are as follows. For $i = 4{:}6$

$$\begin{aligned} K_{i1} &= -K_{i4} \\ K_{i2} &= -K_{i5} \\ K_{i3} &= -\left(K_{i4} * f(x_l)\right) + (K_{i5} * x_l) - K_{i6} \end{aligned} \tag{3-43}$$

Equations (3-1 to 3-43) generate the stiffness matrix $[K_c]_{6\times6}$ for a general curved beam $f(x)$ defining the corrugated core unit cell. In order to calculate the stiffness matrix of the coating $[K_{el}]_{6\times6}$, which is illustrated schematically in Figure 3-2(a), the same procedure is repeated for a general line segment with the equation $g(x) = \frac{f(x_l)}{x_l}x$, $\forall x \in [0\ x_l]$. Therefore the stiffness matrix of the super element is obtained

from assembling stiffness matrix of these elements which have nodes in common, in other words:

$$K_s = K_c + K_{el} \tag{3-44}$$

3-4 Validation

Different models are considered in this section to verify the accuracy and efficiency of the presented super element of the corrugation curve symbolically and numerically. In the first part, the mechanical behaviour of a rotated straight beam predicted by the super element model is compared symbolically to those presented in the finite element literature. In the second part, a number of periods of a sine function were considered for the proposed super element and its mechanical behaviour under combined loading is compared to those calculated by ABAQUS.

3-4-1 Rotated straight beam

In order to validate the performance of the proposed super element symbolically, the simplest form of curved element is considered; a rotated straight beam element with rotation angle θ. According to finite element theory, the global stiffness matrix of a rotated beam element is given by $\boldsymbol{K_{global} = T^t * K_{local} * T}$, where $\boldsymbol{T}$ is the rotation transformation matrix. The same result is achieved in Eq. (3-45) by using the function $f(x) = x * \tan(\theta)$ in Eqs. (3-1 to 3-43). The global stiffness matrix of a straight rotated beam is presented as follows where C, S , E , A and I represent the $\cos(\theta)$, $\sin(\theta)$, the Young's modulus, the cross section area and the second moment of area, respectively.

$$\boldsymbol{K_{global}} = \begin{bmatrix} \left(\frac{C^2EA}{l}+\frac{12S^2EI}{l^3}\right) & \left(\frac{CSEA}{l}-\frac{12CSEI}{l^3}\right) & \left(\frac{-6SEI}{l^2}\right) & \left(\frac{-C^2EA}{l}-\frac{12S^2EI}{l^3}\right) & \left(\frac{-CSEA}{l}+\frac{12CSEI}{l^3}\right) & \left(\frac{-6SEI}{l^2}\right) \\ \left(\frac{CSEA}{l}-\frac{12CSEI}{l^3}\right) & \left(\frac{12C^2EI}{l^3}+\frac{S^2EA}{l}\right) & \left(\frac{6CEI}{l^2}\right) & \left(\frac{12CSEI}{l^3}-\frac{CSEA}{l}\right) & \left(\frac{-12C^2EI}{l^3}-\frac{S^2EA}{l}\right) & \left(\frac{6CEI}{l^2}\right) \\ \left(\frac{-6SEI}{l^2}\right) & \left(\frac{6CEI}{l^2}\right) & \left(\frac{4EI}{l}\right) & \left(\frac{6SEI}{l^2}\right) & \left(\frac{-6CEI}{l^2}\right) & \left(\frac{2EI}{l}\right) \\ \left(\frac{-C^2EA}{l}-\frac{12S^2EI}{l^3}\right) & \left(\frac{12CSEI}{l^3}-\frac{CSEA}{l}\right) & \left(\frac{6SEI}{l^2}\right) & \left(\frac{C^2EA}{l}+\frac{12S^2EI}{l^3}\right) & \left(\frac{-12CSEI}{l^3}+\frac{CSEA}{l}\right) & \left(\frac{6SEI}{l^2}\right) \\ \left(\frac{-CSEA}{l}+\frac{12CSEI}{l^3}\right) & \left(\frac{-12C^2EI}{l^3}-\frac{S^2EA}{l}\right) & \left(\frac{-6CEI}{l^2}\right) & \left(\frac{-12CSEI}{l^3}+\frac{CSEA}{l}\right) & \left(\frac{12C^2EI}{l^3}+\frac{S^2EA}{l}\right) & \left(\frac{-6CEI}{l^2}\right) \\ \left(\frac{-6SEI}{l^2}\right) & \left(\frac{6CEI}{l^2}\right) & \left(\frac{2EI}{l}\right) & \left(\frac{6SEI}{l^2}\right) & \left(\frac{-6CEI}{l^2}\right) & \left(\frac{4EI}{l}\right) \end{bmatrix} \tag{3-45}$$

3-4-2 Sine wave profile

In this section the accuracy of the proposed element is investigated as a function of the length and curvature of the element. A number of periods of the function $f(x) = \sin(x)$ were considered for the proposed super element. Figure 3-4(b) shows five deformed and undeformed shapes of a simple sine wave with 2^Nperiods, where $N = 0,1,2,3,4$. In each case, all degrees of freedom at node 1 were fixed and unit displacements in both horizontal and vertical directions, as well as a unit rotation was applied to node 2 as its boundary condition. The nodal reaction forces and moments were compared to those calculated by ABAQUS in which $544 * 2^N$ beam elements with cubic shape functions were used to mesh the sine profile for each case. Figure 3-4(a) shows the percentage error versus the length of the sine profile. The error is smaller than 0.025% for 16 periods of sine profile, which was discretised with 8704 elements in ABAQUS. This shows the efficiency and accuracy of the proposed method.

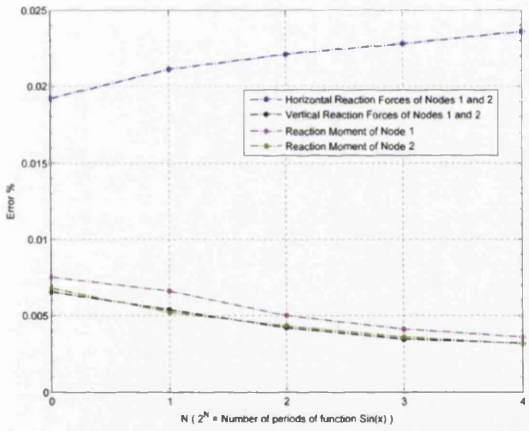

(a) Percentage error

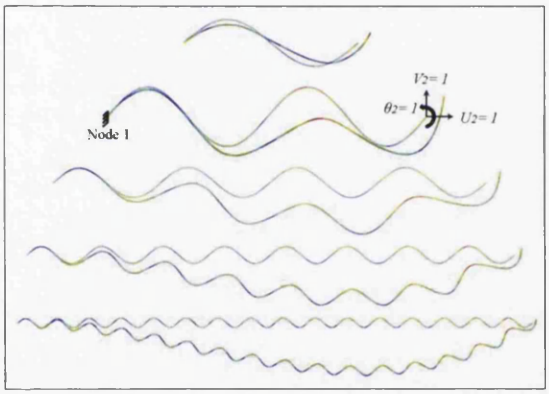

(b) Deformed and undeformed shapes of a simple sine profile

Figure 3-4: Five deformed and undeformed shapes of a simple sine wave

3-5 Corrugation curve study

In morphing skin applications, the in-plane tensile stiffness of the corrugated panel is directly related to the actuation force required to change the camber of the aerofoil. However the out of plane bending stiffness of the corrugated panel is inversely related to the local deformation of the skin of the aerofoil due to the external pressure caused by the airflow. Maximizing the ratio of the equivalent EI to

the equivalent EA, i.e. $\frac{EI_{eq}}{EA_{eq}}$, of the corrugated panel is one of the required design objectives. In this section the effect of the corrugation shape on the ratio $\frac{EI_{eq}}{EA_{eq}}$ is studied. From experimental data (Dayyani et al., 2013), the Young's modulus of the corrugated core and the elastomeric skin were assumed to be 4500MPa and 13.5MPa, while their thicknesses were assumed to be 1mm and 0.8mm, respectively. The width of the panel was 25mm.

3-5-1 Trapezoidal corrugation shape

Trapezoidal corrugated cores have received most interest in comparison to other corrugation configurations in the literature, mainly due to their ease of manufacture. In this section the effect of parameters defining the trapezoidal corrugation shape on the ratio of $\frac{EI_{eq}}{EA_{eq}}$ is investigated. As shown in Figure 3-5(b) any symmetric trapezoidal shape is defined by means of four independent parametersa_1, a_2, a_3 and h. To reduce the number of parameters, a constraint of $a_1 = a_3$ is applied. By means of the Heaviside step function, the trapezoidal shape function $f(x)$ is defined as Eq. (3-46). The length of the corrugation unit cell is assumed to be 30mm, which imposes another constraint: $2a_1 + a_2 = 15$.

$$f(x) = \frac{h}{a_2}(x - a_1) * (\langle x - a_1 \rangle - \langle x - (a_1 + a_2) \rangle) + h * (\langle x - (a_1 + a_2) \rangle - \langle x - (3a_1 + a_2) \rangle) - \frac{h}{a_2}(x - (3a_1 + 2a_2)) * (\langle x - (3a_1 + a_2) \rangle - \langle x - (3a_1 + 2a_2) \rangle) \quad (3\text{-}46)$$

Figure 3-5(a) shows the effect of a_2 and h on the ratio of $\frac{EI_{eq}}{EA_{eq}}$, and highlights that this ratio is sensitive to both h and a_2. As the height of the corrugated unit cell increases, the equivalent axial stiffness of the panel reduces more quickly than the bending stiffness. On the other hand, for a constant height of corrugation when the parameter a_2 decreases, the angle of the corner of the corrugated unit cell decreases, which results in a significantly smaller equivalent tensile stiffness. More details for the mechanism of deformation of the trapezoidal corrugation unit cell are reported in the literature (Xia et al., 2012).

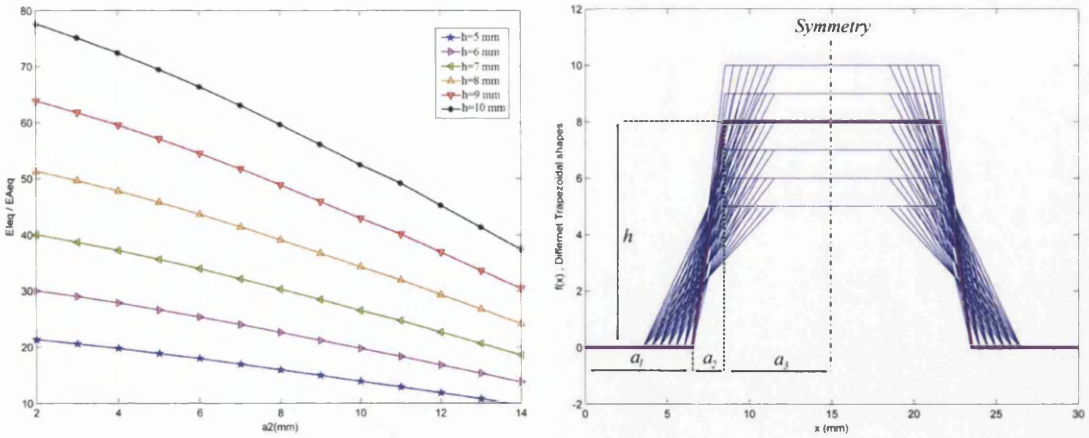

(a) (b)

Figure 3-5: Different variations of the trapezoidal corrugated unit cell and the corresponding $\frac{EI_{eq}}{EA_{eq}}$

3-5-2 Polynomial corrugation shape

An important question in the application of coated corrugated cores for morphing skins is the optimum curve for the corrugation that satisfies the different objective functions such as: maximum $\frac{EI_{eq}}{EA_{eq}}$ and minimum weight. Although topology optimization is beyond the scope of this chapter, the capability of the presented method to estimate the equivalent stiffnesses for unusual geometries is presented briefly in this section. As mentioned before, members 2 and 3 in Figure 3-2(a) have a major role in the deformation mechanism of the coated corrugated core. One possible corrugation curve for member 2 is a polynomial function $f(x)$ introduced in Eq. (3-47). It is assumed that the length of member 1 and the height of the corrugation are 5mm and 10mm, respectively. Therefore the boundary conditions of $f(x)$ are: $f(0) = 0$ and $f(20) = 0$.

$$f(x) = 10^{-2n+1} * \big(x * (20 - x)\big)^n \tag{3-47}$$

Figure 3-6(b) shows the polynomial function $f(x)$ for $n = 1{:}\,10$ as a corrugation curve. The ratio of $\frac{EI_{eq}}{EA_{eq}}$ for both coated and uncoated corrugated unit cells is shown in Fig. 3-6(a).

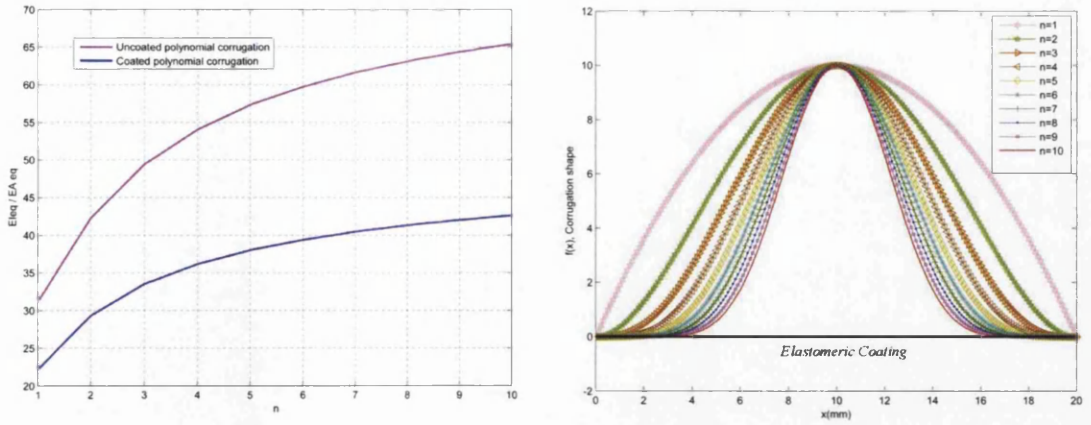

(a) (b)

Figure 3-6: Different variations of the polynomial function for the corrugation unit cell with and without elastomeric coating and the corresponding $\frac{EI_{eq}}{EA_{eq}}$

The key role of the elastomer in reducing the stiffness ratio $\frac{EI_{eq}}{EA_{eq}}$ is shown in Fig. 3-6(a). This is mainly because the out of plane stiffness of the elastomer coating is very low and the elastomer behaves as a spring that undergoes only tension. Thus the elastomer resists the gap opening between two adjacent crests of each unit cell of the corrugated core and hence the equivalent axial stiffness of the coating, EA_{eq}, increases more that the equivalent bending stiffness, EI_{eq}.

3-6 Conclusion

By considering the geometric and mechanical properties of the corrugated panel, a generic super element of corrugated core unit cell with elastomeric coating for the application in morphing structures is investigated in this chapter. The importance of this work, in contrast to the literature, is that it provides an exact analytical equivalent model which avoids any homogenization assumptions. By using the direct stiffness method and Castigliano's second theorem, and by applying proper boundary conditions, the stiffness matrix of the generic super element is derived which can capture the small deformation of 2D thin curved beams with variable curvatures. Different numerical and analytical symbolic models are investigated to verify the accuracy and efficiency of the presented super element. The super element uses the geometric and mechanical properties of the panel as variables, and hence the model may be used for topology optimization studies. The parametric studies of

trapezoidal and polynomial corrugation shapes demonstrate the suitability of the proposed super element for application in further complex design investigations.

Chapter 4:
The Design of a Coated Composite Corrugated Skin for the Camber Morphing Aerofoil

4-1 Introduction

This chapter presents the design and optimization of an elastomer coated composite corrugated skin for the Fish Bone Active Camber morphing aerofoil concept. This morphing structure consists of an internal compliant core composed of a thin chord wise bending beam spine with periodic stringer reinforcement to support the skin surface. Recently, the static behaviour of coated composite corrugated panels has been investigated independently of the internal wing structure through experimental analysis, numerical simulations and analytical equivalent modelling. However, as a proposed candidate for the skin of a morphing wing, the behaviour of these corrugated panels must be investigated comprehensively and optimized in terms of aero-elastic effects and the boundary conditions arising from the internal wing structure. In this chapter, the geometric parameters of the coated composite corrugated panels are optimized to minimize the in-plane stiffness and the weight of

the skin and to maximize the flexural out-of-plane stiffness of the corrugated skin. The effect of the stringers of the FishBAC as the boundary conditions for the elastomer coated corrugated panel is considered in the optimization process. A finite element code for thin beam elements is used with the aggregate Newton's method to optimize the geometric parameters of the coated corrugated panel. The trend of the optimized objectives and parameters are discussed in detail. The obtained results provide important insights into the design of morphing corrugated skins. The advantages of the corrugated skin over the elastomer skin for the FishBAC morphing structure are discussed. Moreover, a finite element simulation of the FishBAC internal structure with the corrugated skin is performed under typical aerodynamic and structural loadings to check the design approach.

4-2 Problem statement

Actively varying an aerofoil's camber is an effective way to change the aerodynamic forces and moments generated by a wing. This allows for control of the vehicle's flight path and optimization of the aerodynamic performance over different flight regimes. Traditionally, camber variation has been accomplished through the use of discrete trailing edge flaps, and indeed this is the solution employed by nearly all aircraft currently flying. However, there has long been an interest in the aerospace industry in technologies which would allow for a more smooth and continuous change in camber than that of a flap. The many different concepts explored over the last several decades have been summarized in several review papers (Barbarino et al., 2011). These systems are being pursued for the promise of a reduction in the significant drag penalty associated with flap deflections. In order to be effective, the control authority of the morphing mechanism must be substantial. The primary motivation for the use of a given morphing technology must be that it can radically alter the performance of the wing. Without a significant impact on the net aerodynamic performance, it is very hard to justify the added weight, complexity, and cost of morphing systems, and they are therefore not likely to come to fruition. Moreover, it is of necessity that the morphing design be as simple as possible. The simplicity of the design would result in rapid reduction of the cost, minimization of the use of mechanical elements, and potentially a reduction in the weight of the

mechanism. Avoiding design complexity decreases the maintenance requirements as well.

The Fish Bone Active Camber (FishBAC) concept (Woods and Friswell, 2012) has been designed in light of these design criteria. It combines several different structural aspects into a single concise design concept. The biologically inspired compliant structure consists of a thin chord wise bending beam spine with stringers branching off to connect it to the coated corrugated skin surface. Actuators mounted in the non-morphing leading edge induce bending moments on the spine through an antagonistic pair of tendons. Figure 4-1 shows the baseline FishBAC concept built around an anisotropic compliant structural core. The baseline design uses a pre-tensioned elastomeric matrix composite (EMC) skin. Continuous bending deflections are driven by a high stiffness, non-backdrivable, antagonistic tendon system. This chapter considers the same morphing concept with the EMC replaced with an elastomer coated composite corrugated skin.

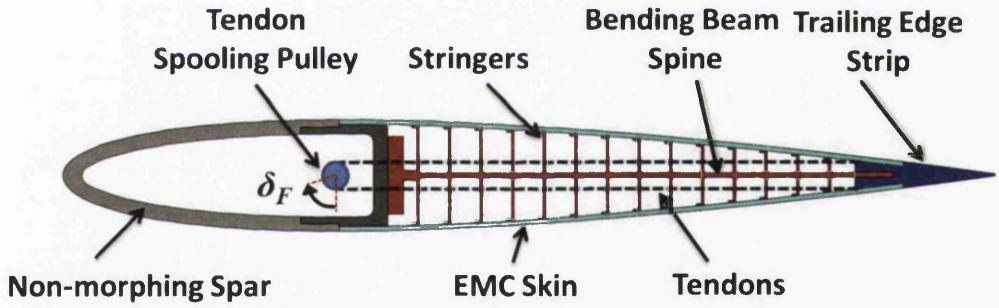

Figure 4-1: The baseline FishBAC concept (Woods and Friswell, 2012)

Although some research has been performed on the mechanical behavior of corrugated structures, no investigations have considered the corrugated skin on top of a morphing internal structure. As a result of considering the interaction of the skin and internal structure in the real application, new effects will arise, such as the effects of boundary conditions and constraints. Hence the applicability of the papers in the literature to system level optimization and the design of a morphing wing is still an open question. This chapter considers the FishBAC compliant concept for the internal structure of a camber morphing aerofoil. The elastomeric matrix composite (EMC) in this concept is replaced with an elastomer coated composite corrugated skin. Figure 4-2 shows the FishBAC concept which uses the coated corrugated core

as its morphing skin. This compliant structure consists of a thin chord wise bending beam spine with stringers branching off to connect it to the skin.

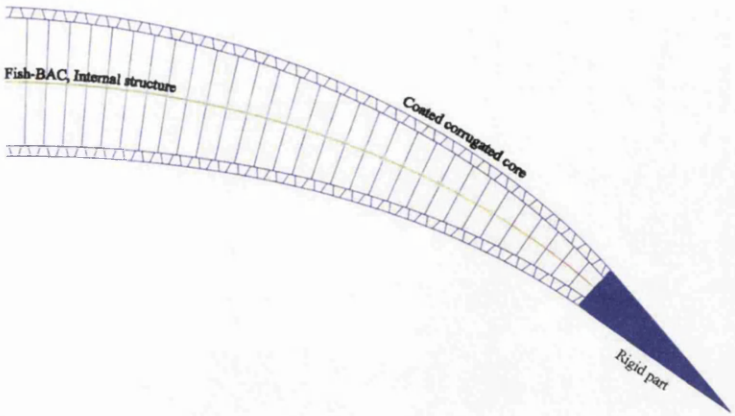

Figure 4-2: Schematic of the application of the coated corrugated skin on the camber morphing trailing edge

Considering the application of a corrugated panel for the morphing skin, the first question to be answered is which corrugation shape has more out-of-plane stiffness and less in-plane stiffness. These parameters are important because higher out-of-plane stiffness of the skin results in smaller bending deformation under aerodynamic loading. Moreover this increases the buckling stiffness of the skin, when the skin is subjected to compression due to morphing actuation. In other words the higher out-of-plane stiffness of the skin results in a smoother surface of the wing during flight. In contrast to the out-of-plane stiffness, minimizing the in-plane stiffness results in less resistance of the skin to actuation of the morphing FishBAC deformations, thereby reducing the force and energy requirements. A perfect skin for morphing application should have a very high out of plane stiffness and a very low in plane stiffness. However in practice these two stiffnesses are coupled; the increase in one results in the increase of the other. Hence, investigating the effect of the various corrugation shapes on the balance of these two stiffnesses and selecting the proper corrugation shape is a necessary step before starting the optimization.

4-2-1 Mechanical properties of different corrugation shapes

To find the optimum corrugation shape that has high out-of-plane stiffness and low in-plane stiffness, three typical configurations are selected as shown in Fig. 4-3. The

sinusoidal corrugation shape is not included since the presence of a single line of contact between the elastomer coating and corrugated core, as opposed to the rectangular contact surfaces of the other configurations, provides insufficient area for bonding. In this initial study the portion of the elastomer coating which overlaps the corrugation is neglected since the ratio of elastomer Young's modulus to composite core material Young's modulus is very small (Dayyani et al., 2013). The composite corrugated core and elastomeric coating are labelled in Fig. 4-3.

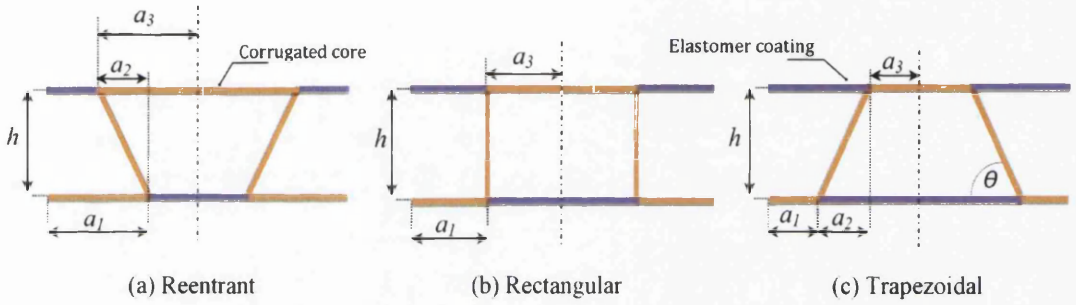

(a) Reentrant (b) Rectangular (c) Trapezoidal

Figure 4-3: Three typical corrugation shapes

Based on Fig. 4-3, six corrugated cores with and without elastomeric coating were modelled in ABAQUS. Each model consisted of 10 unit cells. In order to make a true comparison between these configurations, the values of parameters in each configuration are selected to keep the consistency of the length and the height of the corrugated unit cell in all cases. Table 4-1 presents the values corresponding to the parameters of the three corrugation configurations of Fig. 4-3. The thickness of the corrugated core and elastomeric coatings and the width of the panel for all cases were 1mm, 0.8mm and 25mm respectively. Glass fibre and elastomer with Young's modulus of 4.5 GPa and 13 MPa were considered for the corrugated core and coatings respectively. More details are presented in the literature (Dayyani et al., 2013).

Table 4-1: Parameters of the three corrugation configurations of Fig. 4-3, all values in (mm)

Parameters/ Configuration	a_1	a_2	a_3	h
Reentrant	10	5	10	10
Rectangular	7.5	0	7.5	10
Trapezoidal	5	5	5	10

Two sets of boundary conditions were applied to each model. In the first set, all degrees of freedom of one end of the panel were fixed whereas a displacement boundary condition of 200 mm in the out-of-plane direction was applied to the other end of the panel, to simulate cantilever bending. In the second set, all degrees of freedom of one end of the panel were fixed, and a displacement boundary condition of 100 mm for the in-plane displacement was applied to the other end of the panel, to give a simple tensile test. In all cases a fine mesh of beam elements was used.

Figure 4-4 shows the force displacement curves for reentrant, rectangular and trapezoidal corrugated cores with and without elastomeric coating. The interesting point in Fig. 4-4 is that although the uncoated trapezoidal corrugated core has maximum tensile and bending stiffness, adding the elastomeric coating to the corrugated core results in minimum bending and tensile stiffness in contrast to other configurations. This story is reversed for the reentrant corrugation shape.

Considering the mechanism of deformation in the corrugated core, applying a tensile boundary condition to the reentrant corrugated core results in deformations that change the reentrant corrugation pattern to a rectangular and then to a trapezoidal configuration. Moreover the presented analytical solutions for tensile and bending stiffness of the uncoated corrugated cores (Dayyani et al., 2012) revealed that, with a fixed length of unit cell, the unit cell with smaller θ, as illustrated in Fig. 4-3(c), has a more flattened shape and therefore has increased tensile and bending stiffness. Therefore the uncoated trapezoidal corrugation has more stiffness compared to the uncoated rectangular and reentrant corrugations. But adding the elastomeric coating to the corrugated core, reverses the order of each configuration stiffness. This is due to the fact that the gap between two adjacent corners of a unit cell of a reentrant corrugated core is smaller than it is for the rectangular and

trapezoidal corrugations and hence there is less available elastomer length to strain, resulting in higher elastomer strains to achieve a given global skin strain and an increase in stiffness.

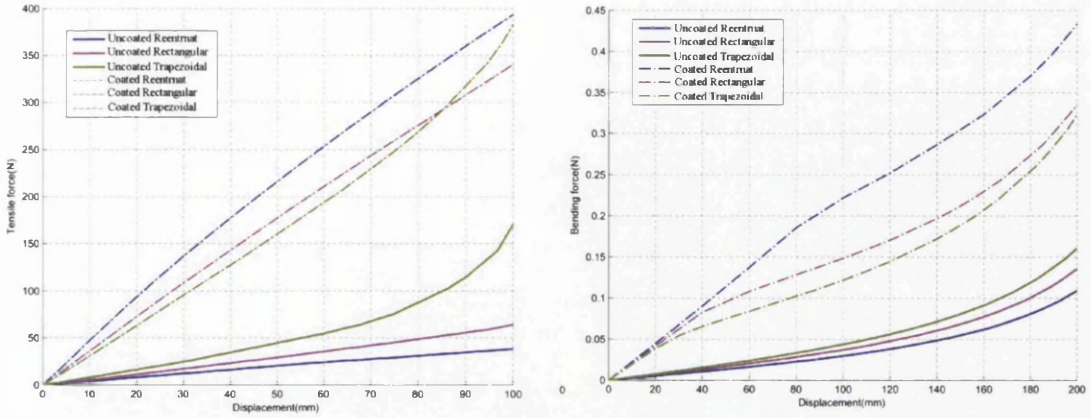

(a) Tensile (b) Bending

Figure 4-4: Force displacement curves for reentrant, trapezoidal and rectangular corrugated core with and without elastomeric coating

Figure 4-5 shows a comparison of the bending flexibility and tensile stiffness for different corrugation types. The different configurations of the uncoated corrugated cores have 6.7 times more out-of- plane flexibility than the coated corrugated configurations on average. In contrast, although the coated corrugated cores have better aerodynamic surfaces and smaller out-of -plane flexibility, they have 5.5 times more in-plane stiffness than the uncoated corrugated configurations on average.

Moreover, considering the corrugation geometries and the corresponding values of their parameters represented in Fig. 4-3 and Table 4-1 and the density of the composite core and elastomeric coating presented in Table 4-4, the mass of the skin for different corrugation types were calculated precisely by including the elastomeric coating in the overlapped regions with the corrugated core. The calculation reveals that the coated re-entrant and coated rectangular corrugated cores are 30% and 11% heavier than the coated trapezoidal corrugated core.

In terms of the morphing skin application, the preferred skin must have the minimum tensile stiffness and bending flexibility as well as a smooth aerodynamic surface. Therefore as a starting point of the multi-objective optimization of the corrugated skin, the coated trapezoidal configuration is selected as the preferred configuration for the morphing skin.

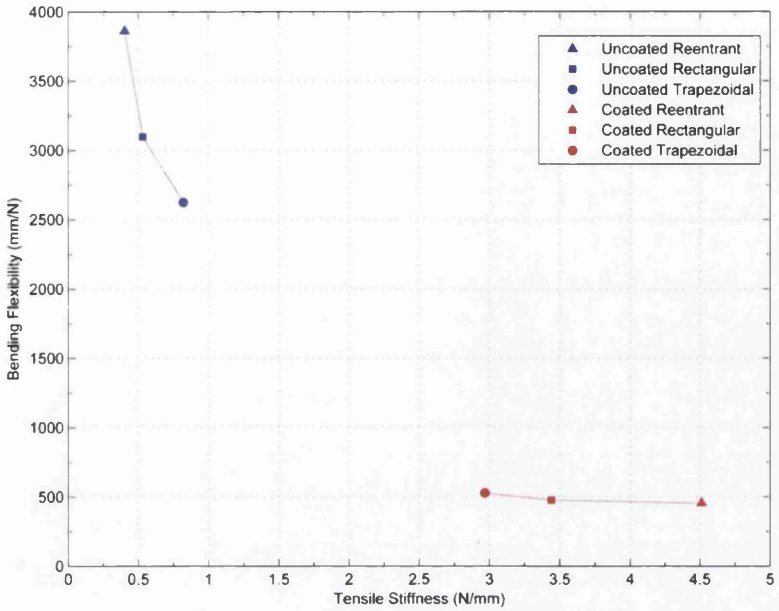

Figure 4-5: A comparison of the bending flexibility and tensile stiffness for different corrugation shapes

4-2-2 Finite element analysis

After selecting the configuration of the corrugation, a finite element code for beam elements was generated in MATLAB that calculates the equivalent tensile, flexural stiffness and the mass of a coated trapezoidal corrugated core with 4 unit cells. The parameters a_1, a_2, a_3 and h defining the geometry of a trapezoidal corrugated unit cell, and t_c and t_e representing the thickness of the corrugated core and elastomeric coating, were the inputs to the FE code. The width of the panel was set to 25 mm. Furthermore, the material properties were defined by means of $\rho_c$and ρ_e representing the density of the composite core and elastomeric coating, and E_c and E_e representing the Young's modulus of the composite core and elastomeric coating. As mentioned in section 4-2-1 since the ratio of elastomer Young's modulus to glass fibre Young's modulus is very small, the elastomer coatings were neglected in the areas overlapped with the composite corrugated core. This assumption is valid because these two materials are assumed to be well adhered together. Consequently they would have the same displacement and hence the strain energy of the coating would be very small compared to the strain energy of the corrugated core in the overlapped areas (Dayyani et al., 2013).

Three degrees of freedom U_x, U_y and θ_z in the global coordinate system were considered at each node. The coated corrugated structure was discretized by 26 elements. The global stiffness matrix of each element with rotation angle of θ is given below, as described in chapter 3, Eq. 3-45. It must be mentioned that the proposed super element in chapter 3 is exactly the same as classic finite element theory for straight thin beams. In this chapter the classic finite element method is used to reduce the computation time, especially when considering several optimization loops in which the equivalent FE code is called.

$$K_{global} = \begin{bmatrix} \left(\frac{C^2EA}{l}+\frac{12S^2EI}{l^3}\right) & \left(\frac{CSEA}{l}-\frac{12CSEI}{l^3}\right) & \left(\frac{-6SEI}{l^2}\right) & \left(\frac{-C^2EA}{l}-\frac{12S^2EI}{l^3}\right) & \left(\frac{-CSEA}{l}+\frac{12CSEI}{l^3}\right) & \left(\frac{-6SEI}{l^2}\right) \\ \left(\frac{CSEA}{l}-\frac{12CSEI}{l^3}\right) & \left(\frac{12C^2EI}{l^3}+\frac{S^2EA}{l}\right) & \left(\frac{6CEI}{l^2}\right) & \left(\frac{12CSEI}{l^3}-\frac{CSEA}{l}\right) & \left(\frac{-12C^2EI}{l^3}-\frac{S^2EA}{l}\right) & \left(\frac{6CEI}{l^2}\right) \\ \left(\frac{-6SEI}{l^2}\right) & \left(\frac{6CEI}{l^2}\right) & \left(\frac{4EI}{l}\right) & \left(\frac{6SEI}{l^2}\right) & \left(\frac{-6CEI}{l^2}\right) & \left(\frac{2EI}{l}\right) \\ \left(\frac{-C^2EA}{l}-\frac{12S^2EI}{l^3}\right) & \left(\frac{12CSEI}{l^3}-\frac{CSEA}{l}\right) & \left(\frac{6SEI}{l^2}\right) & \left(\frac{C^2EA}{l}+\frac{12S^2EI}{l^3}\right) & \left(\frac{-12CSEI}{l^3}+\frac{CSEA}{l}\right) & \left(\frac{6SEI}{l^2}\right) \\ \left(\frac{-CSEA}{l}+\frac{12CSEI}{l^3}\right) & \left(\frac{-12C^2EI}{l^3}-\frac{S^2EA}{l}\right) & \left(\frac{-6CEI}{l^2}\right) & \left(\frac{-12CSEI}{l^3}+\frac{CSEA}{l}\right) & \left(\frac{12C^2EI}{l^3}+\frac{S^2EA}{l}\right) & \left(\frac{-6CEI}{l^2}\right) \\ \left(\frac{-6SEI}{l^2}\right) & \left(\frac{6CEI}{l^2}\right) & \left(\frac{2EI}{l}\right) & \left(\frac{6SEI}{l^2}\right) & \left(\frac{-6CEI}{l^2}\right) & \left(\frac{4EI}{l}\right) \end{bmatrix} \quad (3\text{-}45)$$

where C, S, E, A and I represent the $\cos(\theta)$, $\sin(\theta)$, the Young's modulus, the cross section area and the second moment of area of the element, respectively. Enlarging and assembling the stiffness matrix of all of the elements resulted in the assembled stiffness matrix of the coated corrugated core as: $[K_{structure}]_{60*60}$. While almost all degrees of freedom at one end of the panel were fixed, two prescribed displacements in the x direction and y direction were applied separately to one end of the panel for each model to calculate the tensile and bending stiffness of the panel. The boundary conditions applied to the coated corrugated core in tensile and bending models are presented in Table 4-2.

Table 4-2: Prescribed boundary conditions applied to the coated corrugated core in tensile and bending models

Node Labels (Fig. 4-6)	Prescribed DOFs					
	Tensile modelling			Bending modelling		
	U_x	U_y	θ_z	U_x	U_y	θ_z
1	0	0	0	0	0	0
18	3(mm)	0	0	free	-1(mm)	free
19	3(mm)	free	0	free	-1(mm)	free
20	0	free	0	0	0	0

Figure 4-6 shows the deformed and undeformed configurations of the coated corrugated core subjected to the tensile and bending displacements. The obtained results were verified against ABAQUS results with a fine mesh and the difference between them was smaller than 1%. This high accuracy is because the cubic shape functions of the beam element interpolate the deformations precisely. Although discretising the corrugated structure with more beam elements would modify the results slightly it would increase the computation time, especially since FE code is called more than10000 times in the optimization loops for each configuration of the FishBAC stringers and corrugation unitcells. Moreover, it must be mentioned that the difference between the equivalent properties of a long corrugated panel and a corrugated panel with 4 unit cells was examined in ABAQUS and was smaller than 1%.

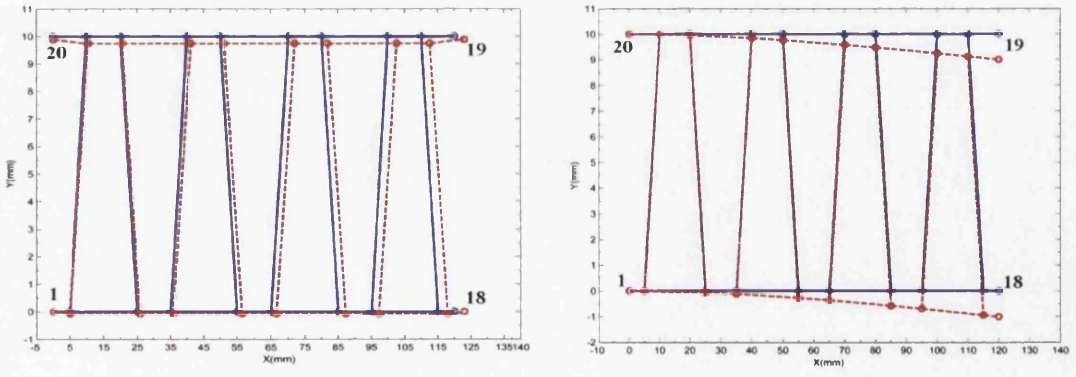

(a) Tensile (b) Bending

Figure 4-6: The deformed and undeformed configurations of coated corrugated panel

4-2-3 Multi-objective optimization

Figure 4-7 illustrates the geometry of the FishBAC which supports the coated corrugated skin. The length l_{morph}, between the rigid leading edge and rigid trailing edge, was fixed as 160mm, which is equivalent to 52% of the chord length.

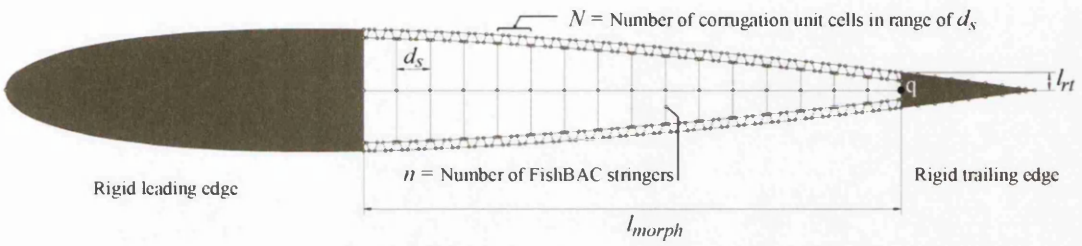

Figure 4-7: FishBAC geometry with the coated corrugated skin

Different possible configurations of FishBAC stringers and the corrugated skin were considered in the optimization problem. The number of FishBAC stringers, n, was allowed to vary between 3 to 15. Based on the distance between two adjacent stringers, i.e. d_s, and manufacturing constraints the number of corrugation unit cells, N, was allowed to vary from 1 to N_{final} which is calculated by rounding down the ratio d_s/L_{uc_a}. The parameter L_{uc_a} refers to the minimum allowable length of a corrugation unit cell which was set to 5mm due to manufacturing limits. Table 4-3 presents different configuration of stringers and unit cells in the optimization problem.

Table 4-3 Different configuration of stringers and unit cells in the optimization

$n_{stringers}$	3	4	5	6	7	8	9	10	11	12	13	14	15
$N_{unitcells}$	[1-8]	[1-6]	[1-5]	[1-4]	[1-4]	[1-3]	[1-3]	[1-2]	[1-2]	[1-2]	[1-2]	[1-2]	[1-2]

Table 4-3 presents the fact that increasing the number of stringers reduces the range of the number of unit cells due to the minimum allowable length restriction. The height of the rigid part at the end of trailing edge, which is shown as l_{rt} in Fig. 4-7, was used as a criterion of the upper bound for the height of the corrugated unit cell. The value for this parameter was estimated as 5.21mm in the FishBAC geometry. The materials for the composite core and the elastomer coating in corrugated skin are selected from the literature. Table 4-4 presents the values of the density and Young's modulus for glass fibre and the elastomer coating.

It might be a good idea to mention that so far there was not found any paper in the literature with regards to optimization of the FishBAC internal structure, even with simple elastomeric skin. Therefore, the full optimization of the internal structure and the corrugated skin is required for future studies although it will be much more time consuming and expensive. This is due to the fact that more optimization parameters will play role in this problem. For example the distance between each two stringers or the angle between each stringer and the main spine will be a new parameter. Moreover this set of new parameters will impose new nonlinear constraints on the position of the unit cells of the corrugated skin, since the stringers are supporting the corrugated skin. Furthermore the type of objective functions in the full optimization problem would be different from the current structural objective functions. For instance maximizing lift to drag or minimizing the actuation energy of the whole system will be new objective functions that not necessary can be represented by equivalent structural characteristics such as: EA_{eq} and EI_{eq}. Therefore, more analysis like aerodynamics and kinematics will be involved which increases the complexity and the cost of computations. Hence, the way of selecting uniform distance between stringers not only helps to avoid further complexity and computation costs but provides the opportunity to detect more details of the function of each component. For example the ideal skin has the maximum out of plane stiffness and the maximum inplane flexibility. Hence all the aerodynamic loads will be carried just by the skin, but yet the function of the internal structure for actuation is important. The internal structure imposes the constraints and boundary conditions on the skin to deform as it is desired. This study provides reasonable arguments for further complex optimization studies which consider the effects of aeroelasticity, actuation and fatigue.

Table 4-4: Fixed material properties of the corrugated skin

Variables	Description	Values
ρ_c	density of composite corrugated core (Reddy, 1997)	0.001799 g/mm^3
ρ_e	density of elastomer coating (Bhowmick and Stephens, 2000)	0.000878 g/mm^3
E_c	Young's modulus of composite corrugated core (Reddy, 1997)	34473 MPa
E_e	Young's modulus of elastomer coating (Bhowmick and Stephens, 2000)	10 MPa

The focus of the chapter is the optimization of the geometric parameters of the corrugated skin. However it may be necessary to perform a full optimization of both geometry and material properties of the coated corrugated panel for the design of these structures. The full optimization solution requires an expression to relate the Young's modulus and density of materials. Usually materials with higher Young's modulus have higher density and a database could be used to select a material from a number of candidates. On the other hand, considering the development of technology in material engineering, it is probable to have new materials with higher Young's modulus and lower density, which is beyond the scope of this chapter.

Table 4-5 shows the geometrical parameters of a coated corrugated core and their corresponding upper and lower bounds. The parameter L_{hu} represents the length of half of the unit cell and may be calculated as: $L_{hu} = \frac{d_s}{2N}$.

Table 4-5: The variables of the optimization problem and their bounds

Variables	Description	Lower bound	Upper bound
t_c	Thickness of composite corrugated core	$L_{hu}/30$ (mm)	$2L_{hu}/30$ (mm)
t_e	Thickness of elastomer coating	$L_{hu}/30$ (mm)	$4L_{hu}/30$ (mm)
a_1	Corrugation unit cell geometry	$L_{hu}/6$ (mm)	$2L_{hu}/3$ (mm)
a_2		$L_{hu}/6$ (mm)	$2L_{hu}/3$ (mm)
a_3		$L_{hu}/6$ (mm)	$2L_{hu}/3$ (mm)
h		$l_{rt}/2$ (mm)	$9l_{rt}/10$ (mm)

Selecting the upper and lower bounds for the thickness of both the corrugated core and the elastomeric coatings was based on practical considerations and the consistency of the analysis with Euler-Bernouli beam theory. In other words, the ratio of the thickness to the length of each member in a corrugation unitcell is smaller than 0.1. Furthermore, the properties of the corrugated skin arise from localized bending within the corrugations; if the ratio of the thickness of the corrugated core to the length of a unit cell is too high, then the mechanism of the deformation changes, resulting in a panel that is too stiff, especially when the size of the corrugation is very small. The lower bounds are set by the availability of suitable material and its robustness and handling properties. The upper bound and lower bound for a_1, a_2, a_3 were selected to be consistent with the geometry of a trapezoidal shape. Considering the application of the corrugated panel for a morphing skin, the height of the corrugated unit cell is dependent on the external parameter l_{rt} which is the maximum size that the height of the panel can be. Based on Fig. 4-3 (c) the equation $a_1 + a_2 + a_3 = L_{hu}$ was considered as the only explicit constraint of the optimization problem, where L_{hu} is representing the half of the length of unit cell and is implicitly constrained by the number of FishBAC stringers and corrugation unit cells. The following three objectives are minimized: the

equivalent tensile stiffness EA_{eq}, the inverse of the equivalent flexural stiffness $\frac{1}{EI_{eq}}$ and the mass of the skin. In order to ensure the best performance of the optimization scheme all the parameters are normalized as

$$x_n(i) = \frac{2\big(x(i) - \bar{x}(i)\big)}{x_u(i) - x_l(i)} \quad ,i = 1,2,\dots,6 \tag{4-1}$$

where x is the vector of parameters, x_u and x_l are the corresponding upper and lower bound vectors, $\bar{x}$ is the average vector of upper bound and lower bound values and x_n is the normalised vector of parameters. The objective functions are also normalised as

$$f_n = \frac{f(x)}{f(\bar{x})} \tag{4-2}$$

4-2-4 Selecting the multi-objective optimization method

In general two different types of techniques are used to solve multi objective optimization problems. These two types are known as classical methods and evolutionary methods. The classical methods, which are mainly non-Pareto based techniques, consist of converting the multi objective problem into a single objective problem. This is possible by either aggregating the objective functions or optimizing one objective and treating the other as constraints. This new single objective function will then be optimized for different configurations of weights of objective functions. The classic aggregate method is easy to implement especially for a few objectives and is efficient for some multi-objective optimization problems with convex Pareto fronts. On the other hand the evolutionary methods mainly use nondominated ranking and selection, to move the population towards the Pareto front. These methods require a ranking procedure and a technique to maintain the diversity in the population so as to avoid converging to a single solution, because of the stochastic noise involved in this process (Coello, 1999; Fonseca and Fleming, 1993; Marler and Arora, 2004). These evolutionary approaches are less susceptible to the shape or continuity of the Pareto front. However in many cases the Pareto curves cannot be computed efficiently, even if it is theoretically possible to find all these points exactly. That is because they are often of exponential size and hence quite hard to

compute, which is why approximation methods for these techniques are frequently used. In this section the aggregate method from the classic methods and the Genetic Algorithm (GA) from the evolutionary techniques are used to solve the multi objective optimization problem of the specific case 15.1 corresponding to $n_{stringer}$=15 and $N_{unitcell}$=1. The results obtained from both methods are compared and the multi-objective optimization technique investigated in this chapter is selected.

4-2-4-1 Aggregate method

In this section the multi-objective problem is solved by combining three objectives into a single-objective scalar function. This approach is also known as the ''weighted-sum'' or ''scalarization'' method. In more detail, the aggregate method minimizes a positively weighted convex sum of the objectives as shown in Eq. (4-3). This new single objective optimization problem is then solved using the ''fmincon'' command which is a Newton gradient based method in MATLAB.

$$min \sum_{i=1}^{3} w_i f_i(x) \tag{4-3}$$

where $w_i \geq 0$ are the weighting coefficients representing the relative importance of the objective functions $f_i(x)$ and x is the vector of the input parameters in the optimization problem. It is assumed that the sum of the weights is equal to one, i.e.:

$$\sum_{i=1}^{3} w_i = 1 \tag{4-4}$$

This technique is ideal for cases where preferential information about the objectives is known in advance. However, it is possible to achieve the non-dominated front by considering a broader interval of the aggregation parameters. Since the solutions of this optimization problem can vary significantly as the weighting coefficients change, and because very little is usually known about choosing these coefficients, it is necessary to solve the same problem for many different values of these weights. Hence the weights were considered to vary from 0.01 to 0.99 in increments of 0.01. As a result the optimization function was evaluated for about 5500 times to get the Pareto surface. However, while the

aggregate method is simple to implement, it has some limitations and drawbacks. For instance, obtaining points on non-convex portions of the Pareto optimal set is impossible and varying the weights consistently and continuously may not necessarily result in an even distribution of Pareto optimal points (Das and Dennis, 1997). The results obtained by this method are shown in Fig. 4-9 for the specific case 15.1 corresponding to $n_{stringer}$=15 and $N_{unitcell}$=1.

4-2-4-2 Pareto based GA method

Normally, the multi-objective optimization problems are conflicting in nature and hence there does not exist a single solution that simultaneously optimizes all objectives. A change in the optimization parameters of an individual point which makes at least the value of one objective function better without making any others worse, is called a Pareto improvement. A set of individuals are then defined as "Pareto optimal" when no further Pareto improvements are possible. There are many different techniques in the literature (Hochman and Rodgers, 1969; Deb, 2001) to select the Pareto optimal set, which are beyond the scope of this thesis. In this section the multi-objective problem is solved using the Pareto based GA technique in MATLAB. A brief overview of the fundamentals of genetic algorithms is given here, although more details can be found in (Goldberg and Holland, 1988).

The genetic algorithm is an evolutionary method for solving both constrained and unconstrained optimization problems. The evolution usually starts from a population of randomly generated individuals, and is an iterative process, with the population in each iteration called a generation. In each generation, the fitness of every individual in the population is evaluated; the fitness is usually the value of the objective function in the optimization problem being solved. The more fit individuals are stochastically selected from the current population, and each individual is modified by recombining or possibly randomly mutating to form a new generation. Genetic algorithms do not require gradient information hence they are effective regardless of the nature of the objective functions and constraints, although there is a relatively high computational expense with these algorithms. However in comparison to a single objective GA optimization, the fitness evaluation technique in GA multi objective optimization is quite different due to incorporating the idea of Pareto optimality in the multi-objective optimization. These techniques will be

briefly categorised into Ranking techniques, the Pareto-set filter procedure, Tournament selection and Niche techniques (Coello, 1999; Fonseca and Fleming, 1993; Marler and Arora, 2004). The other difference is that a penalty approach is usually used to treat constraints rather than addressing them directly (Marler and Arora, 2004).

In this section the multi objective optimization problem is solved by use of the ''gaoptimset'' command in MATLAB. All settings were considered as default except two: the population size and the crossover fraction. First with the fixed population size of 200 the effect of crossover fraction was investigated. Neglecting the elite children in each generation, the crossover fraction coefficient specifies the ratio of the crossover children to mutation children. For instance a crossover fraction of 1 means that all children other than elite individuals are crossover children, while a crossover fraction of 0 means that all children are mutation children. In fact neither of these extremes is an effective strategy to optimize a function and the best value for crossover fraction is dependant to the nature of the optimization problem. To select the best crossover fraction in this problem, a set of different crossover coefficients of [0.2, 0.3,..., 0.8] was considered. With each cross over coefficient, seven optimization runs were performed and the corresponding best compromise point was selected. The number of generations and function evaluations as well as the number of points on the Pareto front were 105, 21199 and 70, respectively for each optimization run. In addition the average distance and the spread measure on the Pareto front were 0.011563 and 0.0979551 respectively for each solution. Figure 4-8 shows the means and standard deviations of the best compromise point in all of these optimization runs for each value of the crossover fraction.

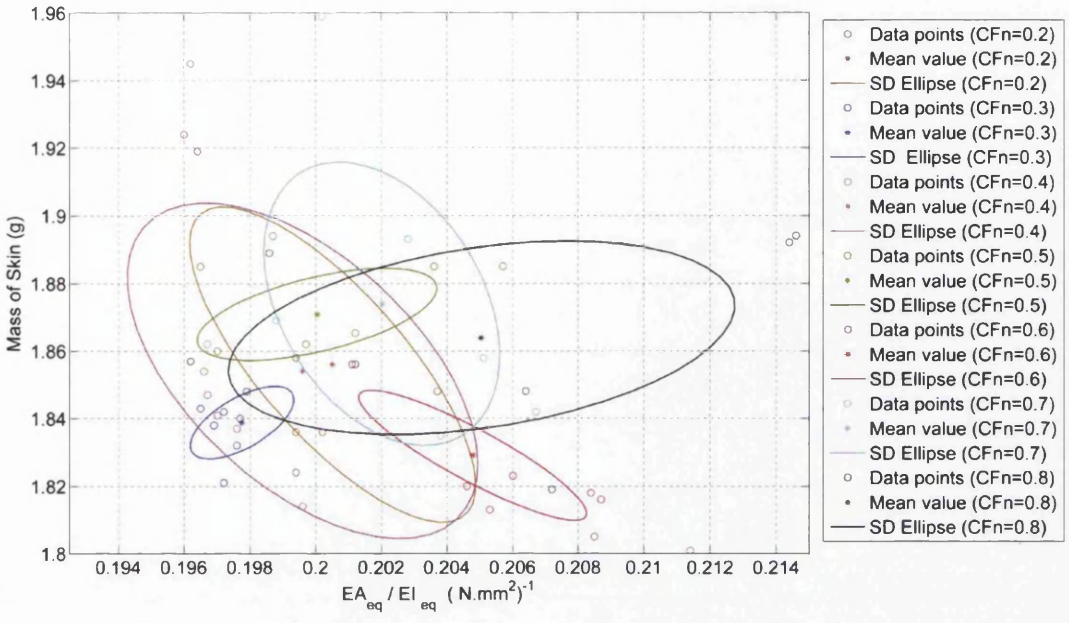

Figure 4-8: Standard deviation analysis of the crossover fraction effect in the GA, and selection of CFn=0.3 in the optimization problem

It is evident in Fig. 4-8 that for this multi objective problem, setting the crossover fraction to 0.3 yields the best result since it has the minimum deviation and minimum mean value for each objective functions. Due to the stochastic behaviour of the genetic algorithm this procedure must be done prior to proper use of this method. In Fig. 4-8 the two objectives of EA_{eq} and $\frac{1}{EI_{eq}}$ are combined into $\frac{EA_{eq}}{EI_{eq}}$, to produce a better illustration as a 2D standard deviation rather than a 3D standard deviation. Another parameter which increases the efficiency of the Pareto front in GA is the size of population. Population sizes of [50,100, 200, 400] were tried in the optimization and finally a population size of 200 was selected because of time efficiency and better fitness values. The results obtained by GA method are illustrated in Fig. 4-9 for the specific case of 15.1 corresponding to $n_{stringer}$=15 and $N_{unitcell}$=1.

4-2-4-3 Comparison of the GA and aggregate methods

In a quick overview of these two methods, the aggregate Newton's method differs from the GA in two main ways. The aggregate Newton's method generates a single point at each iteration and the next point is selected in the sequence by a deterministic computation. At the end the sequence of points approaches the optimal solution. On the other hand the genetic algorithm generates a population of

individuals at each iteration and the next population is selected by stochastic computation. Finally the points with higher ranking in the population approach the Pareto optimal.

Figure 4-9 shows the Pareto front for the specific case of 15.1 corresponding to $n_{stringer}$=15 and $N_{unitcell}$=1, obtained from both the aggregate Newton's method and the GA multi-objective optimization method. Figure 4-9 shows a non- convex curvature of the Pareto front of the multi objective optimization problem and there is a difference in the smoothness of the Pareto front obtained from these two methods. As discussed earlier one of the main drawbacks of the aggregate method is the inability to obtain points on non-convex portions of the Pareto optimal set. Hence before using the aggregate method there must be some information which verifies the non-convex curvature of the Pareto front. The verification here is obtained by observing the good correlation of results obtained by the aggregate method with those GA Pareto front. In addition Fig. 4-9 shows that the weight distribution in the aggregate problem has resulted in an even distribution of Pareto optimal points. Moreover the Pareto curve is less smooth for the genetic algorithm, compared to the aggregate Newton's method, which is due to the randomness and stochastic nature of the genetic algorithm. Considering all these points, the aggregate Newton's method is selected to solve the multi-objective optimization problem described in section 4-2-3.

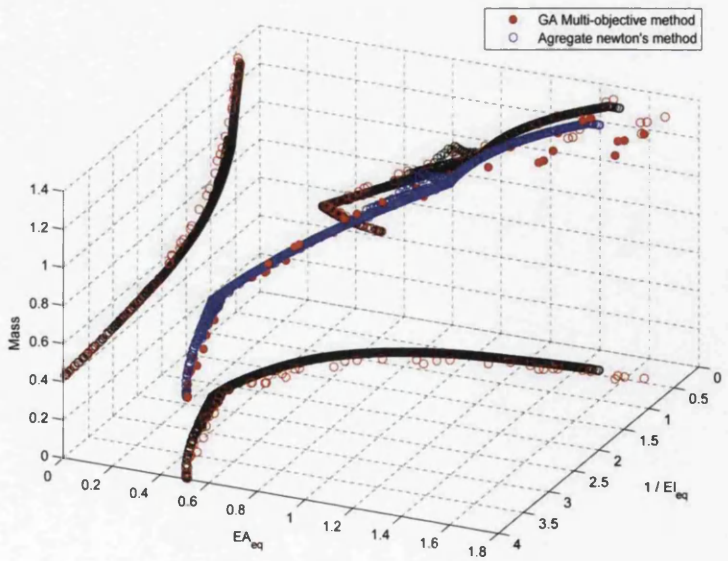

Figure 4-9: Comparison of the GA and the aggregate Newton's based methods, for the specific case 15.1 corresponding to $n_{stringer}$=15 and $N_{unitcell}$=1

4-3 Discussion and Results

Selecting the proper method to solve the multi-objective optimization problem, the results were obtained for different numbers of FishBAC stringers and corrugation unit cells as presented in Table 4-3. Figure 4-10(a) and Figure 4-11(a) show the normalized Pareto surface and its projection on three planes for the case 8.1$(n_{Stringer} = 8, N_{Unitcell} = 1)$ and case 14.2 $(n_{Stringer} = 14, N_{Unitcell} = 2)$ respectively. The Pareto fronts for the other cases are similar to one of these two cases. The best compromise point of these two configurations is also highlighted as red in Fig. 4-10(a) and Fig. 4-11(a). The best compromise point was selected by first identifying the ideal reference point as the coordinates of minimum normalized objective values, i.e:

$$P_{ref} = \left(\left(\frac{1}{EI_{eq}}\right)_{min}, (EA_{eq})_{min}, (Mass_{skin})_{min}\right) \quad (4\text{-}5)$$

Then the point which had the minimum distance from the ideal reference point, in the normalized objective function space, was selected as the best compromise point. Table 4-6 presents the corresponding weights of the optimization technique, the real values of the objectives and the optimized parameters corresponding to the best compromise point for the case 8.1 and the case 14.2. The range of the weights shows that all of the three objectives are involved efficiently in the process of optimization for the best compromise point. Another point which must be noted in Table 4-6 is the range of differences in the value of the optimized parameters and objectives in these two cases, which is due to contracting the size of the corrugation in contrast to increasing the number of stringers. The comparison of the best compromise point of these two cases implies that more desirable objective values will be attained by reducing the size of corrugation.

Table 4-6 (a): Corresponding weights, real values of objectives for the best compromise point in case 8.1 and case 14.2

Configuration of FishBAC stringers and corrugation unit cells	Weights			Real Values of Objectives		
	w_1	w_2	w_3	$\frac{1}{EI_{eq}}$ $(\text{N.mm})^{-2}$	EA_{eq} (N)	Mass of skin (g)
$n_{Stringer}$=8 $N_{unitcell}$=1	0.35	0.33	0.32	$1.2*10^{-4}$	1944.93	6.30
$n_{Stringer}$=14 $N_{unitcell}$=2	0.40	0.36	0.24	$1.3*10^{-4}$	152.52	2.49

Table 4-6 (b): Corresponding optimized parameters for the best compromise point in case 8.1 and case 14.2

Configuration of FishBAC stringers and corrugation unit cells	Optimized parameters (mm)					
	t_c	t_e	a_1	a_2	a_3	h
$n_{Stringer}$=8 $N_{unitcell}$=1	0.51	0.30	3.72	1.49	3.68	4.69
$n_{Stringer}$=14 $N_{unitcell}$=2	0.09	0.19	0.90	0.91	0.86	4.69

Figure 4-10(b) and Figure 4-11(b) show the effect of weight distribution on the Pareto surfaces for case 8.1 and case 14.2. Generally, the relative value of the weights reflects the relative importance of the objectives. The dominance of each objective function is highlighted when its corresponding weight in Eq. (4-3) is in range of [0.7-1]. In these Pareto surfaces, the relatively horizontal plane highlighted as magenta is obtained when the weight w_3 corresponding to the third objective, i.e.

the mass of skin, is dominant. In other words this plane has mainly minimized the mass of skin but not the two other objectives: $\frac{1}{EI_{eq}}$ and EA_{eq}. The plane highlighted as green is obtained when the $w_1$corresponding to the first objective i.e. $\frac{1}{EI_{eq}}$, is dominant since the two other objectives are not minimized significantly. Likewise the region highlighted as orange is obtained when the weight w_2 corresponding to the second objective is dominant.

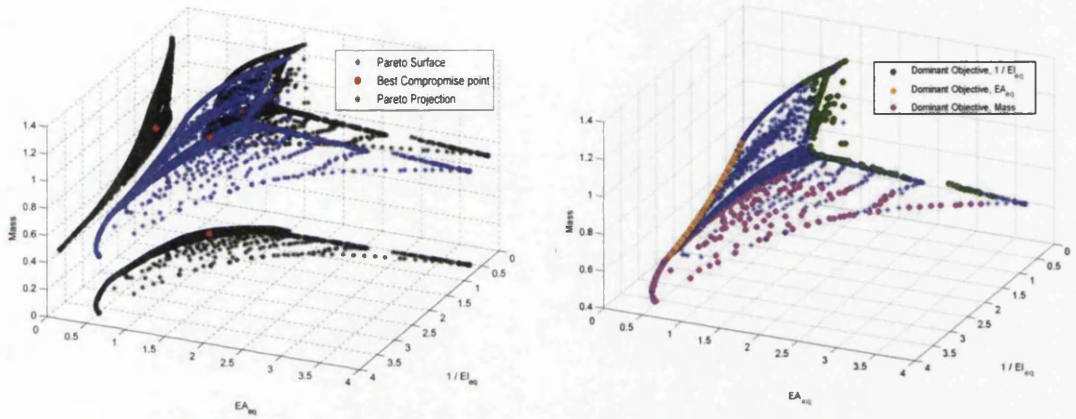

(a) Best compromise point (b) Weight distribution

Figure 4-10: Pareto surface for the case 8.1; $n_{Stringer}$=8, $N_{Unitcell}$=1

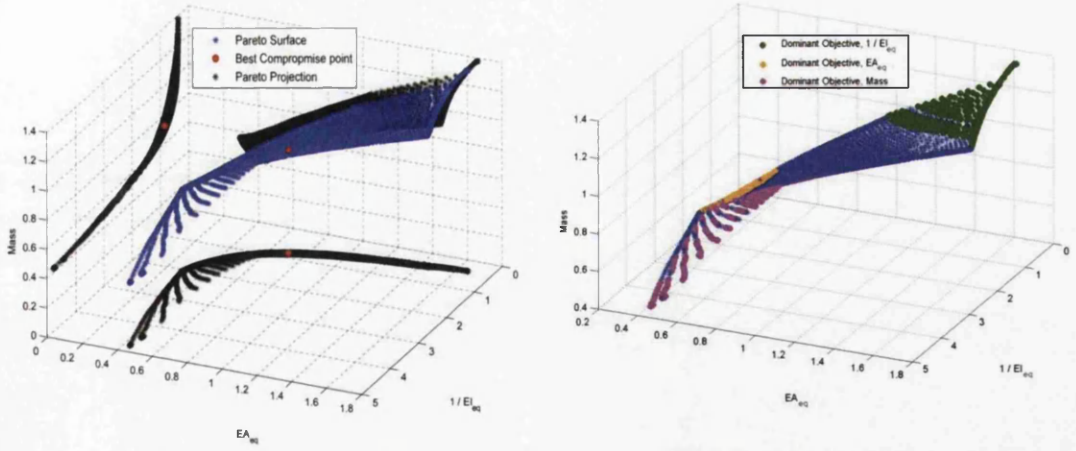

(a) Best compromise point (b) Weight distribution

Figure 4-11: Pareto surface for the case 14.2 ; $n_{Stringer}$=14, $N_{Unitcell}$=2

4-4 Trends of parameters and objective functions

In order to investigate the trend of the optimized parameters and objectives the best compromise points in all of the configurations of FishBAC stringers and corrugation

unit cells are collected and studied in this section. Figure 4-12 shows the trend of first optimized objective function $\frac{1}{EI_{eq}}$ for different length of unit cells. Figure 4-12 shows that the out of plane compliance of the corrugated core with elastomeric coating decreases as the length of the corrugation unit cell increases. For a corrugated panel with a fixed length, as the length of the corrugation unit cells decreases the number of unit cells and consequently the number of corrugation lines increase. Thus the number of corners of a corrugated unit cell increase in the whole panel, as the corrugation unit cell gets smaller. These corners or corrugation lines which act like joints with torsional stiffness have the main role in the mechanism of deformation of the corrugated structures (Dayyani et al., 2012). Hence the increase in the number of corrugation coroners leads to more out of plane compliance of the panel. The minimum value for the out of plane compliance which is obtained at $L_{uc} = 40\text{mm}$ is equal to $1.15 * 10^{-5}(\text{N.mm})^{-2}$as reported in the zoomed region provided in Fig. 4-12.

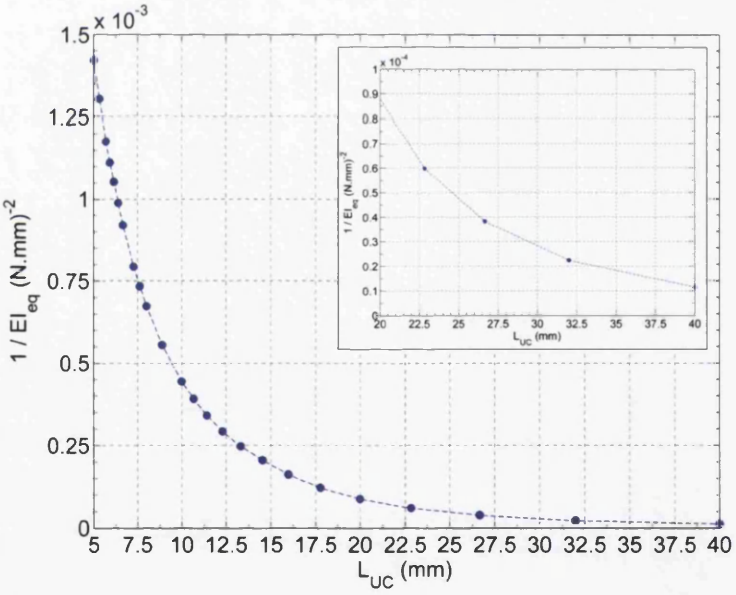

Figure 4-12: The trend of optimized objective function $\frac{1}{EI_{eq}}$ for different lengths of unit cell

Figure 4-13 shows the trend of the second optimized objective function EA_{eq} for different lengths of unit cell. The in plane stiffness of the corrugated core with elastomeric coating decreases as the length of the corrugation unit cell reduces. The minimum value for the in plane stiffness which is obtained at $L_{uc} = 5\text{mm}$ is equal

to 139.5N as reported in the zoomed region provided in Fig. 4-13. With the same analogy the observed trend can be explained. As the corrugation unit cell gets smaller the number of corrugation lines increase in the whole panel and leads to more in-plane flexibility.

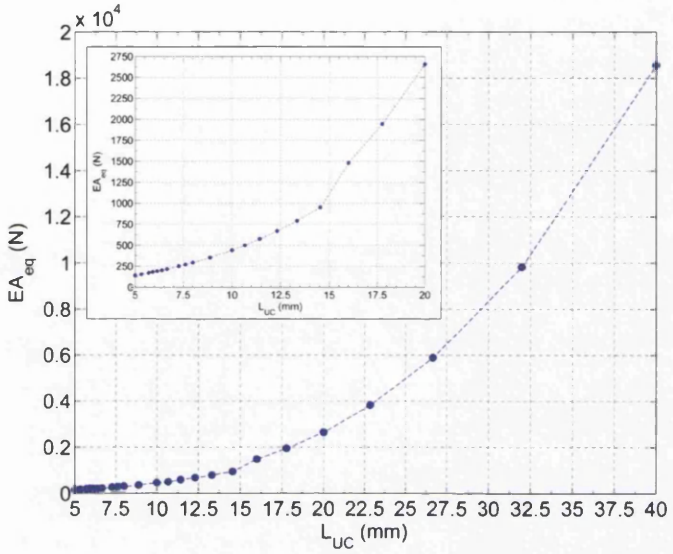

Figure 4-13: The trend of optimized objective function EA_{eq} for different lengths of unit cell

Comparing Fig. 4-12 and Fig. 4-13 implies that the in plane and out of plane stiffness of the corrugated panel are correlated. In other words minimizing the in plane stiffness is conflicting with maximizing the out of plane stiffness. Figure 4-14 illustrates the linear behavior between the optimized in-plane stiffness and out of plane stiffness. This plot justifies the Fig. 4-8 in which two objective functions $\frac{1}{EI_{eq}}$ and EA_{eq} were combined into a single objective function $\frac{EA_{eq}}{EI_{eq}}$. The slope of the plot is about 0.21 (N.mm^2), which is in the range of values illustrated in Fig. 4-8 which were obtained by the GA multi objective optimization. The interesting point here is that although the trend of both objectives in Fig. 4-12 and Fig. 4-13 are smooth the trend for the combination of them is non-smooth about EI_{eq} equivalent to 5000(N.mm)^2. The small jump in Fig. 4-14 may be explained by considering that the domain of changes of parameters gets smaller as the length of corrugation unit cells decrease as shown in Table 4-5. In other words the bounds for the points in Fig. 4-14 with $EI_{eq} \leq 5000$ make the domain of parameters tighter in contrast to the rest of points and hence they have different linear trend.

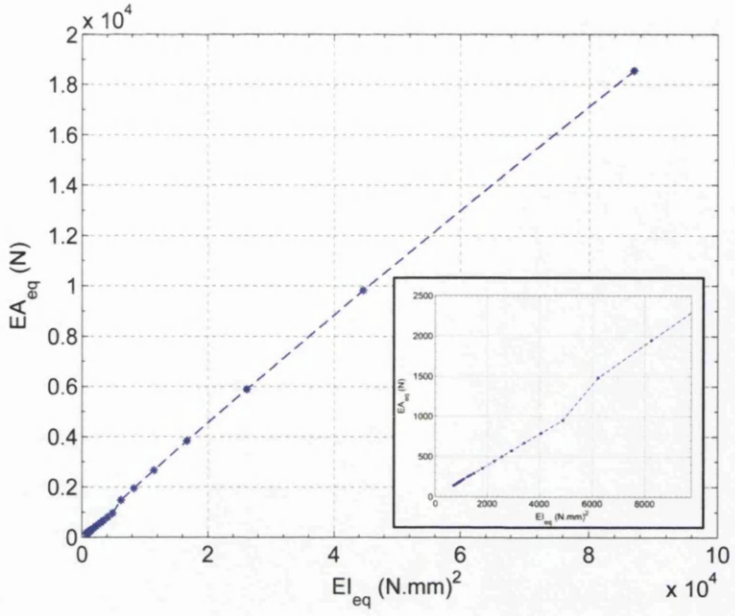

Figure 4-14: The linear behaviour between the optimized in-plane stiffness and out of plane stiffness

Figure 4-15 shows the trend of the third optimized objective function ''mass'' for different lengths of unit cell. The trend implies that, for all configurations of FishBAC stringers and corrugation unit cells, reducing the length of the unit cells decreases the mass of skin. The small jump in Fig. 4-15 is because the optimization algorithm has minimized the parameters t_c andt_e in a different way. As indicated in Table 4-7 the thickness of the core t_c has hit the lower bound for the points with unit cell length less than 14.55 mm while for the points with unit cell length more than 16 mm the thickness of the elastomer coating t_e has hit the lower bound.

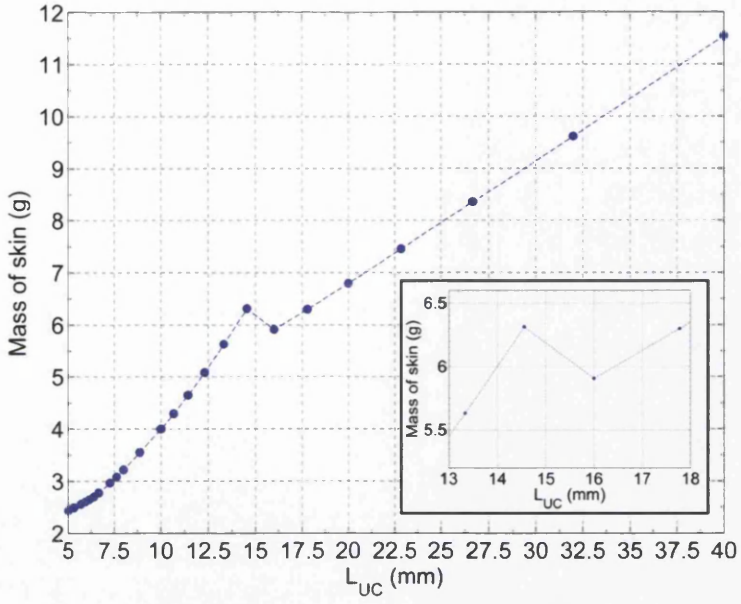

Figure 4-15: The trend of optimized objective function ''Mass'' for different lengths of unit cell

Table 4-7 presents the optimized parameters and objectives of four points in the vicinity of the jump as highlighted in Fig. 4-15. The indices ''lb'' and ''ub'' represents hitting the upper bound and lower bound of optimized parameters respectively. The optimization algorithm has also selected the corresponding values at the lower bound for the parameter a_2, while for the parameter h the upper bound is selected. This implies that increasing the height of the corrugation gives a higher ratio of bending stiffness to tensile stiffness.

Table 4-7: The optimized parameters and objectives for four points in the vicinity of the jump highlighted in Fig. 4-15

L_{uc} (mm)	Real values of objectives			Optimized parameters (mm)					
	$\frac{1}{EI_{eq}}$ $(\mathrm{N.mm})^{-2}$	EA_{eq} (N)	Mass of skin (g)	t_c	t_e	a_1	a_2	a_3	h
13.33	$2.47*10^{-4}$	789.03	5.63	0.22_{lb}	0.76	2.81	1.11_{lb}	2.74	4.69_{ub}
14.55	$2.05*10^{-4}$	950.00	6.31	0.24_{lb}	0.90	3.06	1.21_{lb}	3.01	4.69_{ub}
16	$1.61*10^{-4}$	1479.42	5.91	0.46	0.27_{lb}	3.33	1.33_{lb}	3.33	4.69_{ub}
17.78	$1.21*10^{-4}$	1944.93	6.30	0.51	0.30_{lb}	3.73	1.48_{lb}	3.68	4.69_{ub}

Figure 4-16 shows the upper bounds, lower bounds and the trend of optimized parameter t_c and t_e for different lengths of unit cell. As illustrated in Fig. 4-16(a) the thickness of the corrugated core t_c, increases as the length of unit cells increases. As mentioned earlier, this ascending trend can be considered as two phases. In the first phase, which is for unit cell length less than 14.55 mm, the parameter t_c has hit the lower bound in the optimization process. In the second phase, which is for unit cell length more than 16 mm, the parameter t_c is optimized without approaching to the bounds. The constant slopes in these two phases of Fig. 4-16(a) expresses that the ratio between the thickness of the core and the length of unit cell, $\frac{t_c}{L_{uc}}$ reaches a constant value in each phase. This constant value in the first phase is because of the optimization process which has selected the lower bound with a constant slope for the thickness of the corrugated core. However the value of $\frac{t_c}{L_{uc}}$ in the second phase, which is almost equal to 0.0275, is independent of the constant slopes of the bounds and implies that the optimized thickness of the core is linearly proportional to the length of unit cell. Moreover, Figure 4-16(b) reveals that the thickness of the elastomer coating t_e, increases as the length of unit cells increases in both phases independently. In the first phase, for unit cell lengths less than 14.55 mm, the parameter t_e is optimized without approaching the bounds. In the second phase which, for unit cell lengths more than 16 mm, the parameter t_e has hit the lower bound in the optimization process and hence has a constant value of $\frac{t_e}{L_{uc}}$.

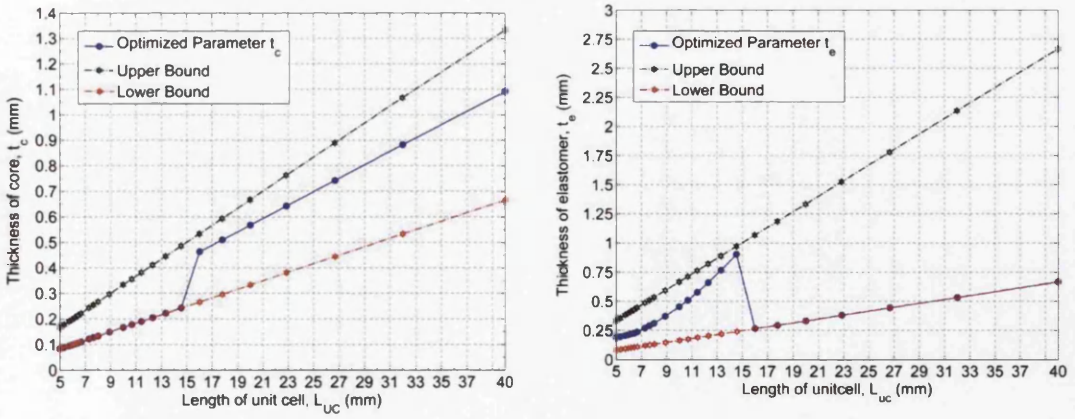

(a) (b)

Figure 4-16: Thickness variation of corrugated core and elastomeric coatings for different length of unit cells

Figure 4-17 shows the upper bounds, lower bounds and the trend of parameters a_1, a_2 and a_3 as a function of the length of corrugation unit cell. The parameters a_1 and $a_3$which represent the horizontal members of the corrugation geometry show a very close correlation as they are optimized. This means that there is a possibility of defining the geometry of corrugation with three parameters rather than four and it is likely to save more computation costs in future optimization studies. The ascending trend of parameters a_1 and a_3 can be considered in two phases. The first phase corresponding to the unit cell length smaller than 6.67 mm, is when the parameter a_2 has a descending trend, before hitting the lower bound. However in the second phase, which corresponds to a unit cell length of more than 6.67 mm, the parameter a_2 hit the lower bound which resulted the descending trend changing into the ascending trend. The constant slope of the trends of the parameters a_1 and a_3 expresses the ratio of these parameters to the length of unit cells. The ratio of $\frac{a_1}{L_{uc}}$ and $\frac{a_3}{L_{uc}}$ in the first phase, where parameter a_2 has not hit the lower bound, is about 0.39. The slope of the trend of parameter a_2 is about -0.31 in the first phase which implies an inverse relationship between parameters a_2 and L_{uc}. However in the second phase, the constraint of $a_1 + a_2 + a_3 = L_{hu}$ and the approximate equivalence $a_1 \cong a_3$ explains the constant slope of parameters a_1 and a_3, which is because the parameter a_2 has hit the lower bound with a constant slope of 0.167.

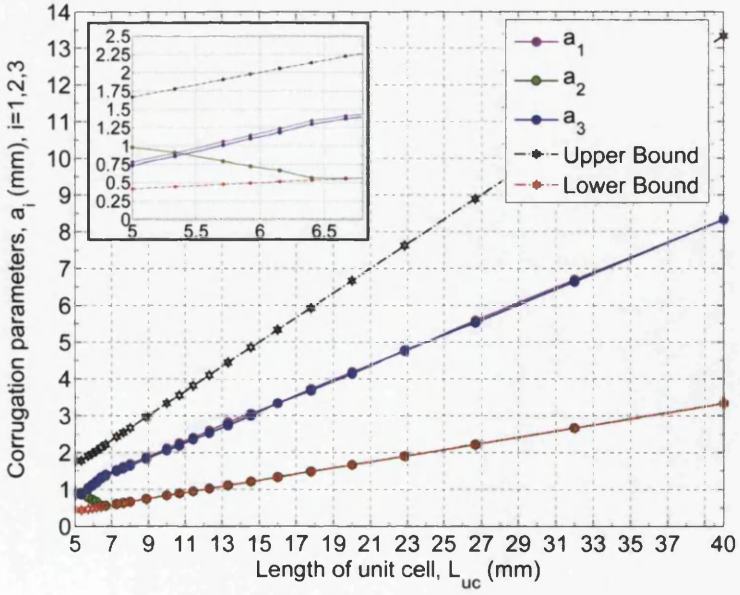

Figure 4-17: The upper bounds, lower bounds and the trend of parameters a_1, a_2 and a_3 as a function of the length of corrugation unit cell

For the parameter h, which represents the height of the corrugation, the optimization algorithm has selected values at the upper bound. In many cases the optimization algorithm has selected the corresponding values at the lower bound for the parameter a_2 which implies that maximizing the angle of corrugation would result in a higher ratio of bending stiffness to tensile stiffness. Figure 4-18 shows the optimized $\tan(\theta)$ as a function of the length of the unit cell.

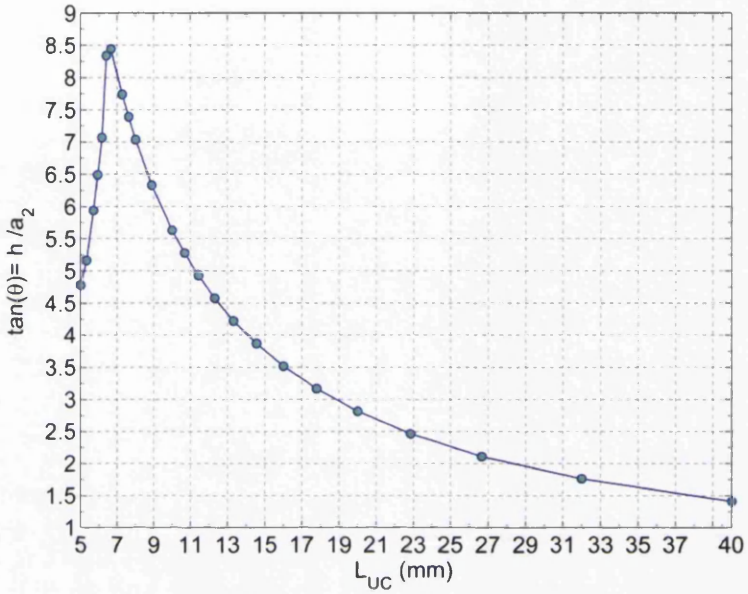

Figure 4-18: The optimized $\tan(\theta)$ as a function of the length of the unit cell

In terms of design, the trend of the three optimized objectives at the best compromise points for the entire range of configurations of FishBAC stringers and corrugation unit cells are illustrated together in Fig. 4-19(b). The design decision was made by repeating the process of finding the best compromise point among the collection in a normalized space of objectives. Figure 4-19(a) shows the distance of the best compromise points of different unit cell lengths to the ideal reference point presented in Eq. (4-5).

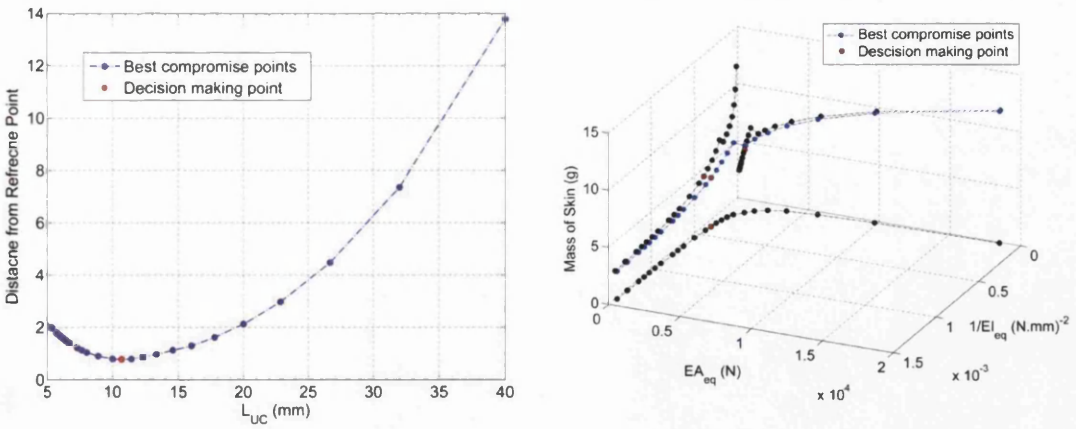

(a) (b)

Figure 4-19: Entire best compromise points for different length of unit cells

The decision point of the best design is highlighted as red in Fig. 4-19. However it must be mentioned that this point would be different if more importance is given to certain objective functions such as the in-plane compliance of the corrugated skin which reduces the required energy to morph. Table 4-8 shows the corresponding objective values and parameters at the decision point of the design. According to the Table 4-8 the length of a corrugation unit cell at the decision point is 10.7 mm. Consequently all of the configurations of FishBAC stringers and corrugation unit cells which are compatible in the equation of $(n_{stringer} + 1) \times N_{unitcell} = 15$ represent the highlighted decision point, i.e. case 4.3 ($n_{stringer}$=4, $N_{unitcells}$=3), case 5.2 ($n_{stringer}$=5, $N_{unitcells}$=2), and case 14.1 ($n_{stringer}$=14, $N_{unitcells}$=1). It must be mentioned that the equation $(n_{stringer} + 1) \times N_{unitcell} = 15$ is derived by replacing the values of the geometric parameters in the corresponding formulas in section 4-2-3. Although these cases have the same geometry of the skin, the number of the stringers of the FishBAC internal structure is different and hence the structural and aerodynamic characteristics of the assembled structure will be different. It is also possible to consider variable spacing of the stringers for the selected geometry of the skin. However such optimization and analysis are beyond the scope of this thesis.

Table 4-8: Corresponding optimized parameters at the decision point of the design

Optimized objective functions			Optimized parameters (mm)					
$\frac{1}{EI_{eq}}$ (N. mm)$^{-2}$	EA_{eq} (N)	Mass of skin (g)	t_c	t_e	a_1	a_2	a_3	h
$3.9*10^{-4}$	500.40	4.29	0.18	0.51	2.26	0.89	2.20	4.69

4-5 Benefits over simple elastomeric skin

Increasing thickness of the skin of the aerofoil allows the skin to resist more pressure caused by the airflow and increases the critical buckling load due to the morphing actuation. In other words the thicker skin allows the FishBAC structure to have fewer stringers with smaller length. But the problem is that increasing the thickness of the skin increases the tensile stiffness of the skin which requires more force to actuate the aerofoil and it increases the mass of skin, whereas the mass reduction of the stringers is negligible.

However the coated corrugated skin has some benefits over the simple elastomeric skin to tackle these challenges. Firstly, the possibility of using a compatible corrugated skin with more height (thicker corrugated skin) that increases the bending stiffness of the skin without increasing mass of skin significantly in comparison to a simple elastomeric skin. Secondly, considering the mechanism of deformation in the corrugated core, the corrugated skin with more height decreases the in-plane tensile stiffness of the panel that results in a smaller actuation force required for morphing deformation. This structural advantage of a corrugated skin provides the possibility of having fewer FishBAC stringers which reduces the weight of the structure. Although more details about the interaction of the corrugated skin and the internal structure are presented in section 4-6, a comparison of the mechanical behaviour of the FishBAC with a coated corrugated skin and a simple elastomeric skin helps to understand the importance of the corrugated skin for morphing wing application.

In this regard, the geometry of FishBAC as described in Table 4-10 was considered. Firstly, the mass of the coated corrugated skin with the geometric parameters and material properties presented in Table 4-8 and Table 4-4 was

calculated without the assumption of neglecting the coating sections that overlap with the corrugated core. The mass of the corrugated skin consisting of two elastomeric coatings and a composite corrugated core was calculated as 35.12 g. This mass and the material properties of the elastomer coating were set fixed to compare both skins. Considering the length of the skin between the rigid leading edge and the rigid trailing edge as 161.08 mm, the thickness of the simple elastomeric skins was calculated as1.66mm, more than 9 times thicker than the elastomeric coating of the corrugated skin. Considering the density of the material used for the FishBAC stringers as 0.0011 g/mm^3, the effective mass of the FishBAC with a corrugated skin, i.e. the mass of non-common parts (skin and stringers) was 17.3% smaller than the FishBAC with a simple elastomeric skin. Moreover, comparing the mechanical behaviour of these two skins reveals that the corrugated skin is almost 5 times more flexible to stretch in the morphing actuation process and has almost 4.5 times more resistance to out of plane deformation due to aerodynamic loads and buckling deformations caused by actuation. Table 4-9 presents more details about the comparison of these two skins.

Table 4-9: A comparison of mechanical properties of the coated corrugated skins and simple elastomeric skin for the FishBAC internal structure

NACA 0012	Coated Corrugated Skin	Simple elastomeric Skin
Mass of skin (fixed) (g)	35.12	35.12
Mass of skin and stringers (g)	100.82	118.34
EA_{eq} (N)	500.4	2490
EI_{eq} (N.mm)^2	2564	571.79

Furthermore, in contrast to the simple elastomeric skin, the corrugated skin has the feature of the structural anisotropy which helps the skin to withstand more aerodynamic loads in the spanwise direction. Considering the pressure distribution over a NACA 0012 aerofoil shown in Fig. 4-20, the corrugated skin allows the internal structure to have variable distance between stringers; more distance between the stringers in regions exposed to lower pressure. In addition, the geometrical parameters of the corrugation provide the facility of having continuous variable out-of-plane and in-plane stiffness along the length of the skin, which leads to a further

reduction of the mass of the skin. The mechanical behaviour of both of these skins can be improved more by using more advanced materials such as a curvilinear fibre composite elastomeric skin (Murugan et al., 2012), or applying pre-stressed elastomeric coatings. However in the case of pre-stressed skins the corrugated core provides more regions for attaching and adhering such pre-stressed coating and hence would have smaller shearing stresses between the elastomer and the corrugated core, compared to a simple elastomeric skin.

4-6 Morphing design considerations

As mentioned earlier the skin of the morphing wing is one of the most critical parts of the wing. This is because the skin is the boundaries of the domain. Consequently the aerodynamic loads are first tolerated and transferred through the skin and the local and global deformations of the skin have significant effects on the aerodynamic performance. The discussion in the chapter has thus far considered the skin in isolation, and presented the advantages of the coated corrugated skin over the elastomer skin. The optimum design was obtained by identifying the best compromise on the Pareto surface between the in plane stiffness, the out of plane stiffness and the mass of the skin.

In practice the shape optimization of the morphing aerofoil with the objective of achieving the highest possible lift to drag ratio will be the first milestone of the design process. After finding the optimum morphed aerofoil which has the highest lift to drag ratio and designing the internal adaptive structure to enable the required deformation the skin would be optimized simultaneously with the internal structure. The coupled optimization of the internal structure and the corrugated skin which considers the boundaries and the constraints from the geometric consistency, material and manufacturing is required for future studies. In addition more objective functions with regards to the efficiency of aerodynamics performance, actuation energy and structural health monitoring should be included or redefined. Each of these objective functions requires different investigation in background. For instance in terms of the aerodynamic performance, fluid structure interaction (FSI) analysis is required which uses CFD and FE codes to capture the effects of the local and global deformations of the skin on the aerodynamic loads. In terms of actuation energy, a topology optimization is needed to minimize the required strain energy to morph and

to reduce further the mass of the whole structure. In terms of structural health monitoring, fracture mechanic analysis is of great importance. For example, once the occurrence of cyclic stress can be predicted reliably then a constraint may be added into the morphing aerofoil optimization to ensure that the structural components of the skin would not fail at stress levels much lower than those experienced by static mechanical loading. This requires an in-depth analysis of the cyclic loading of corrugated skins, and in particular, the development of accurate fatigue models of corrugated panels. Moreover the optimum skin would be different if more importance is given to certain objective functions such as the flexibility of the whole structure which reduces the required energy to morph and results in a lighter actuation system. Alternatively it is possible to convert some of the objectives to constraints. For example, a constraint on EI_{eq} is obtained from the maximum out of plane deformation due to the airflow or to prevent buckling due to the actuation of the internal structure. Such an optimization is beyond the scope of this thesis, although a finite element simulation of the skin and internal structure under typical aerodynamic and structural loadings is performed to verify the design approach.

Prior to simulation of the internal structure with the corrugated skin, it is necessary to have a good insight of the aerodynamic loads on the morphed aerofoil. In this regard, the air flow over the morphing trailing edge of the NACA0012 aerofoil was simulated using XFOIL panel method code. This code included a viscous boundary layer component to predict skin friction drag and flow separation, offering a more complete drag prediction than inviscid codes. Using a viscous formulation of linear vorticity potential flow theory, XFOIL calculated the distribution of pressure coefficient over the airfoil. The aerodynamic input conditions to this code were Mach number and Reynolds number which were equal to 0.1 and 360000, respectively for an air speed of 30m/s. Figure 4-20 shows the estimated surface pressure distribution. This aerodynamic loading and its distribution over the trailing edge is important in terms of the deformation of the skin and the structural modelling of the FishBAC stringers.

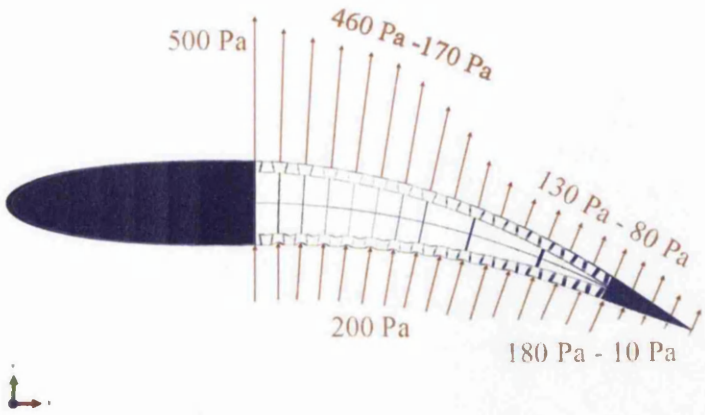

Figure 4-20:The simulated pressure distribution over the NACA0012 aerofoil at 30m/s

Based on the optimized geometry of the corrugated skin presented in Table 4-8, different compatible geometries for the FishBAC internal structure can be considered as: case 14.1 ($n_{stringer}$=14 , $N_{unitcells}$=1) or the case in which the distance between the stringers increases as the pressure distribution decreases, as shown in Fig. 4-20. As mentioned earlier in section 4-5 the last case is one of the important benefits of the interaction of the corrugated skin and the internal structure, which leads to further reduction in the mass of the whole structure and must be considered in the full optimization. However the geometry of the aerofoil section for the case 14.1 ($n_{stringer}$=14 , $N_{unitcells}$=1) corresponds approximately by chance to those used in the original design of the FishBAC structure with elastomer skins. In this section more attention is paid to the skin rather than to the internal structure and hence the internal design is not optimized but assumed identical to the existing aerofoil that has been studied in simulation and experiment (Woods and Friswell, 2012). The geometric parameters, taken from (Woods and friswell, 2012), are given in Table 4-10.This design currently has a simple elastomer skin and here this is replaced with a coated corrugated skin in this study. The Young's modulus and Poisson's ratio of the FishBAC material were assumed to be 2.14GPa and 0.3. These values are in range of the material properties of the previous manufactured FishBAC which were printed from Acrylonitrile Butadiene Styrene (ABS) plastic using an HP Designjet 3D Fused Deposition Modelling printer.

Table 4-10: FishBAC prototype geometric parameters

baseline aerofoil	NACA 0012
chord (c)	305 mm
span (b)	150 mm
start of morph (x_s)	$0.35c$ =107 mm
end of morph (x_e)	$0.85c$ =260 mm
spine thickness (t_b)	2 mm
# of stringer pairs	14
stringer thickness (t_{st})	0.8 mm

Four different corrugated skins were modelled and assembled on the FishBAC internal structure in ABAQUS. These four skins which were compatible with the geometry of the internal structure and correspond to the following points with the: best compromise, minimum $\frac{1}{EI_{eq}}$, minimum EA_{eq} and minimum mass, as presented in Table 4-8 and Table 4-11 respectively. Figure 4-3(C) shows a schematic of the corrugated core unit cell and the corresponding values of parameters presented in Table 4-8 and Table 4-11. In terms of the material properties, the corrugated cores are assumed to be made of three-plies of woven glass fibre with epoxy resin matrix (Aird, 1996; May, 1987), with the material properties given in Table 4-4. The upper and lower skins of the sandwich panel are polyurethane elastomer (Harper, 2002; Callister and Rethwisch, 2007; Bhowmick and Stephens, 2000) with Young's modulus also given in Table 4-4.

Table 4-11: The optimized parameters corresponding to the different dominant objectives of the design

Dominant Objectives	Optimized objective functions			Optimized parameters in (mm)					
	$\frac{1}{EI_{eq}}$ $(\text{N.mm})^{-2}$	EA_{eq} (N)	Mass of skin (g)	t_c	t_e	a_1	a_2	a_3	h
$\frac{1}{EI_{eq}}$	0.0002	1162.32	6.85	0.36	0.71	2.81	0.89	1.64	4.69
EA_{eq}	0.0011	206.01	2.68	0.18	0.18	1.46	2.43	1.44	4.69
Mass	0.0018	401.27	2.28	0.18	0.18	1.97	1.52	1.84	2.61

The FishBAC and coated corrugated skin were modelled as described earlier. A fine mesh of cubic beam elements of approximate size of 0.5mm was used for the assembled structures to simulate the mechanical behaviour of the morphing wing. Large deformation analysis was considered in case the deformations were outside the linear elastic range. The tendon actuation system was modelled as a moment on node q in the rigid part at the trailing edge, as shown in Fig. 4-7. The nodes at the leading edge of the morphing section were fixed. Figure 4-21 shows the trailing edge displacement as an almost linear function of the actuation moment for the FishBAC internal structure with different corrugated skins. Fig. 4-21 clearly shows that the optimum skin would be different if more importance is given to different objective functions. The skins with minimum in-plane stiffness and minimum mass require less actuation energy in contrast to best compromise point for the morphing deformation.

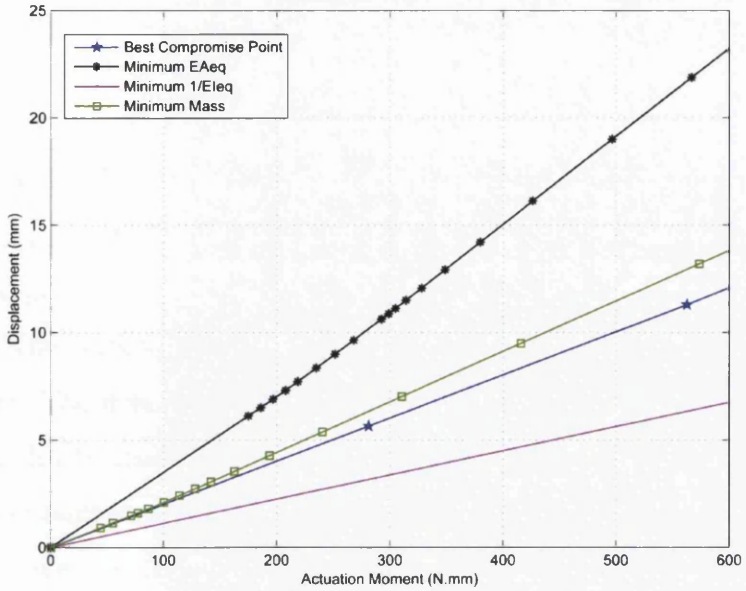

Figure 4-21: Displacement-Actuation moment behaviour of the structure with different corrugated skins

Figure 4-22 shows the deformed configuration of the FishBAC, with both the aerodynamic pressure distribution shown in Fig. 4-20 and the actuation moment required to give the tip deformation for the skin with the best compromise properties. The interaction of the structural behaviour between the corrugated skin and the FishBAC spine and stringers is important. In particular Fig. 4-22 shows that higher strains are present in the skin rather than the FishBAC spine.

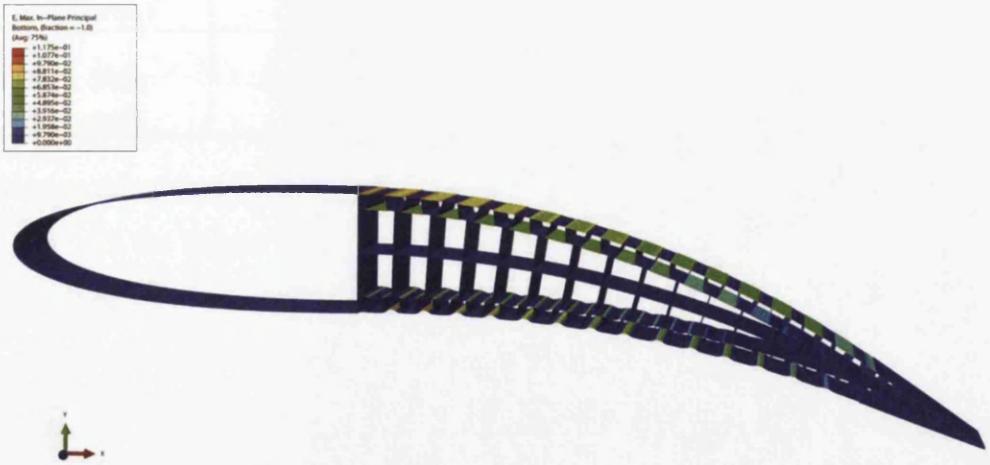

Figure 4-22: Morphed FishBAC with a coated corrugated skin for the given pressure distribution and actuation moment.

As implied earlier, the out of plane deformation of the skin can occur because of buckling of the skin due to the actuation of the internal structure. There are two sorts

of buckling modes for the corrugated skin: global corrugated core buckling and local buckling of the elastomer coating. This highlights the importance of simultaneously optimizing the skin with the internal structure. To demonstrate this phenomenon, three models of the FishBAC with a width of 150 mm and different numbers of stringers ($n_{stringers}$ = 3, 7 and 15) were simulated. Two configurations for each number of stringers were modelled with different heights of corrugated skin, namely 2.5 and 5mm. The parameters a_1, a_2 and a_3 were set equal to 1.667mm for both thin and thick skins. The material properties were selected as those described in section 4-2-1. A large displacement of 54mm transverse to the chord direction was applied as a boundary condition to the tip of the trailing edge of the FishBAC in each model. Table 4-12 presents a comparison of the stiffness resisting the actuation of the FishBAC with thin and thick corrugated skins for three different configurations of unit cells and stringers. Increasing the distance between the FishBAC stringers reduces the structural stiffness resisting the morphing actuation.

Table 4-12: A comparison of stiffness of FishBAC with corrugated skins for different configurations of unit cells and stringers

Stiffness resisting the Actuation of FishBAC	d_s=10mm ($n_{stringers}$=15, $N_{unitcells}$=2)	d_s=20mm ($n_{stringers}$=7, $N_{unitcells}$=4)	d_s=40mm ($n_{stringers}$=3, $N_{unitcells}$=8)
Thin Skin (h=2.5 mm)	0.1469 N/mm	0.1441 N/mm	0.1309 N/mm (Buckled)
Thick Skin (h=5 mm)	0.1060 N/mm	0.1050 N/mm	0.1040 N/mm

However the global buckling of the corrugated core is observed for the case of the thin skin with the largest distance between the stringers i.e. d_s=40mm. This problem can be solved by increasing the height of the corrugation. This increase in height not only postpones the global buckling of the skin but also reduces the stiffness resisting the morphing actuation. However, the local buckling mode appears as wrinkling of the elastomer coating for all the simulated cases. This problem can be avoided by applying pre-stressed elastomeric coatings. This pre-stretching of the elastomer coating not only delays the local buckling of the elastomer coating but also decreases the out of plane deformations due to the pressure distribution over the aerofoil. Figure 4-23 shows these two modes of buckling for both thin and thick corrugated skins for the case of d_s=40mm in Table 4-12.

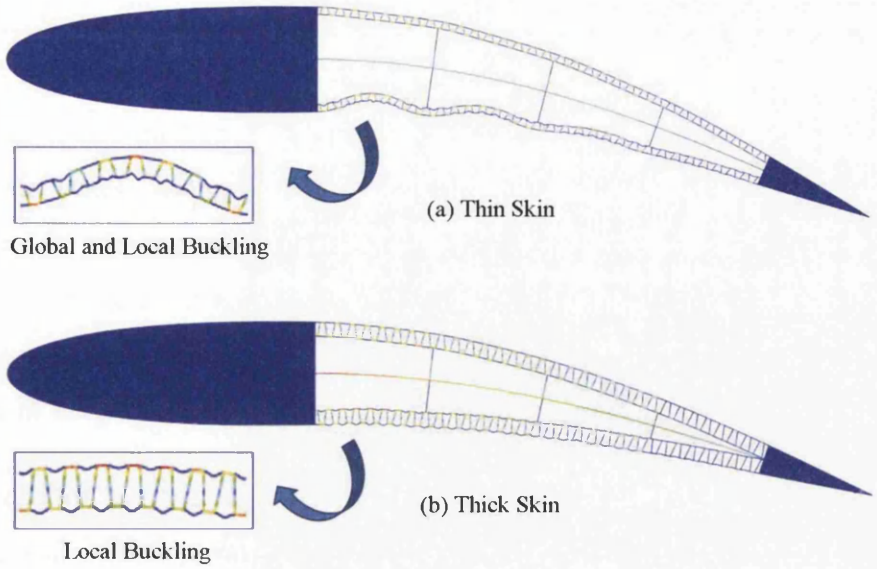

Figure 4-23: Two modes of buckling for both thin and thick corrugated skins for the case of d_s=40mm in Table 4-12

4-7 Conclusion

In this chapter the force displacement curves for reentrant, trapezoidal and rectangular corrugated cores with and without elastomeric coating were investigated in tensile and bending simulations. Comparing the results allowed the selection of a suitable corrugation configuration with regards to morphing skin applications. The geometric parameters of the coated trapezoidal composite corrugated panels were then optimized to minimize the in-plane stiffness and the mass of skin and to maximize the out-of-plane stiffness skin. To do so, a finite element code for beam elements was written in MATLAB to calculate the equivalent tensile and flexural stiffness of coated corrugated panels.

Bearing in mind the manufacturing limitations, different possible configurations of FishBAC stringers and corrugated skin were considered in the optimization problem. Especially when the size of the corrugation was very small, the upper bounds and the lower bounds of the geometric parameters of the corrugation were chosen carefully based on practical considerations. The entire parameters of corrugation were normalized in order to ensure the best performance of the optimization scheme. The advantages and limitations of the aggregate Newton's method and the GA multi-objective method were investigated for solving the multi objective optimization problem for the corrugated skin. The results obtained from

both methods were compared and finally the aggregate Newton's method was utilized in this chapter. The dominance of each objective function due to the weight distribution in this method was discussed and highlighted in the Pareto surface of two sample cases. Moreover, by identifying the ideal reference point as the coordinates of minimum normalized objective values, the best compromise point was selected in each configuration of FishBAC stringers and corrugation unit cells. The range of the weights showed that all of the three objectives were involved efficiently in the process of optimization for the best compromise point.

The trend of optimized parameters and objectives were then investigated by collecting and studying the best compromise points in all the configurations of FishBAC stringers and corrugation unit cells. It was justified that the out of plane and in-plane compliances of the corrugated core with elastomeric coating decreased when the length of the corrugation unit cell increased. For almost all configurations of FishBAC stringers and corrugation unit cells, reducing the length of the unit cells decreased the mass of the skin. In terms of the trends of the optimized geometric parameters, it was shown that the thickness of the core hit the lower bound for the points with a unit cell length less than 14.55 mm while for a unit cell length more than 16 mm the thickness of the elastomer coating hit the lower bound. This switch in the way that the optimization algorithm optimized these two parameters resulted in a small jump in the trend of objective functions. Moreover, the optimization algorithm selected the corresponding values at the lower bound for the parameter a_2, while for the parameter h the upper bound was selected, implying that increasing the height of the corrugation gives a higher ratio of bending stiffness to tensile stiffness. Finally, the design decision was made by repeating the process of finding the best compromise point among the collection in a normalized space of objectives. As a result all the configurations of FishBAC stringers and corrugation unit cells which were well-matched in the equation of $(n_{stringer} + 1) \times N_{unitcell} = 15$ represented the highlighted decision point, i.e. case 4.3 ($n_{stringer}$=4, $N_{unitcells}$=3), case 5.2 ($n_{stringer}$=5, $N_{unitcells}$=2), and case 14.1 ($n_{stringer}$=14, $N_{unitcells}$=1).

The important advantages of using a corrugated skin rather than simple elastomeric coatings on the FishBAC internal structure were also discussed. Using a compatible corrugated skin with more height increases the bending stiffness of the skin to resist

more pressure caused by the airflow and buckling forces due to morphing actuation. It was also shown that the corrugated skin with more height decreased the in-plane tensile stiffness of the panel that results in smaller actuation energy required for morphing deformation. The structural advantage of a corrugated skin provides the possibility of a smaller number of FishBAC stringers which reduces the weight of the structure. A finite element simulation of the skin and internal structure under typical aerodynamic and structural loadings was performed to verify the design approach. The important interaction of the structural behaviour of the corrugated skin and the FishBAC structure was studied. The necessity of a full optimization which considers the geometry and material properties of both FishBAC internal structure and corrugated skin was discussed.

Chapter 5:
Conclusions and Recommendations

5-1 Conclusions

There are two different attitudes in the literature toward the morphing aircraft, namely optimistic and pessimistic view points. Some researchers have been so positive and have proposed concepts for morphing technology that are far from the level of current technology, and hence not practical in reality. On the other hand, some researchers look toward morphing aircraft as an improbable dream. To the author of this thesis, the attitude towards morphing aircraft should not be optimistic or pessimistic, but realistic. The fact that current traditional aircraft cannot be optimized for every single point of the flight envelop highlights the necessity of an aircraft which can adapt its shape to different flight configurations for further improvements of the flight performance. However, the requirements of such an aircraft are conflicting, for example the skin must be flexible enough to enable the shape changes and stiff enough to withstand the aerodynamic loadings. The use of

corrugated panels as a skin of a morphing aircraft is discussed comprehensively in this thesis to extend further the borders of the technology in this field.

In chapter 1 of this thesis, a detailed review of the literature on corrugated structures was presented. The specific characteristics of corrugated structures such as: high anisotropic behaviour, high stiffness and good durability, lightness and cost effectiveness, as well as recyclability and sustainability with the environment, were discussed. It was highlighted how these features have led to a wide range of industrial applications and academic research. Then concepts and developments of the corrugated structures to extend their application were investigated and classified into two categories: innovation based on different material properties and innovation based on topology and geometric parameters. Next a comprehensive set of analyses about the flexural, tensile, shear and out of plane compressive strength of corrugated panels that have been developed in the literature by means of experimental and finite element analysis were reviewed in details. The nonlinear effect in the mechanical behaviour of these structures due to material properties, geometric parameters, various boundary conditions and loading configurations was highlighted in the review. When available, homogenisation and equivalent modelling techniques were highlighted in support of these investigations. In addition a concise discussion on the buckling of these structures was presented, where homogenization techniques and finite element simulations were used to check for global and local buckling modes. Furthermore, the literature was explored in terms of optimization techniques for the optimum design of corrugated structures. The importance of such a review arises because the use of corrugated structures in morphing applications needs a study which comprises interdependent resources of research in different distinct disciplines. This ensures that all likely aspects of the morphing skin will be considered, and integrated into a complete analysis. Finally, the specific boundary conditions and constraints imposed by morphing applications were considered in the literature review of the corrugated skins. The lack of knowledge in the literature on specific fields of research such as: homogenization methods which consider the function of elastomer coating, a generic super element for corrugation curves, the multi-objective optimization and the design of corrugated skin in interaction with morphing internal structure, were considered as an introduction to the research in this thesis.

In chapter 2, two analytical solutions to calculate the equivalent tensile and bending flexural property of the corrugated core with elastomer coating in the longitudinal and transverse directions were presented based on Castigliano's second theorem. The results obtained by the analytical model were compared to those given by numerical simulations and experiments. In the experimental part, both coated and uncoated corrugated cores were studied in tensile and three point bending tests. The ratio of the in plane and out of plane stiffness of coated corrugated structure to uncoated corrugated structure was 2.28 and 2.14, respectively. This provided a better insight into the mechanical behavior of coated composite corrugated panels as candidates for morphing skin. Furthermore, the effect of combined loading and the number of unit cells on the mechanical behavior of the coated corrugated core were investigated and verified with numerical simulations. The physical description of the behavior that the relation between the coefficient of the distribution of forces in the elastomeric members and the Young's modulus of the elastomer converges when the Young's modulus of elastomer tends to infinity was also discussed. The comparison studies demonstrated the suitability of the proposed method for further design investigations.

In chapter 3, a generic super element of a corrugated core unit cell with elastomeric coating was investigated for application to morphing structures. The importance of this work, in contrast to the previous chapter, was that it provides an exact analytical equivalent model which avoids any homogenization and periodicity assumptions. By using the direct stiffness method and Castigliano's second theorem, and by applying proper boundary conditions, the stiffness matrix of the generic super element was derived which could capture the small deformation of 2D thin curved beams with variable curvatures. Different numerical and analytical symbolic models were investigated to verify the accuracy and efficiency of the presented super element. The super element uses the geometric and mechanical properties of the panel as variables, and hence the model may be used for further topology optimization studies. The parametric studies of trapezoidal and polynomial corrugation shapes demonstrated the efficiency of the proposed super element for application in further topology optimization or complex design investigations.

In chapter 4, the force displacement curves for reentrant, trapezoidal and rectangular corrugated cores with and without elastomeric coating were investigated in tensile and bending simulations. Comparing the results allowed the selection of a suitable corrugation configuration with regards to morphing skin applications. The geometric parameters of the coated trapezoidal composite corrugated panels were then optimized to minimize the in-plane stiffness and the mass of skin and to maximize the out-of-plane stiffness skin. To do so, a finite element code for beam elements was written in MATLAB to calculate the equivalent tensile and flexural stiffness of coated corrugated panels. Bearing in mind the manufacturing limitations, different possible configurations of FishBAC stringers and corrugated skin were considered in the optimization problem. Specially when the size of the corrugation was very small, the upper bounds and the lower bounds of the geometric parameters of the corrugation were chosen carefully based on practical considerations. The entire parameters of the corrugation were normalized in order to ensure the best performance of the optimization scheme. The advantages and limitations of the aggregate Newton's method and the GA multi-objective method were investigated for solving the multi objective optimization problem for the corrugated skin. The results obtained from both methods were compared and finally the aggregate Newton's method was utilized in this chapter. The dominance of each objective function due to the weight distribution in this method was discussed and highlighted in the Pareto surface of two sample cases. Moreover, by identifying the ideal reference point as the coordinates of minimum normalized objective values, the best compromise point was selected in each configuration of FishBAC stringers and corrugation unit cells. The range of the weights showed that all of the three objectives were involved efficiently in the process of optimization for the best compromise point. The trend of optimized parameters and objectives were then investigated by collecting and studying the best compromise points in all the configurations of FishBAC stringers and corrugation unit cells. It was justified that the out of plane and in-plane compliances of the corrugated core with elastomeric coating decreased when the length of the corrugation unit cell increased. For almost all configurations of FishBAC stringers and corrugation unit cells, reducing the length of the unit cells decreased the mass of the skin. In terms of the trends of the optimized geometric parameters, it was shown that the thickness of the core achieved the lower bound for the points with a unit cell length less than 14.55 mm while for a

unit cell length more than 16 mm the thickness of the elastomer coating achieved the lower bound. This switch in the way that the optimization algorithm optimized these two parameters resulted in a small jump in the trend of objective functions. Moreover, the optimization algorithm selected the corresponding values at the lower bound for the parameter a_2, while for the parameter h the upper bound was selected, implying that increasing the height of the corrugation gives a higher ratio of bending stiffness to tensile stiffness. Finally, the design decision was made by repeating the process of finding the best compromise point among the collection in a normalized space of objectives. As a result all the configurations of FishBAC stringers and corrugation unit cells which were well-matched in the equation of $(n_{stringer} + 1) \times N_{unitcell} = 15$ represented the highlighted decision point, i.e. case 4.3 ($n_{stringer}$=4, $N_{unitcells}$=3), case 5.2 ($n_{stringer}$=5, $N_{unitcells}$=2), and case 14.1 ($n_{stringer}$=14, $N_{unitcells}$=1). The important advantages of using a corrugated skin rather than simple elastomeric coatings on the FishBAC internal structure were also discussed. Using a compatible corrugated skin with more height increases the bending stiffness of the skin to resist more pressure caused by the airflow and buckling forces due to morphing actuation. It was also shown that the corrugated skin with more height decreased the in-plane tensile stiffness of the panel that results in smaller actuation energy required for morphing deformation. The structural advantage of a corrugated skin provides the possibility of a smaller number of FishBAC stringers which reduces the weight of the structure. A finite element simulation of the skin and internal structure under typical aerodynamic and structural loadings was performed to verify the design approach. The important interaction of the structural behaviour of the corrugated skin and the FishBAC structure was studied. The necessity of a full optimization which considers the geometry and material properties of both FishBAC internal structure and corrugated skin was discussed.

5-2 Some recommendations for future works

Certainly morphing as a promising technology is still far from flight readiness and significant work remains in maturing component technologies. The most critical component may be the skin which must be flexible but load carrying. While large scale morphing commercial aircraft may not be practical in the near future, opportunities exist on smaller unmanned aircraft where current or near-term

technology can be applied to achieve morphing (Friswell, 2014). In this regard precise manufacturing technology is needed to maintain the thickness and the dimensions of the composite corrugated sheet, especially when the scale of the morphing skin is small. The following recommendations are presented for further investigations on the application of corrugated skin in morphing aircraft.

Structural investigation of the skin

1- Practical concept developments which further decouple the out of plane stiffness from the in-plane stiffness of the skin might be difficult, but tempting. This is important since it increases the benefits of the corrugated skin for the application in morphing aircraft.

2- Performing buckling analysis on the corrugated skin specifically in the direction of the corrugation profile is important since the morphing actuation subjects the skin to compressive forces which tend to buckle in the mentioned direction. This opportunity of research was also addressed in camber morphing deformation in chapter 4.

3- Vibration and control analysis of the corrugated skin is very important since it imposes extra constraints on the design of the skin. It is crucial, for instance, to design the skin so that its natural frequencies are a safe distance from the frequency of excitation which is dependent on aerodynamic characteristics such as air speed. In addition, considering the lightness of the corrugated skin, there is an opportunity to harvest energy from this vibration, if piezoelectric materials can be integrated to the skin.

4- Investigation of the damage propagation arising from cyclic deformations either due to airflow induced vibration or the actuation process is also very important. For example, once the occurrence of cyclic stress can be predicted reliably then a constraint may be added into the morphing aerofoil optimization to ensure that the structural components of the skin would not fail at stress levels much lower than those experienced by static mechanical loading. This requires an in-depth analysis of the cyclic loading of corrugated skins, and in particular, the development of accurate fatigue models of corrugated panels. Such a study will

introduce new constraints for the extension of the lifetime of the composite corrugated skin.

5- A multi-objective optimization which considers the objective functions, material properties and geometric parameters is required due to the possible conflicting nature of the objective functions.

System level design of the skin

1- The shape optimization of the morphing aerofoil with the objective of achieving the highest possible lift to drag ratio followed by designing the internal adaptive structure to enable the required deformation of the corrugated skin.

2- Optimizing the skin simultaneously with the morphing internal structure. The coupled optimization of the internal structure and the corrugated skin which considers the boundaries and the constraints from the geometric consistency, material and manufacturing is required for future studies.

3- Fluid structure interaction (FSI) analysis is required which uses CFD and FE codes to capture the effects of the local and global deformations of the corrugated skin on the aerodynamic loads.

4- In terms of actuation energy, a topology optimization is needed to minimize the required strain energy to morph and to reduce further the mass of the whole morphing internal structure and corrugated skin.

Thesis References

A:

ABS:American Bureau of Shipping, (2004), Buckling and ultimate strength assessment for offshore structures

Ahmed, E. and Badaruzzaman, W.H., 2003. Equivalent elastic analysis if profiled metal decking using finite element method. *Steel Structures*; 3, 9-17.

Aird, F. (1996). Fibre glass & composite materials: an enthusiast's guide to high performance non-metallic materials for automotive racing and marine use. Penguin.

Argüelles, P., Bischoff, M., Busquin, P., Droste, B. A. C., et al., (2001), European Aeronautics: A vision for 2020. Report of the Group of Personalities, *The European Commission*, 12.

ASTM (2000), C393S. tandard test method for flexural properties of sandwich constructions. ASTM C393-00. ASTM International, *Philadelphia*, Pa, 19103.

ASTM D. (2000). 3039/D 3039M-00. Standard Test Method for Tensile Properties of Polymer Matrix Composite Materials, 10.

B:

Bapanapalli, S. K., Martinez, O. M., Gogu, C., Sankar, B. V., Haftka, R. T., & Blosser, M. L. (2006). Analysis and Design of Corrugated Core Sandwich Panels for Thermal Protection Systems of Space Vehicles. *AIAA Paper*, 1942, 2006

Barbarino, S., Bilgen, O., Ajaj, R. M., Friswell, M. I., & Inman, D. J. (2011). A review of morphing aircraft. *Journal of Intelligent Material Systems and Structures*, 22(9), 823-877.

Bartolozzi, G., Pierini, M., Orrenius, U., & Baldanzini, N. (2013). An Equivalent Material Formulation for Sinusoidal Corrugated Cores of Structural Sandwich Panels. *Composite Structures*, 100, 173-185.

Beaverstock, C. S., Ajaj, R. M., Friswell, M. I., De Breuker, R., & Werter, N. P. M. (2013). Optimising Mission Performance for a Morphing Mav. In 7th Ankara International Aerospace Conference.

Bhowmick, A. K., & Stephens, H. (Eds.). (2000). Handbook of Elastomers., 2nd edition, CRC Press.

Biancolini, M. and Brutti, C. (2003). Numerical and Experimental Investigation of the Strength of Corrugated Board Packages. *Packaging Technology and Science*, 16(2):47–60.

Bitner, J. R., & Reingold, E. M. (1975). Backtrack Programming Techniques. *Communications of the ACM*, 18(11), 651-656.

Briassoulis, D. (1986). Equivalent Orthotropic Properties of Corrugated Sheets. *Computers & structures*, 23(2), 129-138.

Brown, W. (2002, January). The Suitability of Various Gasket Types for Heat Exchanger Service. In ASME 2002 Pressure Vessels and Piping Conference (pp. 45-51). American Society of Mechanical Engineers.

C:

Carlsson, L. A., Nordstrand, T., & Westerlind, B. (2001). On The Elastic Stiffnesses of Corrugated Core Sandwich. *Journal of Sandwich Structures and Materials*, 3(4), 253-267.

Chang, W. S., Ventsel, E., Krauthammer, T., & John, J. (2005). Bending Behavior of Corrugated-Core Sandwich Plates. *Composite structures*, 70(1), 81-89.

Chekkal, I., Cheung, R., Wales, C., Cooper, J. E., Allen, N., Lawson, S., ... & by Institutions, F. (2014). Design of a Morphing Wing Tip., AIAA conference, SCITECH, Maryland, USA,

Coello, C. A. C. (1999). A Comprehensive Survey of Evolutionary-Based Multiobjective Optimization Techniques. *Knowledge and Information systems*, 1(3), 269-308.

Corrugate. Merriam-Webster.com. 2014. http://www.merriam-webster.com.

Corrugated Pipes for Sewage and Drainage Applications, 2011, Corma.com

D:

Daxner, T., Flatscher, T., & Rammerstorfer, F. G. (2007, May). Optimum Design of Corrugated Board under Buckling Constraints. In Proceedings 7th World Congress on Structures and Multidisciplinary Optimization, BMD Co., Seoul (pp. 349-358).

Das, I., & Dennis, J. E. (1997). A Closer Look at Drawbacks of Minimizing Weighted Sums of Objectives for Pareto Set Generation in Multicriteria Optimization Problems. *Structural optimization*, 14(1), 63-69.

Dayyani, I., Ziaei-Rad, S., & Friswell, M. I. (2013). The Mechanical Behavior of Composite Corrugated Core Coated With Elastomer for Morphing Skins. *Journal of Composite Materials*, 0021998313488807.

Dayyani, I. and Ziaei-Rad, S., (2011), Nonlinear Finite Element Analysis of Composite Corrugated Boards with Elastomeric Coatings, (Master dissertation), Isfahan university of Technology, Iran

Dayyani, I., Ziaei-Rad, S., and Salehi, H. (2012). Numerical and Experimental Investigations on Mechanical Behavior of Composite Corrugated Core. *Applied Composite Materials*, 19(3-4), 705-721.

Deb, K. (2001). Multi-Objective Optimization Using Evolutionary Algorithms, (Vol. 16). John Wiley & Sons.

Diani, J., Fayolle, B., & Gilormini, P. (2009). A Review on the Mullins Effect. *European Polymer Journal*, 45(3), 601-612.

Drela M., 1989 Xfoil: An Analysis and Design System for Low Reynolds Number Aerofoils Low Reynolds Number Aerofoil Aerodynamics, (Notre Dame, IN)

Dubina, D., Ungureanu, V., & Gîlia, L. (2013). Cold-Formed Steel Beams with Corrugated Web and Discrete Web-To-Flange Fasteners. *Steel Construction*, 6(2), 74-81.

E:

Elgaaly, M., Hamilton, R. W., & Seshadri, A. (1996). Shear Strength of Beams with Corrugated Webs. Journal of Structural Engineering, 122(4), 390-398.

European Commission. (2011). Flightpath 2050. Europe's Vision for Aviation. Report of the High Level Group on Aviation Research, Publications Office of the European Union, Luxembourg.

F:

Fincham, J. H., Ajaj, R. M., & Friswell, M. I. (2014). Aerodynamic Performance of Corrugated Skins for Spanwise Wing Morphing. 14th AIAA Aviation Technology, Integration, and Operations Conference, Atlanta, Georgia, 16-20 June 2014. DOI: 10.2514/6.2014-2724

Fonseca, C. M., & Fleming, P. J. (1993, June). Genetic Algorithms for Multiobjective Optimization: Formulation Discussion and Generalization. InICGA (Vol. 93, pp. 416-423).

Forrester, A., Sobester, A., & Keane, A. (2008). Engineering Design via Surrogate Modelling: A Practical Guide. John Wiley & Sons.

Friswell, M. I., (2014), ''MORPHING AIRCRAFT: AN IMPROBABLE DREAM?'', Proceedings of the ASME 2014 Conference on Smart Materials, Adaptive Structures and Intelligent Systems, SMASIS2014, September 8-10, 2014, Newport, Rhode Island, USA

G:

Callister, W. D., & Rethwisch, D. G. (2007). Materials Science and Engineering: An Introduction (Vol. 7, pp. 665-715). New York: Wiley.

Gilchrist, A. C., Suhling, J. C., & Urbanik, T. J. (1998). Nonlinear Finite Element Modeling of Corrugated Board. ASME, *Applied Mechanics Division-Publications-Amd*, 231, 101-106.

Goldberg, D. E., & Holland, J. H. (1988). Genetic Algorithms and Machine Learning. *Machine Learning*, 3(2), 95-99.

H:

Hachemi, H., Kebir, H., Roelandt, J. M., & Wintrebert, E. (2011). A Study of The Braided Corrugated Hoses: Behavior and Life Estimation. *Materials & Design*, 32(4), 1957-1966.

Harper, C., (2002), Handbook of Plastics, Elastomers and Composites, 4th edition, New York, McGraw-Hill.

Hochman, H. M., & Rodgers, J. D. (1969). Pareto Optimal Redistribution. *The American Economic Review*, 542-557.

I:

Isaksson, P., Krusper, A., & Gradin, P. A. (2007). Shear Correction Factors for Corrugated Core Structures. *Composite structures*, 80(1), 123-130.

J:

Jim Noll, Steve Tysl, and Matt Westrich, (2009),The Use of Corrugated Metal Pipe and Structural Plate for Aggregate Tunnel and Conveyor Enclosure Applications, Professional Development Advertising Section , CONTECH Construction Products Inc.

Johnson, M. W., & Urbanik, T. J. (1989). Analysis of the Localized Buckling In Composite Plate Structures with Application to Determining the Strength of Corrugated fibreboard. *Journal of Composites Technology and Research*, 11(4), 121-128.

K:

Kampner, M., & Grenestedt, J. L. (2008). On Using Corrugated Skins to Carry Shear in Sandwich Beams. *Composite Structures*, 85(2), 139-148.

Kazemahvazi, S., & Zenkert, D. (2009). Corrugated All-Composite Sandwich Structures. Part 1: Modeling. *Composites Science and Technology*, 69(7), 913-919.

Kazemahvazi, S., Tanner, D., & Zenkert, D. (2009). Corrugated All-Composite Sandwich Structures. Part 2: Failure Mechanisms and Experimental Programme. *Composites Science and Technology*, 69(7), 920-925.

Khalid, Y. A., Chan, C. L., Sahari, B. B., & Hamouda, A. M. S. (2004), Bending Behaviour of Corrugated Web Beams. *Journal of Materials Processing Technology*, 150(3), 242-254

Knox, E. M., Cowling, M. J., & Winkle, I. E. (1998). Adhesively Bonded Steel Corrugated Core Sandwich Construction for Marine Applications. *Marine structures*, 11(4-5), 185-204

Kooistra, G. W., Deshpande, V., & Wadley, H. N. (2007). Hierarchical Corrugated Core Sandwich Panel Concepts. *Journal of applied mechanics*, 74(2), 259-268.

Kress, G., Winkler, M., 2010. Corrugated Laminate Homogenization Model. *Composite Structures*, 92 (3), 795–810.

Kress, G., Winkler, M., 2011. Corrugated Laminate Analysis: A Generalized Plane-Strain Problem. *Composite Structures*, 93 (5), 1493–1504.

L:

Leekitwattana, M., Boyd, S. W., & Shenoi, R. A. (2011). Evaluation of the Transverse Shear Stiffness of a Steel Bi-Directional Corrugated-Strip-Core Sandwich Beam. *Journal of Constructional Steel Research*, 67(2), 248-254.

Li, L., Kim, S. M., Song, S. H., Ku, T. W., Song, W. J., Kim, J., ... & Kang, B. S. (2008). Finite Element Modeling and Simulation for Bending Analysis Of Multi-Layer Printed Circuit Boards Using Woven Fibre Composite. *Journal of materials processing technology*, 201(1), 746-750.

Liang, C. C., Yang, M. F., & Wu, P. W. (2001). Optimum Design of Metallic Corrugated Core Sandwich Panels Subjected to Blast Loads. *Ocean Engineering*, 28(7), 825-861.

Libove, C. (1973). On the Stiffness, Stresses and Buckling Analysis of Corrugated Shear Webs. In Second Specialty Conference On Cold-Formed Steel Structures. Missouri S&T (formerly the University of Missouri-Rolla).

Liew, K. M., Peng, L. X., & Kitipornchai, S. (2006). Buckling Analysis of Corrugated Plates Using a Mesh-Free Galerkin Method Based on the First-Order Shear Deformation Theory. *Computational Mechanics*, 38(1), 61-75.

Liew, K.M., Peng, L.X., Kitipornchai, S., 2007. Nonlinear Analysis of Corrugated Plates Using A FSDT and A Meshfree Method. *Computer Methods in Applied Mechanics and Engineering*, 196 (21-24), 2358–2376.

Lu, T. J., Chen, C., & Zhu, G. (2001). Compressive Behaviour of Corrugated Board Panels. *Journal of composite materials*, 35(23), 2098-2126

Luo, R., & Edlund, B. (1996). Shear Capacity of Plate Girders with Trapezoidally Corrugated Webs. *Thin-walled structures*, 26(1), 19-44.

Luo, S., Suhling, J. C., Considine, J. M., & Laufenberg, T. L. (1992)., The Bending Stiffnesses of Corrugated Board., *Mechanics of Cellulosic Materials*, ASME, AMD-Vol. 145/MD-Vol. 36,

M:

Mallick, P. K., & Boorle, R. (2014). Sandwich Panels with Corrugated Core-A Lightweighting Concept with Improved Stiffness (No. 2014-01-0808). SAE Technical Paper

Martinez, O. A., Sankar, B. V., Haftka, R., Bapanapalli, S. K., & Blosser, M. L. (2007). Micromechanical Analysis of Composite Corrugated-Core Sandwich Panels for Integral Thermal Protection Systems. AIAA journal, 45(9), 2323-2336

Marler, R. T., & Arora, J. S. (2004). Survey of Multi-Objective Optimization Methods for Engineering. *Structural and Multidisciplinary Optimization*, 26(6), 369-395.

May, C. (Ed.). (1987). Epoxy Resins: Chemistry and Technology. CRC Press.

McFarland, D.E., 1967. An Investigation of The Static Stability of Corrugated Rectangular Plates Loaded in Pure Shear. Ph.D. thesis, University of Kansas, Lawrence, KS

Megson, T. H. G. (2012). Aircraft Structures for Engineering Students. Elsevier

Melin, T. (2000). A Vortex Lattice MATLAB Implementation for Linear Aerodynamic Wing Applications. Master's Thesis, Department of Aeronautics, Royal Institute of Technology (KTH), Stockholm, Sweden.

Miehe, C., Schotte, J., Schröder, J., 1999. Computational Micro–Macro Transitions and Overall Moduli in the Analysis of Polycrystals at Large Strains. *Computational Materials Science*, 16, 372–382.

Miehe, C., Schotte, J., Lambrecht, M., 2002. Homogenization of Inelastic Solid Materials at Finite Strains Based on Incremental Minimization Principles. Application to the Texture Analysis of Polycrystals. *Journal of the Mechanics and Physics of Solids*, 50 (10), 2123–2167.

Mostaghim, S., & Teich, J. (2003, April). Strategies for Finding Good Local Guides in Multi-Objective Particle Swarm Optimization (MOPSO). In Swarm Intelligence Symposium, 2003. SIS'03. *Proceedings of the 2003 IEEE* (pp. 26-33). IEEE.

Murugan, S., Saavedra Flores, E. I., Adhikari, S., & Friswell, M. I. (2012). Optimal Design of Variable Fibre Spacing Composites for Morphing Aircraft Skins. *Composite Structures*, 94(5), 1626-1633.

N:

Nordstrand, T. (2004). Analysis and Testing Of Corrugated Board Panels into the Post-Buckling Regime. *Composite structures*, 63(2), 189-199.

Nordstrand, T., Carlsson, L. A., & Allen, H. G. (1994). Transverse Shear Stiffness of Structural Core Sandwich. *Composite structures*, 27(3), 317-329.

Nordstrand, T. M., & Carlsson, L. A. (1997). Evaluation of Transverse Shear Stiffness of Structural Core Sandwich Plates. *Composite structures*, 37(2), 145-153.

Norman, A. D., Guest, S. D., & Seffen, K. A. (2007, April). Novel Multistable Corrugated Structures. In Proceedings of the 48th AIAA/ASME/ASCE/AHS/ASC Structures, Structural Dynamics and Materials Conference, April 23C26, Waikiki, Hawaii.

Ng, C. F., & Zheng, H. (1998). Sound Transmission Through Double-Leaf Corrugated Panel Constructions. *Applied Acoustics*, 53(1), 15-34.

P:

Patel, P., Nordstrand, T., & Carlsson, L. A. (1997). Local Buckling and Collapse of Corrugated Board under Biaxial Stress. *Composite Structures*, 39(1), 93-110.

Pellegrino, C., Galvanetto, U., Schrefler, B.A., 1999. Numerical Homogenization of Periodic Composite Materials with Non-Linear Material Components. *International Journal for Numerical Methods in Engineering*, 46, 1609–1637.

Peng, L., Liew, K., & Kitipornchai, S. (2007). Analysis of Stiffened Corrugated Plates Based On the FSDT via the Mesh-Free Method. *International Journal of Mechanical Sciences*, 364–378

Pignataro, M., Pasca, M., & Franchin, P. (2000). Post-Buckling Analysis of Corrugated Panels in the Presence of Multiple Interacting Modes. *Thin-walled structures*, 36(1), 47-66.

Q:

Queheillalt, D. T., Murty, Y., & Wadley, H. N. (2008). Mechanical Properties of an Extruded Pyramidal Lattice Truss Sandwich Structure. *Scripta Materialia*, 58(1), 76-79.

R:

Ray, H. (1996). U.S. Patent No. 5,543,204. Washington, DC: U.S. Patent and Trademark Office.

Rao, S.S., 1996. Engineering Optimization Theory and Practice, 3rd ed. John Wiley & Sons.

Reddy, J. N., 1997. Mechanics of laminated composite plates- Theory and analysis, Boca Raton, FL: CRC Press.

Rejab, M. R. M., & Cantwell, W. J. (2013). The Mechanical Behaviour of Corrugated-Core Sandwich Panels. *Composites Part B: Engineering*, 47, 267-277

Roux, W. J., Stander, N., & Haftka, R. T. (1998). Response Surface Approximations for Structural Optimization. *International Journal for Numerical Methods in Engineering*, 42(3), 517-534.

S:

Saavedra Flores, E.I., de Souza Neto, E.A., 2010. Remarks on Symmetry Conditions in Computational Homogenisation Problems. *Engineering Computations,* 27 (4), 551–575.

Samanta, A., Mukhopadhyay, M. (1999). Finite Element Static and Dynamic Analyses of Folded Plates. *Engineering Structures*, 277-287.

Sause, R., & Braxtan, T. N. (2011). Shear Strength of Trapezoidal Corrugated Steel Webs. *Journal of Constructional Steel Research*, 67(2), 223-236.

Semenyuk, N. P., and Neskhodovskaya, N. A. (2002a). On Design Models in Stability Problems for Corrugated Cylindrical Shells. *International applied mechanics*, 38(10), 1245-1252.

Semenyuk, N. P., and Neskhodovskaya, N. A. (2002b). Timoshenko-Type Theory in the Stability Analysis of Corrugated Cylindrical Shells. *International applied mechanics*, 38(6), 723-730.

Semenyuk, N. P., Zhukova, N. B., & Ostapchuk, V. V. (2007). Stability of Corrugated Composite Noncircular Cylindrical Shells under External Pressure. *International Applied Mechanics*, *43*(12), 1380-1389.

Seong, D. Y., Jung, C. G., Yang, D. Y., Moon, K. J., & Ahn, D. G. (2010). Quasi-Isotropic Bending Responses of Metallic Sandwich Plates with Bi-Directionally Corrugated Cores. *Materials & Design*, 31(6), 2804-2812

Seydel, E. (1931). Shear Buckling of Corrugated Plates. Jahrbuch die Deutschen Versuchsanstalt fur Luftfahrt 9, 233–245.

SIMULIA, (2011), ABAQUS 6.11-2,

Shaw, A. D., Dayyani, I., & Friswell, M. I. (2015). Optimisation of Composite Corrugated Skins for Buckling in Morphing Aircraft. *Composite Structures*, 119, 227-237.

Singh, S. P., Chonhenchob, V., & Singh, J. (2006). Life Cycle Inventory And Analysis of Re-Usable Plastic Containers and Display-Ready Corrugated Containers Used for Packaging Fresh Fruits and Vegetables. *Packaging Technology and Science*, 19(5), 279-293.

Sun, H. H., & Spencer, J. (2005). Buckling Strength Assessment of Corrugated Panels in Offshore Structures. *Marine structures*, 18(7), 548-565

Suquet, P., 1993. Overall Potentials and Extremal Surfaces of Power Law or Ideally Plastic Materials. *Journal of the Mechanics and Physics of Solids,* 41, 981–1002.

T:

Tan KH, Montague P, Norris C. (1989), Steel Sandwich Panels: Finite Element, Closed Solution, and Experimental Comparisons on 6m × 2.1m Panel, *Struct Eng*, 67(9):159–66.

Thill, C., Etches, J., Bond, I., Potter, K., and Weaver, P. (2008a). Morphing Skins. *The Aeronautical Journal*, 112(1129), 117-139.

Thill, C., Etches, J.A., Bond, I.P., Weaver, P.M. and Potter, K.D., (2008b), Experimental and Parametric Analysis of Corrugated Composite Structures for Morphing Skin Applications. In: 19th International Conference on Adaptive Structures Technology, 6–9 October 2008, Ascona, Switzerland.

Thill, C., Etches, J. A., Bond, I. P., Potter, K. D., and Weaver, P. M. (2010a). Composite Corrugated Structures for Morphing Wing Skin Applications. *Smart Materials and Structures,* 19(12), 124009.

Thill, C., Etches, J. A., Bond, I. P., Potter, K. D., & Weaver, P. M. (2007, October). Corrugated Composite Structures for Aircraft Morphing Skin Applications. In 18th International conference of adaptive structures and technologies, Ottawa, Ontario, Canada.

Thill, C., Etches, J. A., Bond, I. P., Potter, K. D., Weaver, P. M., & Wisnom, M. R. (2010b). Investigation of Trapezoidal Corrugated Aramid/Epoxy Laminates under Large Tensile Displacements Transverse to the Corrugation Direction. *Composites Part A: Applied Science and Manufacturing*, 41(1), 168-176.

Toupin, R. A. (1965). Saint-Venant's Principle. Archive for Rational Mechanics and Analysis, 18(2), 83-96.

Twede, D., & Selke, S. E. (2005). Cartons, Crates and Corrugated Board: Handbook of Paper and Wood Packaging Technology. DEStech Publications, Inc.

U:

Ursache, N. M., Melin, T., Isikveren, A. T., & Friswell, M. I. (2008, January). Technology Integration for Active Poly-Morphing Winglets Development. InASME 2008 Conference on Smart Materials, Adaptive Structures and Intelligent Systems (pp. 775-782). American Society of Mechanical Engineers.

W:

Wadley, H. N., Fleck, N. A., & Evans, A. G. (2003). Fabrication and Structural Performance of Periodic Cellular Metal Sandwich Structures. *Composites Science and Technology*, 63(16), 2331-2343.

Wennberg, D., Wennhage, P., and Stichel, S., 2011. Orthotropic Models of Corrugated Sheets in Finite Element Analysis. *ISRN Mechanical Engineering.*, Article ID 979532, 9 pages

Wicks, N., Hutchinson, J.W., 2001. Optimal Truss Plates. *International Journal of Solids Structures*. 38, 6165–6183.

Winkler, M., 1981. Analysis of Corrugated Laminates. Dissertation for the degree of Doctor Of Sciences. ETH Zurich, Switzerland.

Winkler, M., Kress, G., 2010. Deformation Limits for Corrugated Cross-Ply Laminates. *Composite Structures.* 92 (6), 1458–1468.

Woods, B. K. S., & Friswell, M. I. (2012, September). Preliminary Investigation of a Fishbone Active Camber Concept. In ASME 2012 Conference on Smart Materials, Adaptive Structures and Intelligent Systems (pp. 555-563). American Society of Mechanical Engineers.

X:

Xia, Y., Ajaj, R. M., & Friswell, M. I. (2014). Design and Optimisation of Composite Corrugated Skin for a Span Morphing Wing. 22nd AIAA/ASME/AHS Adaptive Structures Conference, 13-17 January 2014, National Harbor, Maryland, USA, paper AIAA-2014-0762. DOI: 10.2514/6.2014-0762

Xia, Y., Friswell, M.I. and Saavedra Flores, E.I., 2012. Equivalent Models of Corrugated Panels. *International Journal of Solids and Structures.* 49, 1453-1462.

Y:

Ye, Z., Berdichevsky, V.L. and Yu, W., 2014. An Equivalent Classical Plate Model of Corrugated Structures. *International Journal of Solids and Structures.* 51(11-12), 2073-2083.

Yi, J., Gil, H., Youm, K., & Lee, H. (2008). Interactive Shear Buckling Behavior of Trapezoidally Corrugated Steel Webs. *Engineering Structures*, 30(6), 1659-1666.

Yokozeki, T., Takeda, S. I., Ogasawara, T., & Ishikawa, T. (2006). Mechanical Properties of Corrugated Composites for Candidate Materials of Flexible Wing Structures. *Composites Part A: applied science and manufacturing*, 37(10), 1578-1586.

Yokozeki, T., Sugiura, A., & Hirano, Y. Development and Wind Tunnel Test of Variable Camber Morphing Wing. 22nd AIAA/ASME/AHS Adaptive Structures Conference, 13-17 January 2014, National Harbor, Maryland, USA,